

ABERRANT SIGNALING IN ASTROCYTOMAS AND GLIOBLASTOMA MULTIFORME (GBM):
UTILIZING INHIBITORS OF PROLIFERATION AS POTENTIAL THERAPIES

by

Yvette Connell-Albert
A Dissertation
Submitted to the
Graduate Faculty
of
George Mason University
in Partial Fulfillment of
The Requirements for the Degree
of
Doctor of Philosophy
Biosciences

Committee:

_____	Dr. Ancha Baranova, Dissertation Co-Director
_____	Dr. Karlyne Reilly, Dissertation Co-Director
_____	Dr. Daniel N.Cox, Committee Member
_____	Dr. Barney Bishop, Committee Member
_____	Dr. James D. Willett, Committee Member
_____	Dr. James D. Willett, Director, School of Systems Biology
_____	Dr. Timothy L. Born, Associate Dean for Student and Academic Affairs, College of Science
_____	Dr. Vikas Chandhoke, Dean, College of Science
Date: _____	Fall Semester 2012 George Mason University Fairfax, VA

Aberrant Signaling in Astrocytomas and Glioblastoma Multiforme (GBM): Utilizing
Inhibitors of Proliferation as Potential Therapies

A dissertation submitted in partial fulfillment of the requirements for the degree of
Doctor of Philosophy at George Mason University

by

Yvette S. Connell-Albert
Master of Science
Johns Hopkins University, 2002
Bachelor of Science
University of Maryland at College Park, 1994

Co-Directors: Ancha Baranova, Associate Professor
School of Systems Biology
Karlyne Reilly, Principal Investigator
National Cancer Institute at Frederick

Spring Semester 2013
George Mason University
Fairfax, VA

COPYRIGHT@2013 YVETTE S. CONNELL-ALBERT
ALL RIGHTS RESERVED

DEDICATION

This is dedicated to my grandmother and mother both of whom have always believed and taught by example, that a good education was/is the passport to a better life. Thank you for the encouragement and loving support when the going got rough!

ACKNOWLEDGEMENTS

God: the ultimate source of all wisdom, knowledge and understanding. How Great Is Our God!

I would also like to thank my committee chairperson, and mentor, Dr. Ancha Baranova for the opportunity to conduct research in her lab and for her tireless pursuit of alternative options when the research project did not always generate the anticipated results. A special thank you to my dissertation committee members: Drs. Dan Cox, James Willett, Barney Bishop, and Karlyne Reilly, for their dedication, guidance and patience, in the culmination of this research project. I could not have done it without you, so thank you.

I would especially like to thank my Dissertation Director, Dr. Karlyne Reilly for the wonderful opportunity to conduct my dissertation research under her tutelage at the NIH/NCI and for access to the facilities and funding to work on this research project towards the PhD degree. Karlyne, your unwavering support, your exquisite guidance, your patience and respect towards me during my tenure in your lab has left an indelible impression on my mind that not only are you a brilliant scientist, a fantastic mentor and leader; you are probably one of the kindest and most generous people I have encountered in my lifetime. I thank you for who you are and who I have become and continue to aspire to be because of my association with you.

In addition, I would like to acknowledge my fellow lab mates to include Dr. Jessica Hawes for her warm friendship and support, as well as the other members of the Reilly Gang. A sincere thank you! Also, to the members of the Mouse Cancer Genetics Group for their shared time and experience, thank you to all!

Furthermore, I would like to thank the PROMISE Director and Co-Director, Dr. Renetta G.Tull and Dr. Wendy Carter-Veale, respectively, for the opportunity to participate in the Dissertation House and for invaluable advice and support. Thank you!

Finally, I would like to thank my immediate family, mother, spouse and son for their patience and support as we traversed this pathway together. You have been the “wind beneath my wings”. Loving thanks to each of you!

TABLE OF CONTENTS

	Page
List of Tables	vi
List of Figures	viii
List of Abbreviations	x
Abstract	
Chapter 1: Introduction	1
Chapter 2: PI-103, Tricirbine and Rapamycine as Potential Glioma Therapeutics.....	222
Chapter 3: Pre-Clinical Evaluation of Nelfinivir, Chloroquine, Perifosine, PIA-6 and OSU-03012	50
Chapter 4: Pre-clinical Evaluation of Scheinweinfurthin and its Analogues	78
Bibliography.....	95
Appendix: The Role of Pannexins in Intercellular Communication and The Implications for Gliomagenesis	108
Appendix Bibliography	180

LIST OF TABLES

Table	Page
Table 1.1: The five major categories of glioma-derived neoplasms	1
Table 1.2 The grades of astrocytic tumors based on WHO criteria.	3
Table 2.1: Selected Chemical and Physical Properties of PI-103, TCN and Rapamycin that contribute to characteristics of good drug candidates.	27
Table 2.2: The experimental conditions for drug inhibition studies.	35
Table 2.3: IC ₅₀ , GI ₅₀ , and maximum percent inhibition of PI-103, TCN and Rapamycin in various cell lines.	39
Table 3.1: The five inhibitors used in the Alamar Blue cell viability and cytotoxicity assay with mouse and human cell lines.	57
Table 3.2: Selected Chemical and Physical Properties of OSU, Perifosine, Chloroquine, Nelfinivir and PIA-6 that contribute to characteristics of good drug candidates.	57
Table 3.3: The calculated IC ₅₀ values for the five inhibitors tested with mouse and human cell lines.	67
Table 4.1: This shows some of the natural Schweinfurthin compounds and their analogues as tested <i>in vitro</i>	81
Table 4.2: The calculated IC ₅₀ , GI ₅₀ , and maximum percent inhibition of SA and select analogues tested with cell lines.	88
Table A.1a: Comparison of Mouse and Human Pannexin genes.	111
Table A.1b: Bacterial strains and genotype used for recombineering.	133
Table A.2: Primer sets used for generating 5' and 3' Homology arms for Retrieving.	141

Table A.3: Primer sets used for generating the 5' and 3' Homology arms for the Second Mini-targeting construct with pLTM260 5' Neo Reverse cassette.....	146
Table A.4: Primer sets used for generating the 5' and 3' Homology arms for the First mini-targeting construct pLTM332 3' Neo Forward cassette.....	151
Table A.5: Primer sets used for generating the 5' and 3' Probes for Southern blot analysis.....	156

LIST OF FIGURES

Figure	Page
Figure 1.1: Tumor cell lines isolated from NPCis mouse models form tumors subcutaneously and maintain the growth characteristics of respective tumor grade	16
Figure 2.1: This figure shows the chemical structure of PI-103 with Molecular Formula: C ₁₉ H ₁₆ N ₄ O ₃	23
Figure 2.2: This figure shows the chemical structure of Tricirbine	24
Figure 2.3: This figure shows the chemical structure of Rapamycin	26
Figure 2.4: Inhibition of phospho-Akt and phospho-p70S6K by increasing concentrations of PI-103	40
Figure 2.5: Growth inhibition curves as a function of drug concentration for PI-103 (top panel), TCN(middle panel), and Rapamycin (bottom panel).....	41
Figure 2.6: Inhibition of phospho-Akt and phospho-p70S6K by increasing concentrations of TCN.....	44
Figure 2.7: Inhibition of phospho-p70S6K by Rapamycin.....	47
Figure 3.1: This figure shows the chemical structure of Chloroquine.....	51
Figure 3.2: This figure shows the chemical structure of Perifosine	52
Figure 3.3: This figure shows the chemical structure of PIA6	53
Figure 3.4: This figure shows the chemical structure of OSU-03012	54
Figure 3.5: This figure shows the chemical structure of Nelfinivir	56
Figure 3.6: Effects of OSU-03012 on cell viability	69
Figure 3.7: Effects of Perifosine on cell viability	72
Figure 3.8: Effects of Chloroquine on cell viability	73
Figure 3.9: Effects of Nelfinivir on cell viability	74
Figure 3.10: Effects of PIA-6 on cell viability	75
Figure 4.1: Diagram showing the structure of Schweinfurthin A. Top: NSC#735927-3dSB-Schweinfurthin B analogue. Middle: NSC#746620-Schweinfurthin analogue. Bottom: Schweinfurthin A.....	80
Figure 4.2: Effects of Schweinfurthin A on cell lines	89
Figure 4.3: Calculated GI ₅₀ values for 3dSB treated cell lines	91
Figure 4.4: Effects of analogue NSC#746620 on cell viability	92

Figure A.1: This diagram represents the innexin, connexin, and pannexin channel forming proteins in invertebrates and vertebrates.....	112
Figure A.2: This diagram represents the typical structure of the pannexin channel forming protein found in both vertebrates and invertebrates ..	112
Figure A.3A: The expression of PANX2 mRNA in human brain tumor samples	118
Figure A.3B: The Kaplan-Meier survival plot for samples with differential PANX2 gene expression.....	119
Figure A.4: Panx1 is abundantly expressed in mouse primary astrocytes as well as HEK293	121
Figure A.5: Panx2 is abundantly expressed in mouse primary astrocytes and reduced in some other human and mouse cell lines.....	122
Figure A.6: Conditional knock-out vector construction.....	132
Figure A.7: Identification of correctly targeted Bac-Panx2 DNA clones	134
Figure A.8: Diagram to show the pAD253 retrieval vector	139
Figure A.9: Diagram showing pAD253 retrieval plasmid with homology arms and Bac Panx2 DNA.....	140
Figure A.10: Confirmation of Bac-Panx2 DNA in retrieval vector pAD253	140
Figure A.11: Diagram showing the pLTM260 vector containing the Neomycin cassette	148
Figure A.12: Diagram to show the homology arms for the second targeting construct	149
Figure A.13: Diagram showing the construction of the second mini-targeting vector	149
Figure A.14: The second mini-targeting vector containing homology arms and pLTM260 Neomycin cassette	150
Figure A.15: This diagram shows the pLTM332 vector containing Neomycin cassette	152
Figure A.16: Diagram to show the homology arms for first targeting construct	153
Figure A.17: Diagram showing the construction of the first mini-targeting vector...	153
Figure A.18: Mini-targeting vector containing homology arms without Neomycin cassette	154
Figure A.19: Diagram showing the Southern blot design	161
Figure A.20: Southern blot analysis of 3' probe in the WT DNA ES cells	162
Figure A.21: Southern blot analysis of 5' probe in the WT DNA ES cells	162
Figure A.22: Diagram showing the expected pAD253 retrieval plasmid	164
Figure A.23: Diagram showing the KO mutant mice DNA.....	165
Figure A.24: Diagram showing the pcDNA3.1 vector used for sub-cloning.....	166

LIST OF ABBREVIATIONS

Term	Abbreviation
Anaplastic astrocytoma.....	AA
Bacterial artificial chromosome.....	BAC
Blood brain barrier.....	BBB
Bovine serum albumin.....	BSA
Central nervous system.....	CNS
Cerebral spinal fluid.....	CSF
Conditional knock out.....	CKO
Connexin	Cx
Cyclooxygenase-2.....	COX2
Dithiothreitol.....	DTT
Dulbecco Minimum Essential Medium	DMEM
3-deoxy Schweinfurthin B.....	3DSB
Embryonic stem	ES
Ethylenedinitrilo tetraacetic acid	EDTA
Ethylene glycol-bis[β -aminoethyl ether]-N,N,N',N'-tetraacetic acid.....	EGTA
Embryonic stem	ES
Epidermal growth factor receptor	EGFR
Ethidium bromide	ETBR
Glial fibrillary acidic protein	GFAP
Glioblastoma multiforme	GBM
Homology arm	HA
Human brain microvascular endothelial cell	HBMEC
Immunoprecipitation.....	IP
Inhibitory concentration 50.....	IC50
Knock-out	KO
Loss of heterozygosity	LOH
Luria Broth	LB
Low grade glioma	LGG
Malignant peripheral nerve sheath tumors.....	MPNST
Neurofibromatosis type 1.....	NF1
NF1+/-; P53+/-.....	NPcis
OSU03012	OSU
P1 artificial chromosome	PAC
Peripheral nervous system	PNS
Phosphate buffered saline	PBS

Phosphatidylinositol ether lipid analogue 6.....	PIA-6
Picomolar	pM
Phenylmethylsulfonyl fluoride.....	PMSF
Polymerase chain reaction	PCR
Protease inhibitor	PI
3-[4-(4-morpholinyl)pyrido[3',2':4,5]furo[3,2-d]pyrimidin-2-yl]-phenol	PI-103
Rapamycin	RAP
Radio-immunoprecipitation assay buffer.....	RIPA
Revolutions per minute	RPM
Schweinfurthin	SA
Serum free medium.....	SFM
Sodium dodecyl sulfate polyacrylamide gel electrophoresis.....	SDS-PAGE
Tris-Buffered-EDTA.....	TBE
Tris-Acetate-EDTA.....	TAE
Tris-Phosphate-EDTA	TPE
Tricirbine	TCN
Tris-buffered-saline-Tween	TBST-T
Temozolomide	TMZ
Tris buffered saline	TBS
Units	U
Ultra Violet	UV
Weight to volume.....	W/V
Wild type	WT
World Health Organization.....	WHO

ABSTRACT

ABERRANT SIGNALING IN ASTROCYTOMAS AND GLIOBLASTOMA MULTIFORME (GBM): UTILIZING INHIBITORS OF PROLIFERATION AS POTENTIAL THERAPIES

Yvette S. Connell-Albert, Ph.D.

George Mason University, 2013

Dissertation Co-Directors: Dr. Ancha Baranova & Dr. Karlyne Reilly

Glioblastomas (GBMs), the most aggressive malignant astrocytomas, are recurrent, infiltrative, and fatal. In GBMs, receptor tyrosine kinases (RTKs) are often activated by mutations, leading to the dysregulation of cell signaling pathways. The PI3K/Akt1/mTOR pathway, which plays a role in many biological processes such as proliferation, survival, invasion, migration and angiogenesis, is often deregulated in malignant cancers, often by the simultaneous loss of tumor suppressor PTEN, and the hyperactivation of the kinase Akt. Therefore, pharmacological inhibition of the PI3K/Akt1/mTOR pathway may prove beneficial in arresting the growth of astrocytomas and glioblastomas. In order to determine if the candidate molecules Chloroquine, Nelfinivir, PIA-6, OSU03012, Rapamycin, Tricribine (TCN), and PI-103 inhibit the PI3K/Akt-1/mTOR pathway, we used the Alamar blue assay as a measure of cell viability and cytotoxicity in mouse astrocytoma cell lines K1861-10 Grade II; KR158 Grade III;

K130G#3 Grade IV; human astrocytoma cell lines, U87MG and SF295, both Grades IV; and normal proliferating mouse primary astrocytes treated with candidate molecules described above. Inhibitors with low IC_{50} values in tumor cells as compared to normal primary astrocytes were selected. From the select panel of inhibitors, only the AKT inhibitor Tricirbine and dual PI3K/Akt-1 inhibitor PI-103 showed low IC_{50} values in the nM or pM range, suggesting strong inhibition of cell viability in the astrocytoma cell lines tested. Rapamycin, an mTOR inhibitor, showed inconsistent inhibition of cell viability on the cell lines tested, suggesting that rapamycin may be acting through more than one pathway. The results of our study suggest that the PI3K/Akt1/mTOR pathway has potential as a druggable target in astrocytomas and glioblastomas.

CHAPTER 1: INTRODUCTION

Gliomas, which are a group of tumors that may either be benign or malignant, arise in the central nervous system (CNS) from cells of glial origin (David N. Louis 2007). Glioblastoma multiforme (GBM) and malignant astrocytomas are diffusely infiltrating tumors (Table 1.1). They account for more than 50% of all CNS tumors of glial origin (Molina, Hayashi et al. 2010). These tumors are uniformly fatal.

Table 1.1: The five major categories of glioma-derived neoplasms.

Neoplasm	Whether malignant or not
Subependymal giant cell astrocytomas	NO
Desmoplastic cerebral astrocytomas of infancy	RARELY
Pleomorphic xanthoastrocytomas	YES, if progression from benign occurs
Pilocytic astrocytomas	RARELY
Diffusely infiltrating astrocytomas and glioblastoma multiforme	YES

The morbidity, prognosis and ultimate mortality of patients diagnosed with an astrocytoma or GBM is determined by the grade of the tumor. Tumor grading is based on its proliferative potential and histologically evident malignant features, and is performed

according to the criteria established by the World Health Organization (WHO) (David N. Louis 2007).

This dissertation focuses on the diffusely infiltrating astrocytomas. In an effort to reduce the morbidity and mortality associated with astrocytomas and glioblastomas (GBMs), here we study how the aberrant signaling of the PI3K/Akt/mTOR signal transduction pathway may be attenuated by potential therapeutics. In addition, we address the down-regulation of expression of the Pannexin 2 (Panx2) channel protein in astrocytomas and GBM and the role Panx2 may play in gliomagenesis.

GLIOMA TUMOR GRADING

The World Health Organization (WHO) has classified glial tumors into four grades: I, II, III, and IV (Table 1.2). These grades are based on three criteria to include the malignancy of the tumor, which can range in scale from low to high; the histology of the tumor; and whether the tumor has a well-defined border (Rivera and Pelloski 2010; Rivera and Pelloski 2010). The grade of the tumor determines the degree of morbidity and mortality. Thus, tumor grading is important for diagnostics and predicting the prognosis of the disease course.

Table 1.2 The grades of astrocytic tumors based on WHO criteria.

Classification	WHO Grade	Tumor Type
Low-grade gliomas (LGG)	I	Pilocytic astrocytoma
LGG	II	Pleomorphic xanthoastrocytoma
OA	II/III	Oligoastrocytoma
AA	Grade III	Anaplastic astrocytoma
GBM	Grade IV	Glioblastoma multiforme

The grade translates into how rapidly the tumor grows and proliferates, which ultimately determines the standard treatment options to consider, and the aggressiveness to which the treatments should be administered (David N. Louis 2007). For example, Grade I tumors (Pilocytic astrocytomas) are routinely treated by surgical resection as they are characterized as having well-defined borders (Grzmil and Hemmings 2010; Grzmil and Hemmings 2010). Meanwhile, Grade II low-grade tumors often show diffuse infiltration into nearby tissues; Grade III anaplastic tumors tend to be more fatal with increased proliferation and anaplasia; and finally Grade IV tumors demonstrate vascular proliferation; necrosis and are often resistant to chemotherapy and radiation (Grzmil and Hemmings 2010; Grzmil and Hemmings 2010). This increase in malignancy from low to high as characterized by diffuse infiltration and loss of well-defined borders, presents a challenge for the complete surgical resection of higher graded tumors, which contributes to tumor recurrence and the demise of the patient (Thumma, Fairbanks et al. 2012).

ASTROCYTOMAS AND GBMS ARE GRADES II, III, IV OF THE DIFFUSELY INFILTRATING ASTROCYTOMAS

As a group the diffusely infiltrating astrocytomas, which includes grade II astrocytomas, the anaplastic astrocytomas (AA), and glioblastoma multiforme (GBM), are the most common primary brain tumors of the central nervous system (CNS). The incidence or number of new cases of gliomas represent 1.5-3% of all new cancer cases within the USA annually, which is approximately 15-18 cases per 100,000 of population (Stiles and Rowitch 2008; Riemenschneider and Reifenberger 2009). The majority of both new and existing cases of gliomas are predominantly anaplastic astrocytomas or glioblastoma multiforme (GBM) (Stiles and Rowitch 2008), with GBM accounting for 50%- 80% of all malignant astrocytomas alone (Ohka, Natsume et al. 2012).

The WHO grade II gliomas are the slow-growing neoplasms of the CNS that represent 35% of all astrocytic tumors. The low incidence rate of LGG is at approximately 1,800 new cases per year. The overall survival rate of LGG is approximately six to eight years from diagnosis to death (Rivera and Pelloski 2010), as these tumors are relatively amenable to surgery, radiation therapy and chemotherapy. The second main category of diffusely infiltrating astrocytomas is WHO Grade III astrocytoma. These are malignant neoplasms that often progress to malignant GBMs within approximately two years of diagnosis. If the AAs remain as diagnosed and do not progress to GBMs, the median overall survival from diagnosis to death is approximately five years (Rivera and Pelloski 2010). The third category of diffusely infiltrating astrocytomas is the glioblastoma multiforme or GBMs. The moniker “multiforme” refers to the high intratumoral and intertumoral heterogeneity observed among GBM tumors

(Krakstad and Chekenya 2010), a concept which will be elaborated upon in subsequent sections. The GBMs grade IV, are the most common, most malignant, most highly aggressive primary brain tumor in adults, and represent the most fatal of all brain tumors, accounting for approximately 4% of all cancer deaths within the USA annually (Molina, Hayashi et al. 2010; Thumma, Fairbanks et al. 2012). The average five-year survival rate for GBM patients is less than 3%, while the median survival rate from diagnosis to death is measured in months despite the most aggressive treatment (Lathia, Gallagher et al. 2010).

MAIN CHARACTERISTICS OF GBMS

There are several characteristics of GBMs that contribute to its poor prognosis, morbidity and mortality. These characteristics include (a) cell proliferation that is both fast and unregulated; (b) its widespread infiltration especially into nearby brain parenchyma thereby making total surgical resection impossible; (c) its resistance to chemotherapy and radiotherapy; (d) its ability to attract new blood vessels hence giving rise to robust angiogenesis; (e) its compromised blood-brain barrier leading to vascular edema or swelling; and finally (f) its intratumoral heterogeneity contributing to variations within the tumor mass (Inda, Bonavia et al. 2010).

TYPES OF GBM

GBMs can arise *de novo* (so-called primary GBMs) or from a low-grade glioma (LGG) (Wiencke, Zheng et al. 2007; Ruano, Mollejo et al. 2008; Brennan, Momota et al. 2009). Primary GBMs, prevalent in the elderly population, account for over 90% of all

the reported GBMs (Ohka, Natsume et al. 2012). In contrast, the secondary GBMs tend to occur in the younger patients (Rivera and Pelloski 2010).

A primary and a secondary GBM are histologically indistinguishable from each other, yet each tend to have distinctive genetic aberrations (Ohka, Natsume et al. 2012). However, some genetic events may help to differentiate these tumors (Brennan, Momota et al. 2009). For example, primary GBMs often have amplification or mutation of the *EGFR* gene; mutation in the *PTEN* gene; and loss of heterozygosity (LOH) on chromosome 10q (Kapoor, Christie et al. 2007; Theeler and Groves 2011). In contrast, secondary GBMs rarely show mutations or amplifications in the *EGFR* gene. Instead, secondary GBMs are often characterized by *p53* mutations, *PDGFR* gene overexpression, and retinoblastoma (*RB1*) gene abnormalities (Kapoor, Christie et al. 2007; Theeler and Groves 2011).

SUBTYPES OF GBMS

The primary and secondary GBMs can be further sub-divided into four subtypes based on their genomic and transcriptional profiles (Ozawa, Brennan et al. 2010). A recent study by the TCGA group has identified the four GBM subtypes as follows: Classical, Proneural, Mesenchymal, and Neural (Van Meir, Hadjipanayis et al. 2010; Lei, Sonabend et al. 2011; Lim, Llaguno et al. 2011; Vitucci, Hayes et al. 2011).

The classical subtype of GBM shows *EGFR* amplification and *EGFRvIII* mutations; it lacks *TP53* mutations and the *CDKN2A* locus is deleted.

The mesenchymal subtype of GBMs contains mutations in the *NF1*, *TP53* and *PTEN* genes, and presents with necrosis and microvascular proliferation. This suggests

that the mesenchymal subtype of GBM may be amenable to inhibitors of angiogenesis (Vitucci, Hayes et al. 2011).

The proneural subtype of GBM overexpresses PDGF ligand and its receptor PDGFRA, and carries mutations in *IDH1*, *TP53*, and *PIK3CA/PIK3R1*. This implies that patients diagnosed with this GBM-subtype may be more responsive to targeted therapies involving PDGFRA and PI3K inhibitors (Vitucci, Hayes et al. 2011). This subtype also presents with necrosis.

The neural subtype of GBMs expresses markers of neuronal origin. Some of these markers include *SLC125A*, *SYT1*, *GABRA1* and *NEFL* mRNAs (Ohka, Natsume et al. 2012). Altogether, the transcriptional subtypes contribute to the heterogeneity of the GBM tumors and reflect the signaling abnormalities present within these tumors. GBM subtypes respond differently to therapies (Lim et al, 2011). Hence, GBM subtyping becomes important in deciding which patients will benefit from additional molecularly targeted agents specific to the mutation identified (Vitucci et al, 2011).

GBM LOCATION WITHIN CNS

The anatomic location of the gliomas, especially in the case of diffusely infiltrating astrocytomas and GBMs, can influence treatment options and prognosis (Larjavaara, Mantyla et al. 2007). In a study of 267 gliomas, Larjavarra et al found that 40% of the gliomas are found in the frontal lobes, 29% in the temporal lobes; 14% in the parietal lobe and 3% in the occipital lobe (Larjavaara, Mantyla et al. 2007; Theeler and Groves 2011). Interestingly, 51% of the gliomas are found in the right hemisphere of the brain, in contrast to the left hemisphere where only 40% of gliomas are found. The

remaining gliomas are present either in the central areas of the brain or in the cerebellum (Larjavaara, Mantyla et al. 2007).

Therefore, GBMs, whether they are primary or secondary, whether they occur in the young or old, and despite their more frequent frontal lobe location in the brain, are difficult to treat and/or cure by the standard treatment options. The next section discusses the standard of care for GBM patients.

STANDARD TREATMENT OPTIONS FOR GBM PATIENTS

The current standard of care for GBM patients include surgical resection, concomitant radiation therapy followed by post-radiation administration of temozolomide (TMZ) (Goellner, Grimme et al. 2011).

Complete surgical resection of GBMs is virtually impossible. This is due in part to the invasive nature of the GBMs into surrounding parenchyma (Akhavan, Cloughesy et al. 2010). In addition, tumor recurrence is the most difficult aspect of glioma/GBM therapy (Madsen and Hirschberg 2010). Following the debulking surgery with concomitant radiation therapy or chemotherapy with TMZ, the average survival is still no more than 15 months. The mechanism of action for TMZ is the induction of apoptosis and cell death (Goellner, Grimme et al. 2011). Unfortunately, almost all GBM patients eventually relapse by developing TMZ-resistant tumor.

Over the past 30 years, numerous cutting-edge treatment options for advanced GBM patients emerged. Unfortunately, many of these options have not been as successful as originally conceived, so there is a pressing need to develop new therapeutic strategies to treat, cure, and/or extend the life span of this patient population.

Four approaches have been used to concentrate chemotherapies at the site of the tumor to treat, cure and/or extend the life of GBM patients and include:

1. Blood-brain-barrier disruption (BBBD) (Fortin, Desjardins et al. 2005).
2. Wafers at the GBM tumor site (Affronti, Heery et al. 2009).
3. Selective placement of catheters at the GBM tumor site (Kunwar, Chang et al. 2010).
4. Targeted molecular therapy (Sathornsumetee, Reardon et al. 2007; Mercer, Tyler et al. 2009).

Together, these four approaches comprise the bulk of the available auxiliary techniques used in GBM therapeutics. The potential drawbacks for each of these approaches will be discussed below.

The technique of BBBD was developed by Dr. Edward Neuwalt at the Oregon State University (OSU) in an attempt to resolve the problem of how to get antitumor drugs across the BBB in therapeutically relevant concentrations (Fortin, Desjardins et al. 2005). This technique was perfected in over 6000 procedures done on 400 patients, located at 6 different clinics, and utilized 3 unique protocols (Fortin, Desjardins et al. 2005). Mannitol is the most commonly used BBBD agent; an infusion that is usually delivered into either the internal carotid or vertebral artery, depending on the tumor's arterial supply, via percutaneous femoral artery catheterization. In the Phase I/II clinical trials, BBBD was found to be a suitable method to increase the local concentration dose of chemotherapeutic agents (Fortin, Desjardins et al. 2005). However, the review of the literature suggests that the BBBD technique is not a part of the current standard of care

for newly diagnosed or recurrent GBM patients, as it does not contribute to the overall survival of GBM patients.

The second conventional approach used to treat GBM is the implantation of biodegradable polymer wafers at the tumor site (Affronti, Heery et al. 2009). These wafers termed Gliadel® contain the chemotherapeutic drug, BCNU (1, 3-bis (2-chloroethyl)-1-nitrosurea), which was previously shown to be effective against glioma cell lines (Rainov and Heidecke 2011). This method also addresses the need of bypassing the BBB to get chemotherapeutics across. In one study of carmustine wafers, there was a small, however, not significant survival advantage in the treated group compared to the placebo control group (Affronti, Heery et al. 2009).

The direct delivery of chemotherapeutic into the CNS at the tumor site using implanted catheters (Kunwar, Chang et al. 2010), in principle, is similar to the BBBD technique and carmustine wafers and is based on a continuous pressure gradient of chemotherapy. A randomized Phase III clinical trial enrolling 296 patients evaluated the efficacy of the convection enhanced delivery (CED) technique as compared to the carmustine or Gliadel wafer, implanted at the tumor site, with both procedures occurring within 48 hours of surgery (Kunwar, Chang et al. 2010). In this study, the CED technique, while tolerated in GBM patients, unfortunately did not offer a survival advantage over the carmustine (Mueller, Polley et al. 2011).

The fourth approach used to treat GBM patients involves molecular targeted therapy and is not surgically invasive (Sathornsumetee, Reardon et al. 2007; Mercer, Tyler et al. 2009). These approaches may include any of the following:

1. Inhibition of growth factor ligands.
2. Inhibition of growth factor receptors.
3. Inhibition of intracellular effectors.

The typical example of growth factor ligand inhibitor is Bevacizumab/Avastin, a humanized neutralizing monoclonal antibody to VEGF. In fact, Bevacizumab remains the only FDA-approved molecularly targeted drug in GBM; yet its use has only improved progression-free survival without any improvement in overall survival (Patel, Vogelbaum et al. 2012).

In addition to the listed, relatively conventional approaches, some other miscellaneous approaches include the following:

1. Ligand-toxin conjugates.
2. Agents targeting invasion.
3. Deacetylase inhibitors.
4. Proteasome inhibitors.
5. Combination therapy.
6. Multimodal treatment (Sathornsumetee, Reardon et al. 2007; Mercer, Tyler et al. 2009).

Taken together, this is just a fraction of the ongoing clinical efforts to alleviate the morbidity and mortality associated with GBM patients. There is a hope that the repurposing of established, already tested drugs may represent an additional source of compounds available for testing as glioma therapies. Repurposing, sometimes called drug repositioning, is the assignment or application of a new association for known or existing

drugs (Harrison 2011; Swamidass 2011). In other words, it is a method of discovering new uses for the existing FDA-approved medicines that are clinically available. Drug repositioning can reduce the costs involved in research and development and marketing. Secondly, drug repositioning can accelerate the regulatory approval process (Harrison 2011; Swamidass 2011).

WHY GBMs ARE SO DIFFICULT TO TREAT

GBMs are notoriously resistant to chemotherapy and radiation therapy/treatment and complete surgical resection. This can be attributed to the intracranial environment, ability of brain tumors to widely diffuse into surrounding normal parenchyma as well as genetic heterogeneity between tumor subtypes and within the individual (Karkan, Pfeifer et al. 2008),(Molina, Hayashi et al. 2010).

The intratumoral heterogeneity of GBM could be registered both as visible differences in histological presentation of cells within the tumor mass and substantial differences in gene expression profiles as measured in samples taken at different locations (Inda, Bonavia et al. 2010; Lei, Sonabend et al. 2011). The heterogeneous population of a GBM mass often includes areas containing anaplastic astrocytomas (Grade III) or low-grade gliomas (Grade II) including oligodendrogliomas or gliomas with ependymal differentiation (Kyritsis, Bondy et al. 2010). This coupled with different proliferation and differentiation potential, different degree of vascularity and invasiveness suggests that some cells in the GBMs might be inherently resistant to radiation therapy and chemotherapy (Akhavan, Cloughesy et al. 2010).

The blood-brain barrier (BBB) is a seamless, continuous physical layer that separates the CNS from the blood circulation. It is composed of astrocyte foot processes, pericytes or smooth muscle cells, and brain capillary endothelial cells (BEC). These cellular elements are in turn covered by basal membrane and extracellular matrix and secured by tight junctions to seal the paracellular spaces (Rascher, Fischmann et al. 2002). The main function of the BBB is to maintain brain homeostasis by protecting the brain from the transient change in the composition of the blood especially after meals or exercise; and restricting the passage of exogenous and endogenous factors such as blood-borne pathogens into the brain (Rascher, Fischmann et al. 2002; Karkan, Pfeifer et al. 2008; Madsen and Hirschberg 2010). Additionally, the BBB also restricts the passage of compounds with high molecular weights (≥ 400 D), monoclonal antibodies and other agents (Madsen and Hirschberg 2010). Thus cancer cells that penetrate beyond the protective “walls” of the BBB are shielded from the cytotoxic effects of potential therapeutics.

Additionally, the tendency of GBMs to invade nearby brain areas (Molina, Hayashi et al. 2010) adds to the difficulty in treating these tumors. The presence of tumor infiltrating cells within the 2-3 cm of surgical margin is associated with a high rate of tumor reoccurrence (Madsen and Hirschberg 2010). This infiltrating edge may be driven by a small population of cancer stem cells (Yuan, Curtin et al. 2004; Zhang, Atkinson et al. 2010) that are capable of initiating secondary tumors when transplanted into another site (Lathia, Gallagher et al. 2010). These “core” stem cells are often called GBM stem cells.

NF1 AND GLIOMAS/GBMs

NF1 (Neurofibromatosis type 1) is an autosomal dominant disorder that affects about 1 in 3500 individuals worldwide (Hegedus, Banerjee et al. 2008). Children and adults with NF1 have an inherited predisposition to developing multiple tumors. These tumors can be benign or malignant, and can develop most commonly in both the CNS and peripheral nervous system (PNS). PNS tumors of NF1 patients are called neurofibromas and are composed of Schwann cells lacking the *NF1* gene and protein as well as *NF1*+/- fibroblasts, mast cells and vascular elements (Daginakatte and Gutmann 2007).

NF1 patients, especially children, often develop low-grade gliomas (LGGs) which account for 20% of all glial tumors diagnosed (McBride, Perez et al. 2010). These LGGs are classified as pilocytic astrocytomas (Grade I) and often occur in the hypothalamus and the optic pathway (Hegedus, Banerjee et al. 2008).

MOUSE MODELS USED IN GLIOMA STUDIES

To understand the biology and formation of gliomas *in vivo* and to develop effective therapeutics to treat GBM patients, there is a need to develop efficient model systems. There are several important features that are necessary in a GBM model to correctly reflect the human disease condition. Notably, in the GBM model tumors, the abnormal cell should be present along with necrotic areas within the tumor tissue. Additionally, both neo-angiogenesis and invasiveness should be present throughout the CNS (Inda, Bonavia et al. 2010). Tumors should recapitulate the molecular evolution of

brain tumors as they occur *in situ*, while accurately reflecting the genetic and cellular heterogeneity of tumors, and the tumor-stromal interactions (Huse and Holland 2009). The model also should retain important genetic alterations such as EGFR overexpression or amplification, possess a short tumor latency and high penetrance, be simple to generate and easy to use, and finally it should have a built-in mechanism that helps to directly quantify therapeutic effects, such as a bioluminescent reporter (Huse and Holland 2009; Yi, Hua et al. 2011). Genetically engineered mouse models (GEMMs) are preferable as *in vivo* systems over cell culture (Huse and Holland 2009).

For example, one of the GEMM mouse models for GBM is the *Nf1; p53cis* (NPcis) mutant mouse model in the background of the C57BL/6J strain developed by Reilly et al (Reilly, Tuskan et al. 2004). In this model, *Nf1* and *Trp53* are mutated on the same chromosome (chr) 11 of the mouse and are tightly linked (Reilly, Tuskan et al. 2004). These NPcis mice develop low grade tumors which progress through a range of histological grades, attributed to the loss of heterozygosity of the remaining wild-type *Nf1* and *p53* loci. Furthermore, this NPcis mouse model has the features necessary to understand the biology of GBMs.

The NPcis model performance is depicted in Figure 1.1 which shows that tumor cell lines derived from the NPcis mice are tumorigenic when implanted subcutaneously in immunocompromised mice. In Figure 1.1, one can see that four different grade III NPcis astrocytoma cell lines (1395, K1492, K5001, and KR158, as represented by the red graph) grow at a significantly faster rate as compared to three different grade II cell lines (1410, K1861, and K4622, as represented by the blue graph) (Gursel, Connell-Albert et

al. 2011). The result shows a correlation between grade and tumor mass as measured *in vivo*. For instance, the grade III NPcis astrocytoma cell lines generated tumors with greater masses overall as compared to grade II NPcis astrocytoma cell lines which had tumors of lesser mass (Figure 1.1). Hence, the NPcis mouse model and the astrocytoma cell lines derived from this mode are suitable for studying the biology of gliomas and GBMs.

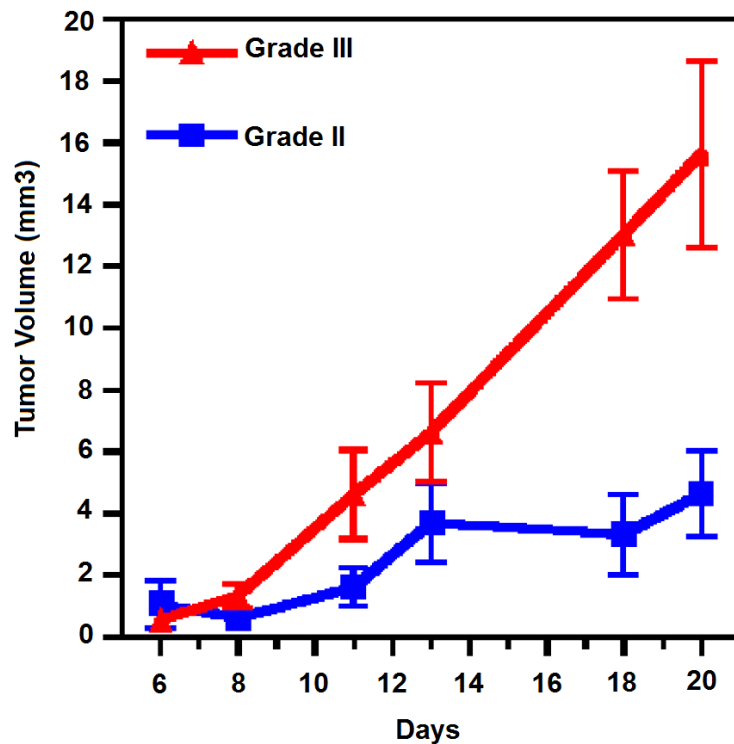


Figure 1.1: Tumor cell lines isolated from NPcis mouse models form tumors subcutaneously and maintain the growth characteristics of respective tumor grade.

Although the GEMM models like NPcis are more expensive to produce and use compared to other mouse models, they more closely mimic the natural tumor

environment (Huse and Holland 2009). This can increase the efficacy of the pre-clinical and clinical trials and lower the tremendous cost involved in bringing a product to market, all in an effort to alleviate the morbidity and mortality associated with astrocytomas and GBMs.

GENETIC MUTATIONS IN PRIMARY AND SECONDARY GBMS

Different genetic alterations are known to be involved in primary and secondary GBMs. The most frequent and the first genetic mutation identified in primary *de novo* GBMs is epidermal growth factor receptor (*EGFR*) gene amplification and *EGFR* activating mutations (Ang, Guiot et al. 2010). Secondary GBMs, on the other hand, harbor inactivating mutations in the tumor suppressor gene p53 (*TP53*) (Wiencke, Zheng et al. 2007). Among other tumor suppressor genes inactivated are *p16*, *RB* and *PTEN*. Apart from the mutations in tumor suppressors, secondary GBMs may also be triggered by the activation of oncogenes such as *MDM2*, *CDK4* and *CDK6* (Maher, Brennan et al. 2006; Wei, Clarke et al. 2006; Rivera and Pelloski 2010).

EPIDERMAL GROWTH FACTOR RECEPTOR (EGFR)

Genomic deletions of parts of the *EGFR* gene, its activation or its chromosomal amplification are known to contribute to primary GBM morbidity and mortality. The activating mutations of the *EGFR* gene are present in more than 45-60% of GBMs (Akhavan, Cloughesy et al. 2010). The *EGFR Δ III* mutant results from a 267-base pair in-frame deletion of exons 2-7. The deleted region corresponds to the extracellular domain of EGFR and results in its constitutive activation. This, in turn, leads to activation of

ERK and PI3K/Akt/mTOR signaling pathways. In addition, the amplification of *EGFR* gene is found in more than 45% of GBMs (Inda, Bonavia et al. 2010; Ozawa, Brennan et al. 2010).

PLATELET DERIVED GROWTH FACTOR RECEPTOR- α (PDGFRA)

Another gene altered in GBM is the *PDGFRA* gene. The mutation of PDGFRA involves an in-frame deletion of 243 base pairs in exons 8 and 9 that correspond to the extracellular portion of the PDGFRA domain (Ozawa, Brennan et al. 2010). As a result the mutant PDGFRA protein (PDGFRA delta8, 9) is constitutively auto-phosphorylated on tyrosine residues resulting in down-stream activation of MAPK and PI3K signaling pathways (Ozawa, Brennan et al. 2010).

Therefore, the activating mutations on the *EGFR* and *PDGFRA* genes result in ligand independent constitutive activation of receptor tyrosine kinases (RTKs) that activates down-stream signaling pathways of Ras/Raf/MAPK, ERK and PI3K pathways in GBMS, which makes these pathways suitable for study. However, apart from the above mentioned signaling pathways activated in primary GBMs, Sonic Hedgehog (SHH), and the Notch pathway are also reported to be involved in GBM pathology (Ohka, Natsume et al. 2012).

THE PI3K/AKT/mTOR PATHWAY

RTKs belong to the family of cell surface receptors which are involved in important functions such as cell-cycle control, cell migration, cell metabolism and survival and cell proliferation (Lemmon, 2010). RTKs are activated when a growth factor

ligand binds to its cognate receptor. Activated RTKs then undergo receptor dimerization, followed by cross auto-phosphorylation of the tyrosine residues on the receptor, which then activates intracellular signaling proteins such as the enzyme PI3K. When PI3K is activated, it catalyzes the phosphorylation of PI (4) P and PI (4, 5) P₂ at the D3 position on PI3K to generate PIP₂ and PIP₃ respectively. PIP₃ then binds to the pleckstrin homology domains of PDK1 and Akt. This interaction causes both proteins to translocate to the cell surface membrane. PIP₃-bound Akt is phosphorylated by PDK1 at threonine T308. To achieve full kinase activity, Akt needs to be phosphorylated at a second key residue, serine S473. This modification is performed by members of the PI3K-related kinase family mTORC2 or DNA-PK, depending on the stimulus and the context (Fayard, Xue et al. 2010).

The activation of Akt is implicated in many cellular processes such as apoptosis, cell cycle progression, transcription and translation (Choe, Horvath et al. 2003; Garrett, Chakrabarty et al. 2011). It is clear that the PI3K/Akt/mTOR pathway integrates a variety of cell survival signals. PI3K/Akt/mTOR pathway alterations are found in various human tumors. The activation of Akt at S473 is commonly detected in gliomas; this phosphorylation event is associated with poor prognosis in cancers such as skin, pancreas, liver, prostate, and breast and brain cancer (Kreisberg, Malik et al. 2004). Additionally, PI3K/Akt/mTOR signalling plays an important role in the development of platinum (cisplatin or carboplatin) and paclitaxel resistance (Priulla, Calastretti et al., 2007; Zhang, Zhang et al., 2009).

THE PI3K/AKT/mTOR PATHWAY TARGETS IN ASTROCYTOMAS AND GBM BIOLOGY

This normal serine/threonine kinase Akt/protein B pathway is important in regulating numerous processes including cell growth, proliferation, survival, migration, invasion, and angiogenesis (Gallia, 2009; Hui, 2008). There are several points at which a hyperactivation of PI3K signaling pathway is reported to occur. One common mechanism is the deregulation of RTK signaling. In normal cells, the activity of RTKs is tightly regulated. Deregulation through mutations or structural alterations results in RTKs functioning as oncogenes (Gschwind, Fischer et al. 2004). Examples of deregulated RTKs which have been causally linked in the development and progression of many types of cancers include proteins encoded by genes *EGFR*, *c-Met*, *VEGFR*, and *PDGFR* (Lemmon, 2010). As such, RTKs and their growth factor ligands have fostered the rapid development of a new class of inhibitors targeting RTK activation and activity.

Another possible mechanism is loss of the tumor-suppressor PTEN, found in approximately 50% of GBMs. The *PTEN* gene encodes a cytoplasmic enzyme which is capable of dual protein and lipid phosphatase activity that negatively regulates the PI3K pathway (Akhavan, Cloughesy et al. 2010). Therefore, when the *PTEN* gene is mutated, epigenetically inactivated or deleted (Abounader, 2009), this regulator cannot function to deactivate the PI3K signaling pathway, resulting in constitutive signaling. Importantly, PTEN is the sole central negative regulator of PI3K signaling as no other protein is capable of compensating for a loss in its function.

The genetic inactivation of *NF1*, resulting in loss of the NF1 protein product neurofibromin, also contributes to gliomagenesis. In particular, heterozygous mutations in *NF1* were observed in glioblastomas (Parsons, Jones et al. 2008). Additionally, *NF1* may be inactivated via excessive proteasomal degradation that is triggered by the hyperactivation of protein kinase C (PKC) (McGillicuddy, Fromm et al. 2009). However, complete genetic loss of *NF1*, which only occurs when p53 is also inactivated, mediates sensitivity of glioma cells to mTOR inhibitors (McGillicuddy, Fromm et al. 2009).

Therefore, targeted therapies against known signaling aberrations may be one of several promising approaches in glioma therapy. Overall the goal of a molecularly targeted anti-glioma approach should be to interrupt the aberrant signal transduction either by 1) specifically preventing the EGFR ligand and receptor interaction, 2) preventing the activation of the secondary effector molecule PI3K, or 3) preventing further downstream activation of effector molecules such as recruitment of Akt or mTOR.

Here we test three inhibitors of Akt/mTOR pathway, PI-103, tricirbine and rapamycin, as these molecules have a potential as candidates for glioma therapy. Typically, a candidate molecule is evaluated on the basis of the following criteria: 1) if the drug-like compound has acceptable toxicity properties (LoRusso, Anderson et al. 2010) and 2) if the drug-like compound has acceptable ADME (Absorption, Distribution, Metabolism and Excretion) properties. When combined, these criteria make the molecule a good candidate for Phase I clinical trial (Lipinski 2000).

CHAPTER 2: PI-103, TRICIRBINE AND RAPAMYCIN AS POTENTIAL GLIOMA THERAPEUTICS

PI-103 is a novel, lipid kinase inhibitor that belongs to the pyridofuro-pyrimidine class of molecules (Lopez-Fauqued, Gil et al. 2010). As a PI3K-alpha-isoform specific, dual PI3K/mTOR inhibitor, PI-103 arrests cells in the G1 phase of the cell cycle (Park, Chapuis et al. 2008; Prevo, Deutsch et al. 2008). In gliomas, PI-103 works as a cytostatic by blocking PIP3 production in a dose-dependent manner, as well as blocking the activity of phosphorylation. However, PK (pharmacokinetic) studies revealed that PI-103 is rapidly cleared from the plasma, suggesting poor ADME properties, as well as being metabolized to glucuronide (Zou, Zhang et al. 2009; Prevo, Deutsch et al. 2008). Despite this shortcoming, PI-103 remains an interesting target, particularly in view of the fact that it has been shown that concurrent treatment with PI-103 and DNA-damaging drugs, such as doxorubicin, increases apoptosis and reduces colony formation via the inhibition of PI3K and DNA-PK via the inhibition of DNA-PK-mediated DNA repair (Westhoff, Kandenwein et al. 2009).

PI-103 is a chemically stable compound, readily absorbed from the digestive tract and distributed into the appropriate bodily compartments (Koehn and Carter 2005; Chaplan, Eckert et al. 2010). It has a favorable molecular weight of 348.35 which is within the acceptable limits of BBB permeability (Madsen and Hirschberg 2010), suitable hydrogen bond donor/acceptor number (Lipinski, Lombardo et al. 2001; Veber, Johnson

et al. 2002), low number of rotatable bonds, and reduced polar surface area (See Table 2.1 for a summary). Additional *in vivo* tests are needed to determine if PI-103 is easily metabolized, and whether it has an acceptable toxicity and safety profile. In fact, recent studies indicate that, in combination with other chemotherapeutic compounds, PI-03 may be a potent and less toxic therapy in the treatment of other cancers such as acute myeloid leukemia (AML) (Ding, Gu et al. 2013).

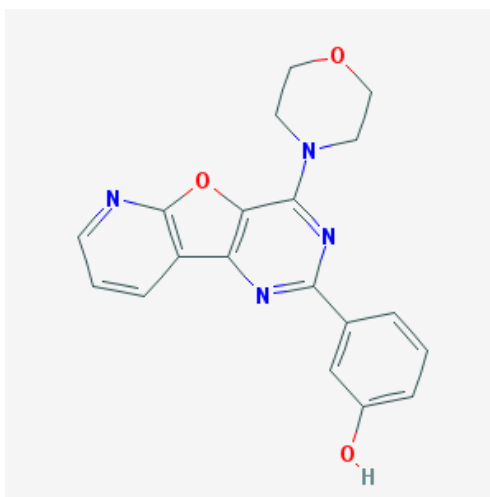


Figure 2.1: The chemical structure of PI-103 with Molecular Formula: C₁₉H₁₆N₄O₃.
(Source of the figure: //PubChem.nlm.nih.gov).

Tricirbine (TCN) is an unusual tricyclic purine analogue that inhibits DNA and protein synthesis. Tricirbine phosphate (TCN-P) is the water soluble phosphate ester of Tricirbine, which is enzymatically dephosphorylated by cellular ecto-5' nucleosidase (Schilcher, Haas et al. 1986). This dephosphorylation event allows Tricirbine to enter into cells, where it is then re-phosphorylated by adenosine kinase. The intracellular form of

the compound is thought to be responsible for the cytotoxic effects exerted by the analogue Tricirbine in transformed cells (Hoffman, Holmes et al. 1996) accumulating in red-blood cells, the pancreas and the liver, which suggest poor elimination (Schilcher, Haas et al. 1986). In human clinical trials, Tricirbine was shown to inhibit DNA and protein synthesis and is cytotoxic to transformed cells in the S-phase of the cell cycle. Tricirbine also prevents amino acids from binding to tRNAs.

Similar to PI-103, Tricirbine also is a chemically stable compound with MW of 320.3 Dalton. It has four donor H-bonds, five acceptor H-bonds, two rotatable bonds and a topological surface area of 142 Å², (<http://PubChem.ncbi.nlm.nih.gov>; Tricirbine), which is slightly more than the recommended polar surface area. This suggests that Tricirbine may be orally available.

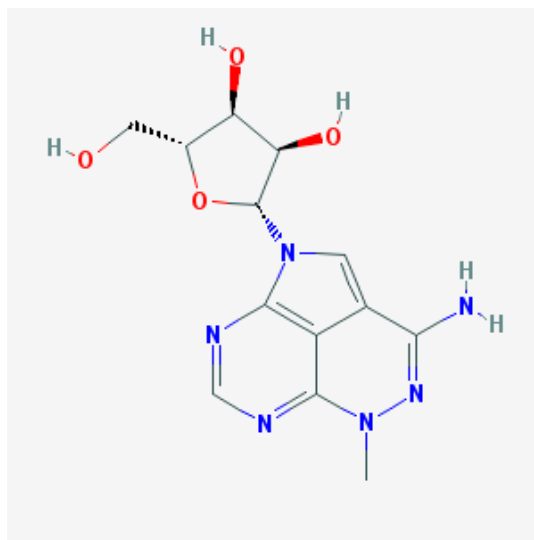


Figure 2.2: This figure shows the chemical structure of Tricirbine with Molecular Formula: C₁₃H₁₆N₆O₄. (Source of the figure: <http://PubChem.ncbi.nlm.nih.gov>).

The therapeutic applicability of Tricirbine is limited due to its toxicity. The *in vivo* Phase I/II human clinical trials showed that Tricirbine leads to the development of hypertriglyceridemia and/or glucose intolerance in a substantial number of patients (Schilcher, Haas et al. 1986). The mechanism of this side effect is unknown, but may possibly be related to the suppression of the production of insulin (Hoffman, Holmes et al. 1996). Apart from these side effects, Tricirbine and its partially metabolized form, TCN-P (phosphate) accumulation was found in the liver and pancreas of patients even 6-12 weeks after the last dosing, while no drug was present in urine samples (Schilcher, Haas et al. 1986). Although Tricirbine has shown some anti-neoplastic potency, the exact mechanism by which this occurs has not been elucidated (Gloesenkamp, Nitzsche et al. 2012).

Rapamycin, also known as Sirolimus, is a macrolide antibiotic that blocks mTOR kinase activity (Puli, Jain et al. 2010). mTOR is a subcomponent of both mTORC1 and mTORC2; mTOR binds to Raptor to form mTORC1, and to Rictor to form mTORC2. The Raptor complex is important for mTOR dependent cell growth. Rapamycin forms a complex with FK506-binding protein FKBP-12, thereby leading to cell cycle arrest at G1 phase. Rapamycin also inhibits the downstream effector molecules of mTOR, p-p70S6K and 4EBP1 (Paternot, Roger et al. 2009). It leads to the activation of Akt and eIF4E survival pathways, which decreases the effectiveness of Rapamycin monotherapy in cancers (Cloughesy, Yoshimoto, et al. 2008). This negative feedback loop may contribute to the cytostatic versus cytotoxic effects exerted by Rapamycin.

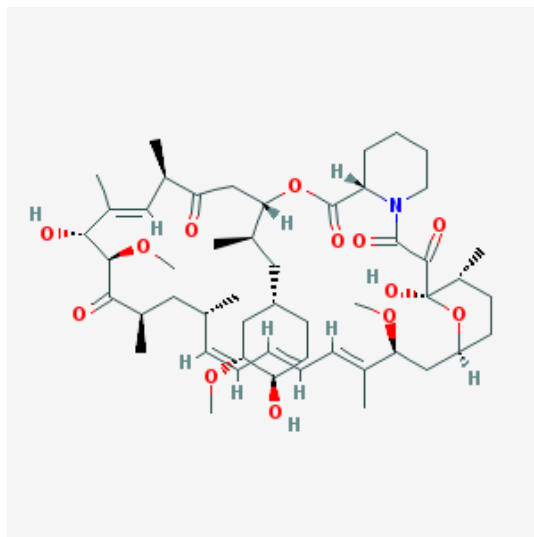


Figure 2.3: This figure shows the chemical structure of Rapamycin with Molecular Formula: $C_{51}H_{79}NO_{13}$. (Source of the figure: <http://PubChem.nlm.nih.gov>).

Rapamycin has a MW of 914.17, which suggests that it may not readily cross the BBB (<http://PubChem.ncbi.nlm.nih.gov>; Rapamycin). It has 13 acceptor H-bonds and a topological polar surface area of $195A^0$ (<http://PubChem.ncbi.nlm.nih.gov>; Rapamycin). These chemical features of Rapamycin suggest relatively poor oral bioavailability *in vivo* (Veber, Johnson et al. 2002). However, Rapamycin has acceptable ADME (Absorption, Distribution, Metabolism, and Excretion) properties, and is currently being administered orally in other disease conditions such as breast cancer (LoRusso 2013). Rapamycin (Sirolimus) is rapidly absorbed and peak concentration obtained within 1 hour after the administration of a single dose in healthy subjects with systemic bioavailability of approximately 14%. The mean distribution of Rapamycin is approximately 7.2 L/kg,

while its elimination occurs within 57-63 hours, predominantly through the feces (91%) and, to a lesser degree, through the urine (2.2%) (<http://Pubchem.ncbi.nlm.nih.gov>).

Table 2.1: Selected Chemical and Physical Properties of PI-103, Tricirbine and Rapamycin that contribute to characteristics of good drug candidates.

Name/ ID of Compound	Molecular Weight	Hydrogen bond donor	Hydrogen bond acceptor	Rotatable bond count	Topological surface area	Predicted oral availability
PI-103/CID 9884685	348 g/mol	1	3	2	84.5 Å ⁰	Yes
TCN/CID 65399	320 g/mol	4	5	2	142 Å ⁰	Yes
Rapamycin/ CID 5284616	914 g/mol	3	13	6	195 Å ⁰	No

Data compiled from PubChem (<http://pubchem.ncbi.nlm.nih.gov>; <http://www.chemspider.com>).

IN VITRO AND IN VIVO EVALUATIONS OF PI-103, TRICIRBINE AND RAPAMYCIN AS POTENTIAL THERAPEUTICS

All three compounds, PI-103, Tricirbine and Rapamycin, were previously evaluated for their cytotoxicity in non-glioma cell lines and some in non-glioma patient populations.

To evaluate the effects of PI-103 on the constitutively active PI3K/Akt/mTOR signaling pathway, bone marrow cells obtained from chemotherapy-naïve AML patients were treated with PI-103 *in vitro* (Park, Chapuis et al. 2008). In these assays, PI-103 inhibited the proliferation of the AML cell lines; its cytostatic effects were exhibited at 1 µM concentration. Importantly, PI-103 caused a dose-dependent decrease in the

phosphorylation status of Akt, the downstream effector of PI3K, and p-p70S6k, the downstream effector of mTOR. These decreases were seen regardless of the PI3K-positive or PI3K-negative status of tested AML cells.

Another example of a tumor with constitutively activated PI3K/Akt/mTOR pathway is non-small cell lung carcinoma (NSCLC) (Zou, Zhang et al. 2009). PI-103 treated lung cancer cell lines showed inhibition of Akt phosphorylation, and p-p70S6K phosphorylation was also blocked, but the inhibitor PI-103 had little effect on the phosphorylation of ERK, suggesting that PI-103 specifically targets PI3K-alpha and mTOR (Zou, Zhang et al. 2009).

Therapeutic effects of tricirbine were studied in Phase I human clinical trial in a cohort of 24 patients with advanced solid tumors. The patients received 48 mg/m²/week over the course of a 42-day cycle. Unfortunately, many patients experienced adverse effects, which included acute liver toxicity and possibly pancreatic islet damage (Schilcher, Haas et al. 1986). In a Phase I/II clinical trial in patients with metastatic breast cancer, the patients received up to a maximum dose of 40 mg/m² of tricirbine with dose-limiting toxicities (DLT) reported, but no clinical effect at all doses tested (Hoffman, Holmes et al. 1996). None of the listed studies included glioma patients. The testing of the effects of tricirbine in mouse glioma models may provide evidence for Phase I trials in glioma patients.

Rapamycin is an FDA approved drug used to treat many conditions, the two most important indications being immunosuppression in patients to prevent allograft rejection of transplants, and the treatment of kidney cancer (Cloughesy, Yoshimoto et al. 2008).

Rapamycin was previously tested in many *in vitro*, *in vivo*, and human clinical phase I-II trials that have been conducted with the aim of modulating the PI3K/Akt/mTOR pathway. *In vitro* studies demonstrated the anti-proliferative effects of Rapamycin on tumor cells, and these earlier studies provided the impetus for further pre-clinical and clinical studies to determine the effect of Rapamycin in patients with a loss or inactivation of *PTEN*, termed *PTEN*-negative or deficient tumors (Cloughesy, Yoshimoto et al. 2008). However, despite the initial favorable response observed in these *in vitro* and *in vivo* pre-clinical trials, the results from actual clinical trials have not been as encouraging (Paternot and Roger 2009).

In one example of a clinical trial with mixed results, patients with various *PTEN*-negative tumors were given Rapamycin at oral daily doses of 2, 5, or 10 mg for one week prior to resection surgery (Cloughesy, Yoshimoto et al. 2008). Post-surgery, the patients resumed the daily dose of Rapamycin until disease progression or death. To determine if the rapamycin had an effect on mTOR inhibition of cell proliferation in the tumor tissue, the study authors measured the phosphorylation status of S6 ribosomal protein, by immunohistochemistry (IHC). The S6 ribosomal protein is a substrate of S6 kinase, which is a direct effector downstream of mTOR (Cloughesy, Yoshimoto et al. 2008). The results among the patients in the clinical trials varied in that some patients with sufficient drug concentration in the tumor tissue were unresponsive to rapamycin therapy or had a very mild reduction in tumor pS6 phosphorylation. This suggests that some patients were resistant to mTOR inhibition with rapamycin therapy even though the volume and concentrations present in the tumor mass was sufficient to cause pS6 inhibition

(Cloughesy, Yoshimoto et al. 2008). The failure of rapamycin to inhibit mTOR in these PTEN-negative rapamycin resistant patients was not cell-type specific (Cloughesy, Yoshimoto et al. 2008). This lack of clinical effectiveness is one of the reasons for the ongoing research into the use of rapamycin in combination therapy with other treatment modalities.

We hypothesized that PI-103, Tricirbine and Rapamycin may inhibit cell viability as a measure of cytotoxicity, in mouse and human glioma cell lines by inhibition of the phosphorylation of Akt substrates or effectors in the PI3K/Akt/mTOR pathway. The results generated from these *in vitro* drug-inhibition studies may prove useful in combination therapies in pre-clinical *in vitro* and *in vivo* studies and in laying the foundation for future, combination clinical trials for GBM.

2.2 MATERIALS AND METHODS

CULTURING OF WILD TYPE PRIMARY MURINE ASTROCYTES

Newborn pups at 24 hours old or less were euthanized on ice; the tails and spleens were saved for genotyping. The brains were removed and placed in sterile, enriched DMEM medium containing 20% FBS (v:v) and 1% Penicillin-Streptomycin (Pen/Strep) (CellGro/Mediatech, Manassas, VA) antibiotics. The meninges were removed from the brains, and the midbrain and neo-cortices minced in enriched medium. The dissociated brain tissues were re-suspended by repeated pipetting in 10-ml of enriched DMEM, spun for 5 minutes at 13,000 RPM and the pellets were resuspended in 1-ml enriched DMEM environment. One million cells were plated per 10-cm dish in 10-ml of enriched DMEM

and incubated at 37°C /5% CO₂ for 10 days. The enriched medium was replaced with complete DMEM media containing 10% FBS (v:v) and 1% Pen/Strep antibiotics.

To confirm homogeneity of the population of primary astrocytes, immunocytochemistry (ICC) was performed with the astrocytic marker glial acidic fibrillary protein (GFAP) (Dako, Carpinteria, CA), and the neural/glial progenitor marker nestin (Millipore, Temecula, CA). The presence of GFAP staining and negligible nestin staining suggests the presence of a nearly homogenous population of primary astrocytes.

SUBCUTANEOUS GROWTH OF TUMOR LINES

One million astrocytoma cells were injected subcutaneously into athymic mice in quadruplicate. Tumor length and width were measured by caliper every week for four weeks starting when tumors were clearly palpable to examine long-term growth; or tumor length, width, and height were measured every other day for 20 days from the day of injection to examine short-term growth. Tumor volumes were approximated with the equation $\text{Volume} = (\text{LXWXW})/2$ or $\text{Volume} = (\text{LXWXH})/2$ (depending on whether measurements were taken in 2 or 3 dimensions) and plotted using GraphPad Prism v4. Statistical analysis was performed in GraphPad Prism using a paired t-test.

ALAMAR BLUE METABOLIC ASSAYS AND IC₅₀ AND GI₅₀ CALCULATIONS

The Alamar blue assay is one of several cytotoxicity assays, such as the MTT and XTT assays, that are readily available and commonly used to test the cytotoxicity of drugs on various cell types, for further *in vitro* studies or to determine the appropriate starting doses for further *in vivo* studies (Zhang, Mu et al. 2007). It is advantageous to the

widely known MTT and XTT assays because it employs a stable, non-toxic, water-soluble dye that enables continuous monitoring of cell cultures over a period of time (Al-Nasiry, Geusens et al. 2007). The Alamar blue assay relies on a redox indicator that changes color in the presence of reduction by living, metabolically active cells, an event mediated by mitochondrial enzymes (Hamid, Rotshteyn et al. 2004). The oxidized form of Alamar blue enters the cytosol of the cells and is converted to the reduced form when it accepts electrons from the NADPH, FADH, FMNH, NADH, or cytochromes. Following the re-dox reaction, there is a shift in the color of the culture medium from blue to pink, measurable on a colorimetric or fluorescent plate reader (Al-Nasiry, Geusens et al. 2007).

In our studies, the Alamar blue cell viability cytotoxicity assay was utilized in a 96-well format, using Z'-factor assessment of assay quality. The Z' factor is a measure of the reliability, reproducibility, suitability, and quality of the assays used for high-throughput-screening (HTS) assays. A HTS assay that has a calculated Z' factor above 0.5 suggests that the assay has been sufficiently optimized and is reproducible (Hamid, Rotshteyn et al. 2004; Hawes and Reilly 2010). The Z' factor for all experimental conditions were calculated and assays with Z' values < 0.5 indicated poor performance of the 96 well plate assay, and these data were discarded (Zhang, Chung et al. 1999).

Furthermore, the four parameters needed to calculate the Z' factor included the mean (μ), and the standard deviation (σ) of both the positive (p) and negative (n) controls. As described in Gursel et al, the Z factor is calculated as $Z' = 1 - \frac{(3 * \sigma_{GM3}) + (3 * \sigma_{GM0})}{(\mu_{GM3} - \mu_{GM0})}$ where σ_{GM3} is the standard deviation of the Alamar blue

measurements for the positive controls on day 3, σ_{GM0} is the standard deviation of the Alamar blue measurements for the positive controls on day 0, μ_{GM3} is the average of the Alamar blue measurements for the positive controls on day 3, and μ_{GM0} is the average of the Alamar blue measurements for the positive controls on day 0 (Gursel, Connell-Albert et al. 2011).

For the assay, the human astrocytoma cell lines SF295 and U87MG and the mouse astrocytoma cell lines K1861-10, KR158, and K130G#3, were plated at a density of 2500 cells/100 μ l DMEM complete medium in a 96-well flat bottom plate. For controls, mouse primary astrocytes were plated at 5000-cells/100 μ l in DMEM complete medium. The plates were incubated at 37° C/5% CO₂ overnight. The next day, select inhibitors at 7 different concentrations were added to cells in triplicate wells. Positive control wells contained media and cells, while negative controls contained only media. Alamar Blue (ABD Serotec, Raleigh, NC) was used according to the manufacturer's protocol. For the Day Zero control readings, 50 μ l of 30% Alamar blue was added to each of the quadruplicate wells containing cells for a final concentration of 10% Alamar blue, incubated for 4 hours and the plate read at 540 nm absorption/630 nm emissions filters, using a Novostar plate reader (Novostar, BMG Lab Technologies, Germany). The plates were further incubated for 72 hours (Day 3) and Alamar blue added and plates read as above. IC₅₀ and GI₅₀ values were calculated using Graph Pad Prism v4 and Microsoft Excel. The GI₅₀ is the concentration of compound required to inhibit growth by 50% (Staunton, Slonim et al. 2001); whereas the IC₅₀ is defined as the concentration of compound required to produce 50% inhibition relative to the control (Riddick, Song et al.

2011). In other words, the GI_{50} is relative to the maximum growth of the cell while the IC_{50} is relative to the maximum activity observed by the drug. Both GI_{50} and IC_{50} concentrations were calculated for each compound studied. All GI_{50} values less than the GI_{50} value of the control cells, were treated as sensitive relative to the controls. Similarly, all GI_{50} values more than the GI_{50} value of the cells, were treated as less sensitive or resistant, relative to the controls.

As described in Gursel et al, to calculate the IC_{50} values, Alamar blue measurements from day 3 were normalized to the average of the positive control wells on day 3. A minimum of 8 independent experiments with triplicate readings were averaged and the IC_{50} was calculated by fitting to the data to the log(inhibitor) vs response-variable slope equation $Y = \text{Bottom} + (\text{Top} - \text{Bottom}) / (1 + 10^{(\text{LogIC}_{50} - X) * \text{HillSlope}})$ in GraphPad Prism v4. GI_{50} values were calculated as $GI_{50} = 10^{(\text{LogIC}_{50} - ((\text{Log}((\text{Top} - \text{Bottom}) / (50 - \text{Bottom})) - 1)) / \text{HillSlope})}$. The fitted value of the Top variable was taken as the maximum % inhibition (Gursel, Connell-Albert et al. 2011).

IN VITRO DRUG INHIBITION STUDIES

Mouse astrocytoma grade III KR 158 cell lines were plated in 6-well plates at 250,000 cells/2 ml DMEM complete medium incubated at 37°C. After 24 hours, the cells were rinsed in 2 ml serum free medium (SFM) (DMEM with 5% Pen-Strep without FBS) and incubated in 2 ml SFM for an additional 24 hours. The cells were treated with varying concentrations of the serially diluted select inhibitors for 1 hour in SFM then stimulated with 10% FBS for 5, 15 or 30 minutes, before collecting protein lysates (See Table 2.2).

Table 2.2: The experimental conditions for drug inhibition studies used in the mouse cell lines.

Well Number	Inhibitor	Inhibitor Time	Condition	Serum Time	Miscellaneous
1	No Drug	NA	No Serum	NA	Control(SFM)
2	No Drug	NA	10% Serum	30 mins	Control
3	1 nM Drug	60 mins	10% Serum	30 mins	Treated
4	10 nM Drug	60 mins	10% Serum	30 mins	Treated
5	100 nM Drug	60 mins	10% Serum	30 mins	Treated
6	1 μ M Drug	60 mins	10% Serum	30 mins	Treated
7	10 μ M Drug	60 mins	10% Serum	30 mins	Treated
8	100 μ M Drug	60 mins	10% Serum	30 mins	Treated
9	1 μ M Drug	60 mins	No Serum	NA	Control(SFM)

PROTEIN EXTRACTION-SDS PAGE-WESTERN BLOT ANALYSIS

Adherent treated and control cells in dishes were rinsed in ice-cold PBS before lysing in 30 μ l – 50 μ l cell lysis buffer (50 mM HEPES, 150 mM NaCl, 25 mM EDTA, 1 mM EGTA, 10% Glycerol, 1% Triton X-100, pH 7.5) supplemented with Leupeptin (5 ug/ml) PMSF (1 mM), Sodium orthovanadate (1 mM), and Aprotinin (10 ug/mL), phosphatase inhibitor cocktail 1 (10 μ l/mL) (Sigma, Cat#P2850) and cocktail inhibitor 2 (10 μ l/mL) (Sigma, Cat#P5726). The cells were scraped and the lysates incubated on ice for 30 minutes. The cell lysates were centrifuged at 120,000 X g for 15 minutes at 4 °C. After centrifugation, the supernatants were removed and stored at -80 °C.

SDS-PAGE AND DETERMINATION OF PROTEIN CONCENTRATION

Two microliters of protein cell lysates were aliquoted in duplicate in a 96-well U-Bottom plate (BD Falcon, Cat# 353911). Two microliters of bovine serum albumin (BSA) (NEB, Ipswich, MA) were added to final concentrations of 5 mg/mL; 2.5 mg/mL; 1.875 mg/mL; 1.25 mg/mL; 0.9375 mg/mL; 0.625 mg/mL; 0.3125 mg/mL; and 0.15625 mg/mL, in duplicate, in a separate row to generate the standard curve. Two hundred microliters of Quick-Start Dye Reagent (BioRad Labs, Hercules, CA) was added to all samples and the plate incubated for 15 minutes at room temperature. The plate was read on a Novostar Plate Reader (BMG LabTech Inc, Cary, NC) at 590 nM. Raw values were used to calculate the standard curve and to determine microgram amounts of protein lysates for equal loading.

Protein lysates of equal concentrations (10ug-50 ug) were boiled at 100 °C in 5X protein sample loading buffer, incubated on ice for 5 minutes and loaded onto a 4-12% SDS PAGE buffer with 1X Tris running buffer. Resolved proteins on the gel were transferred to PVDF membranes at 110 V for 75 minutes at room temperature (RT). After transferring, the membranes were blocked in 5% BSA in 1X TBS-Tween (0.1% Tween-20) (Fisher Scientific, Pittsburg, PA) for 1 hour at room temperature. The blots were analyzed utilizing the appropriate antibody diluted in 5% BSA at 1:1000 and incubated at 4 °C overnight with rocking. Membranes were washed 3 times, 5 minutes each in 1X TBST (0.1% Tween). Membranes were incubated for 1 hour at room temperature with rocking, in the appropriate secondary antibody at 1:1000 dilution in 2.5% non-fat dried milk/TBST (Tween 0.1%), followed by 3 times 5 minute washes with 1X TBST. The

secondary antibodies included goat anti-rabbit-HRP 1:1000 (Jackson ImmunoResearch Laboratories, West Grove, PA), goat-anti-mouse-HRP 1:1000 (Jackson ImmunoResearch Laboratories, West Grove, PA) and anti-alpha-tubulin 1:1000 (Molecular Probes, Eugene, OR). Blots were incubated in ECL-Plus (Amersham, Piscataway, NJ) according to the manufacturer's protocol and visualized with Kodak BioMax XAR or MR film. Bands were further analyzed by densitometry using NIH Image J software program (www.nihimagej.com).

2.3 RESULTS

To determine whether NPCis astrocytoma lines are tumorigenic and whether there is a correlation between grade and tumor growth *in vivo*, we injected astrocytoma lines subcutaneously to immunocompromised mice (Fig 1.1). The average growth rates of four different grade III lines (1395, K1492, K5001, and KR158) were significantly higher than the average growth rates of three grade II lines (1410, K1861, and K4622) (Fig 1.1). This result demonstrates that an inbred C57BL/6J astrocytoma line is tumorigenic in mice.

PI-103 INHIBITS CELL VIABILITY IN SELECT MOUSE AND HUMAN ASTROCYTOMA CELL LINES

In Alamar blue cell viability assay, both mouse and human astrocytoma cell lines were sensitive to the dual PI3 kinase and mTOR inhibitor, PI-103 (Table 2.3).

The normal control mouse primary astrocytes treated with PI-103 had a GI_{50} of 5.15 μ M. In contrast, the more rapidly proliferating mouse and human astrocytoma cell lines showed increased sensitivity towards the PI-103 inhibitor. Specifically, the mouse astrocytoma grade II cell line, K1861-10, had GI_{50} of 0.97 μ M. Likewise, both mouse astrocytoma cell lines, KR158 grade III, with GI_{50} of 0.66 μ M and K130G#3, grade IV, with GI_{50} value of 0.68 μ M, were substantially more sensitive to PI-103 as compared to control mouse primary astrocytes. Similar observations were made when rapidly proliferating human astrocytoma cell lines SF295 (GI_{50} of 0.89 μ M) and U87MG (GI_{50} of 1.10 μ M) were used.

PI-103 produced a dose-dependent inhibition of phosphorylated Akt (Fig. 2.4). In the presence of increasing concentrations of PI-103 inhibitor, phosphorylation of Akt was inhibited at approximately 1 μ M, as evidenced by Western blot analysis. A comparison to total Akt, used as a loading control, indicates that only the activated/phosphorylated Akt was inhibited by PI-103. Similarly, phospho-p70S6K, the downstream effector molecule in the mTOR pathway, was also dose-dependently inhibited in the presence of PI-103 at the 1 μ M concentration. The total p85S6K functioned as a loading control for the non-phosphorylated p-70S6K effector molecule.

Table 2.3: IC₅₀, GI₅₀, and maximum percent inhibition of PI-103, Tricirbine and Rapamycin in various cell lines.

Inhibitor		Astrocytes Mouse Normal	K1861 Mouse Grade II	KR158 Mouse Grade III	KR130 Mouse Grade IV	SF295 Human Grade IV	U87MG Human Grade IV	pAKT/ pS6K
PI-103	IC ₅₀	3.12 μM	0.80 μM	0.59 μM	0.62 μM	0.80 μM	0.63 μM	0.005 μM
	GI ₅₀	5.15 μM	0.97 μM	0.66 μM	0.68 μM	0.89 μM	1.10 μM	
	Max%	83.3%	95.4 %	86.8 %	94.8 %	94.6 %	86.0 %	100%
TCN	IC ₅₀	5.33 μM	0.70 μM	0.31 μM	0.74 μM	0.75 μM	27.67 μM	0.13 μM
	GI ₅₀	13.58 μM	1.73 μM	0.36 μM	1.07 μM	0.99 μM	NA μM	
	Max%	70.7 %	69.0 %	87.1 %	82.3 %	85.9 %	43.2 %	98%
Rapamycin	IC ₅₀	NA	NA	0.26 nM	0.47 nM	0.35 nM	0.58 nM	<1 pM
	GI ₅₀	NA	NA	NA	NA	NA	119.03 nM	
	Max%	NA	NA	33.6 %	45.6 %	46.6 %	50.6 %	100%

NA, data not available

The plots used to calculate the IC₅₀ values by the Western blots for phospho-Akt and phospho-p70S6K against total Akt and total p70S6K are shown at Fig. 2.4 (bottom left & right panels, respectively). The results indicate that the inhibitor PI-103 is active in this *in vitro* model system as evidenced by the dose-dependent dephosphorylation decrease of pAkt at Ser473 and Thr308 at 100 nM concentrations for the Akt and p70S6K at 100 nM. The sigmoidal dose-response curves show the percent inhibition of both the mouse and human astrocytoma cell lines, when treated with the PI-103 dual inhibitor (Fig. 2.5, top panel). The average maximum inhibition by the PI-103 inhibitor

was approximately 80%. Statistical analyses were done using the one-way analysis of variance with Dunnett post-hoc test.

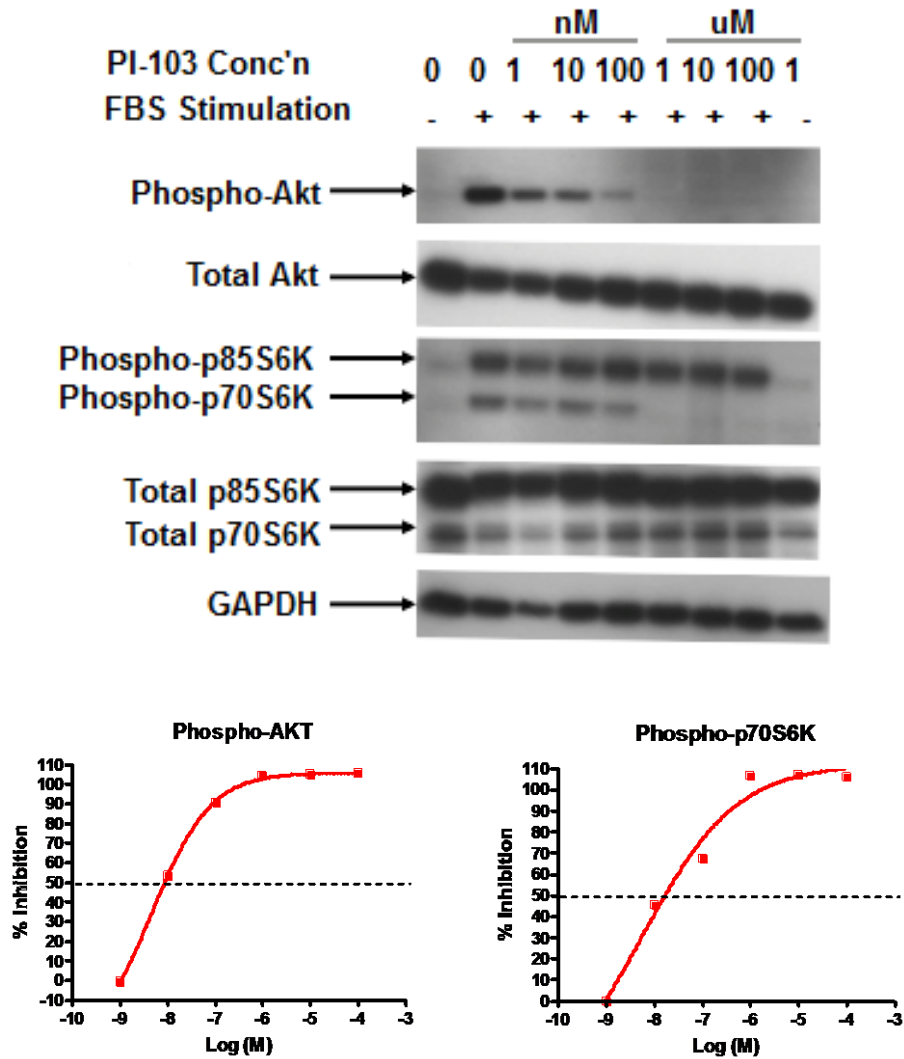


Figure 2.4: KR158 cells were starved and then stimulated with 10% FBS in the presence of different concentrations of PI-103. Western blots for phospho-Akt, downstream of PI3K, and phospho-p70S6K, downstream of mTOR, were quantified using ImageJ software and plotted as the percent inhibition relative to stimulation in the absence of drug. Plots show the curves used to calculate the IC_{50} for inhibition of PI3K.

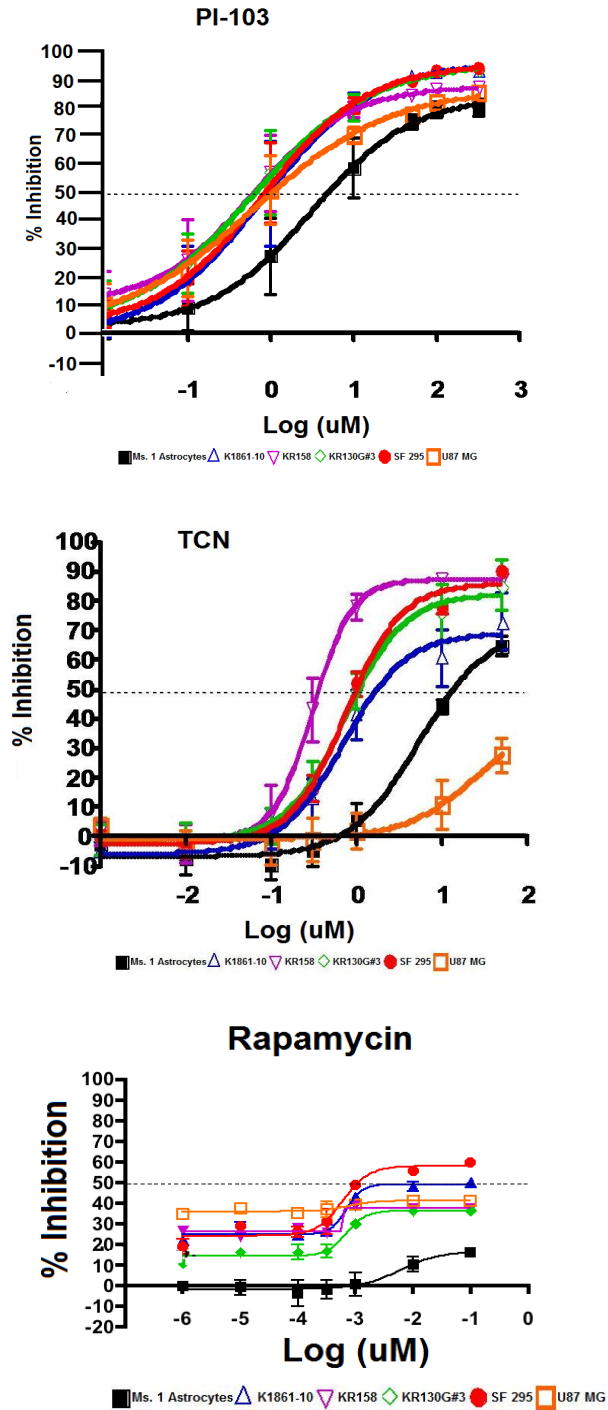


Figure 2.5: Growth inhibition curves as a function of drug concentration for PI-103 (top panel), Tricirbine (middle panel), and rapamycin (bottom panel). Data points are the averages of a minimum of 8 experiments with triplicate samples in each, and standard error is shown by error bars. Averaged data was used to fit the curve for each astrocytoma cell line. Rapamycin showed highly variable results, with inhibition even at very low concentrations, such that data did not show a sigmoidal dose response. Murine primary astrocytes: Ms 1 Astro; murine astrocytoma grade II: K1861; murine astrocytoma grade III: KR158; murine GBM grade IV: KR130; human GBM grade IV: SF-295 and U87MG.

TRICIRBINE INHIBITS CELL VIABILITY IN SELECT MOUSE AND HUMAN ASTROCYTOMA CELL LINES

As tested by the Alamar blue cell cytotoxicity assay, both mouse and human astrocytoma cell lines were sensitive to Tricirbine (Table 2.3).

The normal control mouse primary astrocytes treated with Tricirbine had a GI_{50} of 13.58 μ M. In contrast, the more rapidly proliferating mouse and human astrocytoma cell lines showed more sensitivity towards Tricirbine. Specifically, mouse astrocytoma grade II cell line K1861-10 had a GI_{50} of 1.73 μ M. Mouse astrocytoma cell lines, KR158 grade III, with a GI_{50} of 0.36 μ M, and K130G#3, grade IV, with a GI_{50} value of 1.07 μ M, were even more sensitive to Tricirbine as compared to control mouse primary astrocytes. Similar observations were made for rapidly proliferating human astrocytoma cell lines SF295 (GI_{50} of 0.99 μ M). We were unable to obtain GI_{50} data for the human astrocytoma cell line U87MG. However, based on the IC_{50} value for U87MG compared to the IC_{50} value for the control mouse primary astrocytes cells, it appears that the U87MG astrocytoma cell line may be less sensitive to Tricirbine.

Similarly, the dose response curves for Tricirbine-treated mouse and human astrocytoma cell lines, compared with control mouse primary astrocytes, suggest that both mouse and human astrocytoma cell lines are sensitive to the effects of the Tricirbine inhibitor as tested *in vitro* (Fig. 2.5, middle panel). The average maximum inhibition approaches 80-90%, with one notable exception of U87MG that was not sensitive to the Tricirbine.

Both in serum-starved and in FBS stimulated mouse astrocytoma grade III KR158 cells, Tricirbine produced a dose-dependent inhibition of phosphorylated Akt (Fig. 2.6).

As can be seen in Fig. 2.6, Tricirbine inhibited the phosphorylation of Akt and the downstream effector molecule p-p70S6K at 100 μ M. The curves used to calculate the IC_{50} value for the inhibition of Akt were plotted as a percent of Tricirbine compared to FBS stimulation in the absence of drug (Fig 2.6 bottom panel). Statistical analyses were done using the one-way analysis of variance with the Dunnett post-hoc test.

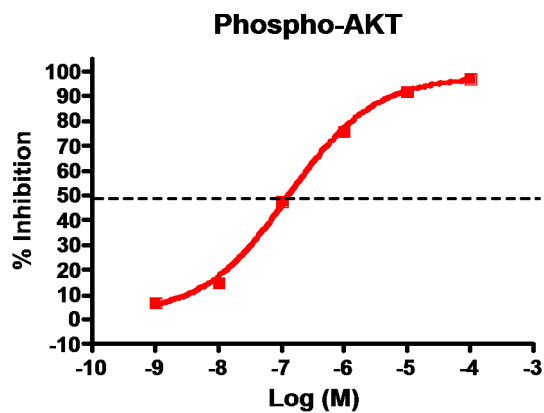
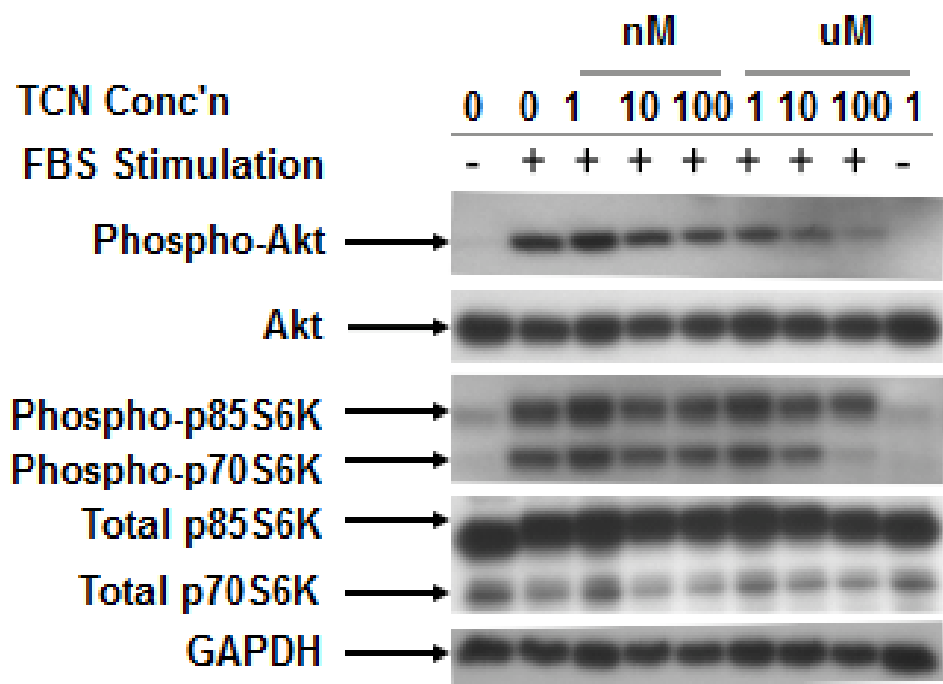


Figure 2.6: Inhibition of phospho-Akt and phospho-p70S6K by increasing concentrations of Tricirbine.

KR158 cells were serum-starved and then stimulated with 10% FBS in the presence of different concentrations of TCN. Western blots for phospho-Akt were quantified using ImageJ software and plotted as the percent inhibition relative to stimulation in the absence of drug. The plot shows the curve used to calculate the IC_{50} for inhibition of AKT.

RAPAMYCIN INHIBITS CELL VIABILITY IN SELECT MOUSE AND HUMAN ASTROCYTOMA CELL LINES

The study of the effects of rapamycin showed inconsistent results. The activities of rapamycin in the mouse and human astrocytoma cell lines are described in Table 2.3. In contrast to the sigmoidal growth inhibition observed with both PI-103 and TCN inhibitors, the outcomes of the treatment with rapamycin varied (Fig. 2.5 bottom panel). Rapamycin demonstrated maximum inhibition approaching 30-40%; an effect that was mostly cytostatic with very low concentrations of inhibitor needed.

The Western blot data (Fig. 2.7) shows the dose-dependent dephosphorylation of phospho-p70S6K, a down-stream effector in the mTOR signaling cascade, in the presence of mTOR inhibitor, Rapamycin. Total Akt and p-Akt remained unchanged in the presence of Rapamycin. In addition, its effects on pAKT phosphorylation status at Ser473 and Thr308 residues were negligible.

Our data indicate that Rapamycin inhibits the phosphorylation of p-p70S6K at approximately 1 pM or less. The unchanged intensity of the bands for GAPDH, total p70S6K, and total Akt used as internal loading controls indicated that only the phosphorylated downstream effector molecule p-p70S6K is affected by Rapamycin treatment. The plot in Fig. 2.7 (bottom panel) shows the observed inhibition of phospho-p70S6K in the presence of Rapamycin, with almost complete inhibition at all concentrations tested.

In the mouse astrocytoma KR158 cell line, treatment with Rapamycin demonstrated dephosphorylation of phospho-p70S6K, at all concentrations tested, starting with the lowest 1 pM concentration all the way to the final 100 μ M

concentration. These low rapamycin concentrations of 1 pM are in agreement with published reports in which the concentrations of rapamycin needed to inhibit proliferation in PTEN-negative cell lines were at or around 1 nM (Cloughesy, Yoshimoto et al. 2008).

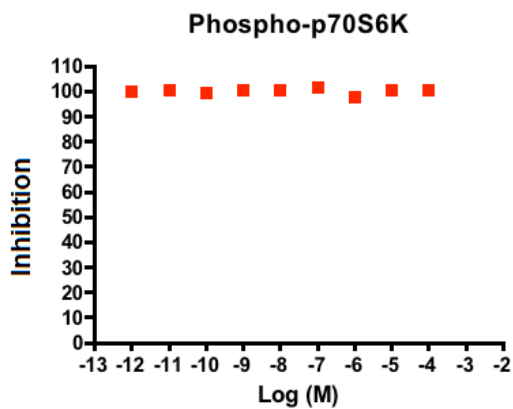
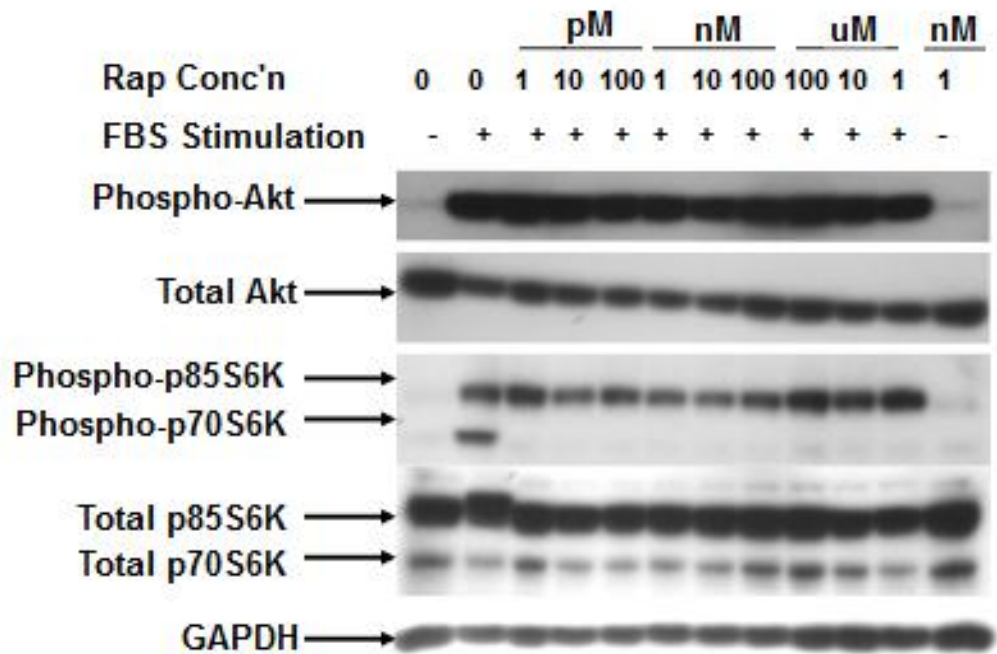


Figure 2.7: Inhibition of phospho-p70S6K by rapamycin.

KR158 cells were serum-starved and then stimulated with 10% FBS in the presence of different concentrations of rapamycin. Rapamycin had no effect on phospho-Akt levels, but inhibited phospho-p70S6K at all concentrations tested. Western blots for phospho-p70S6K, downstream of mTOR, were quantified using ImageJ software and plotted as the percent inhibition relative to stimulation in the absence of drug. Plots show quantification of the inhibition of phospho-p70S6K with close to 100% inhibition at all concentrations tested.

2.4 DISCUSSION

Among the three inhibitors tested in the *in vitro* model system, the dual PI3K/Akt PI-103 inhibitor seemed the most efficient in the dose-dependent dephosphorylation of activated Akt and p-p70S6K as tested. The results suggest that PI-103 inhibited both the cell viability of mouse and human astrocytoma cell lines as compared to the control mouse primary astrocytes cell line. This inhibition was reflected in the low GI₅₀ values. The data from the Western blot analysis indicates that PI-103's intended Akt target was affected as evidenced by the decrease in levels of both the phosphorylated Akt and its effector phospho-p70S6K with increasing concentrations of inhibitor. Furthermore, all tested cell lines were sensitive to PI-103 inhibitor as compared to control cells.

In a similar fashion, the Akt inhibitor Tricirbine was efficient in both mouse and human astrocytoma cell lines. The control mouse primary astrocyte cell line with IC₅₀ value of 5.33 μ M, was significantly higher than the mouse and human astrocytoma cell line SF295 and mouse astrocytoma cell lines with IC₅₀ values less than 1 μ M, indicating their sensitivity to the inhibitor. In contrast, the human astrocytoma cell line, U87MG with IC₅₀ of 27.67 μ M, was resistant to Tricirbine.

Inhibition of astrocytoma with Rapamycin was less pronounced and never achieved more than 75% maximum inhibition. Western blot analysis suggests that Rapamycin inhibited the dose-dependent phosphorylation of activated mTOR at the lowest 1 pM concentration and in all the concentrations tested up to 100 μ M. It is possible that mTOR inhibition alone is not sufficient to inhibit cell growth/viability as

tested, and argues for combination therapy to target both PI3K/Akt and mTOR signaling axes.

LIMITATIONS OF THE STUDY

There are two main limitations of the *in vitro* cytotoxicity assays, including the Alamar blue assay. The first limitation is that *in vitro* cytotoxicity assays cannot predict *in vivo* toxicity (Hamid, Rotshteyn et al. 2004; Zhang, Mu et al. 2007). However, *in vitro* cytotoxicity assays are indispensable as they allow identification of cytotoxic compounds, as well as the ranking of new compounds against other known compounds in terms of their potency.

A second limitation of the Alamar blue fluorescence based assay is that test compounds may either absorb light or emit fluorescence, thus introducing unwanted variables into the determination of drug activity (Koehn and Carter 2005). One way to mitigate the effects of absorbing light or emitting fluorescence is to use 96-well black plates.

CONCLUSION

Both PI-103 and Tricirbine were shown to deactivate Akt in a dose-dependent manner in mouse and human astrocytoma cell lines. These early pre-clinical *in vitro* studies warrant further *in vivo* pre-clinical testing either as monotherapy or in combination therapy with other inhibitors, to justify their advance to human clinical trials as potential therapeutics for astrocytoma and GBM patients.

CHAPTER 3: PRE-CLINICAL EVALUATION OF NELFINIVIR, CHLOROQUINE, PERIFOSINE, PIA-6 AND OSU-03012 AS POTENTIAL ANTI-ASTROCYTOMA THERAPIES

3.1 INTRODUCTION

The aim of this part of the study was to test additional compounds that inhibit the PI3K/Akt signaling pathway either directly or indirectly in astrocytoma cell lines. The five compounds shortlisted for testing include Nelfinivir, Chloroquine, Perifosine, PIA-6 and OSU-03012. In previous studies, Nelfinivir (NFV), Chloroquine (CLQ), and Perifosine (PER) showed dose-responsive inhibitory effects (Gursel, Connell-Albert et al. 2011) at relatively high concentrations, which is consistent with indirect activity on the signaling pathway (See Table 3.3). Additionally, PIA-6 and OSU-03012, which have never been tried in brain tumor models, were included.

The five shortlisted inhibitors exert various types of effects in tumor cells. The only FDA approved drug out of the five, Chloroquine, is a 4-alkylamino substituted quinone that is used in the treatment or prevention of malaria (Fig. 3.1). A strong lysosomotropic and DNA-intercalating agent, Chloroquine, works by inhibiting lysosomal acidification, which prevents autophagy by blocking the formation of autophagosome fusion and degradation (Maycotte, Aryal et al. 2012). Chloroquine is inexpensive, readily available, and easy to use, has low toxicity, its side effects are well known and it has a rapid onset of action (He, Qin et al. 2008).

Perifosine is a synthetic alkylphospholipid which inhibits AKT activity, as well as the assembly of the mTOR complexes, Raptor and Rictor in mechanisms of action unrelated to that of Rapamycin, by promoting the degradation of mTOR components through a GSK3/FBW7-dependent mechanism. In select cell lines, Perifosine also substantially increases the poly(ADP-ribose) polymerase cleavage and levels of type II light chain 3, a hallmark of autophagy, suggesting that Perifosine induces both apoptosis and autophagy (Fu, Kim et al. 2009; Gao, Ishiyama et al. 2011) (Fig. 3.2).

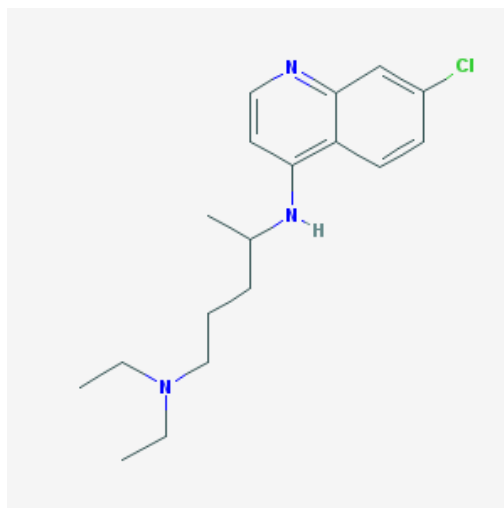


Figure 3.1: This figure shows the chemical structure of Chloroquine with Molecular Formula: $C_{18}H_{26}ClN_3$. (Source of the figure: <http://PubChem.nlm.nih.gov>).

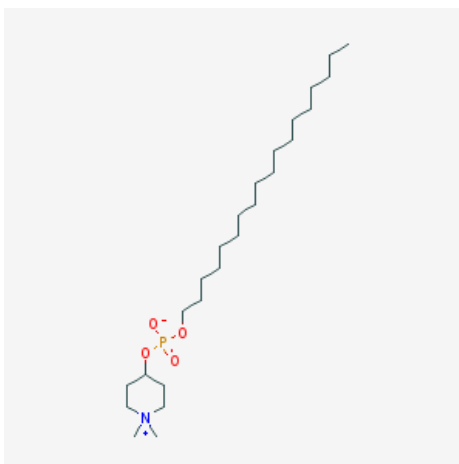


Figure 3.2: This figure shows the chemical structure of Perifosine with Molecular Formula: C₂₅H₅₂NO₄P. (Source of the figure: <http://PubChem.nlm.nih.gov>).

Phosphatidylinositol ether lipid analogue (PIA)-6 specifically inhibits AKT1 (Fig. 3.3). In the presence of PIA-6, cells are blocked or prohibited from forming cyclic phosphates by phosphoinositide-specific phospholipase C (PI-PCC) (Zhang, Elkahloun et al. 2011).

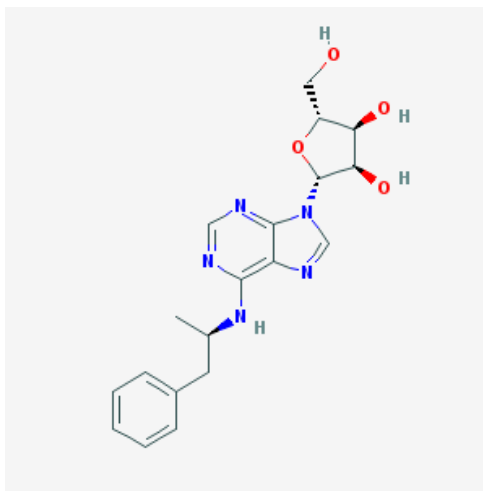


Figure 3.3: This figure shows the chemical structure of PIA-6 with Molecular Formula: $C_{19}H_{23}N_5O_4$. (Source of the figure: <http://PubChem.nlm.nih.gov>).

OSU-03012 {2-amino-N-4, 5-2-phenathrenyl-3 trifluoromethyl-1H-pyrazol-1-yl-phenylacetamide} is a small molecule that is specifically targeted to the PDK-1 pathway, an upstream regulator of Akt (Fig. 3.4). OSU-03012 has been shown to inhibit Akt phosphorylation; inducing apoptosis in transformed cells while leaving normal untransformed cells relatively intact (negligible apoptosis); and has been shown to kill cells by endoplasmic reticulum (ER) stress, lysosomal degradation (autophagy) and BID (BH3-interacting domain)-dependent release of apoptosis inducing factor (AIF) from the mitochondria (Kucab, Lee et al. 2005; Yacoub, Park et al. 2006; Park, Yacoub et al. 2008).

Earlier studies have shown that patients with prolonged exposure to COX-2 or cyclooxygenase inhibitors as part of an anti-inflammatory therapeutic regimen had a lower incidence of developing cancer. This finding suggests that COX-2 inhibitors were cancer preventative. As such, OSU-03012 was developed as an anti-cancer agent on the

scaffold of COX-2 inhibitors. In *in vitro* experiments with select cell lines, OSU-03012 showed greater than an order of magnitude higher anti-tumor activity as compared to that of celecoxib, but no COX-2 inhibitory activity (Kucab, Lee et al. 2005; Yacoub, Park et al. 2006; Park, Yacoub et al. 2008). In gliomas, OSU-03012 has been shown to induce PDK-1/Akt independent cell death. It has been suggested that OSU-03012 may be a multi-targeted inhibitor that exerts its effects in a cell-type dependent manner to include autophagy and apoptosis in select cell lines. OSU-03012 is suitable to pursue as a potential anti-astrocytoma therapy as it crosses the BBB and it interacts synergistically with other chemotherapy drugs such as EGFR inhibitors to suppress tumor growth. In addition, OSU-03012 could sensitize tumor cells to radiation (Kucab, Lee et al. 2005; Yacoub, Park et al. 2006; Gao, Yeh et al. 2008; Park, Yacoub et al. 2008).

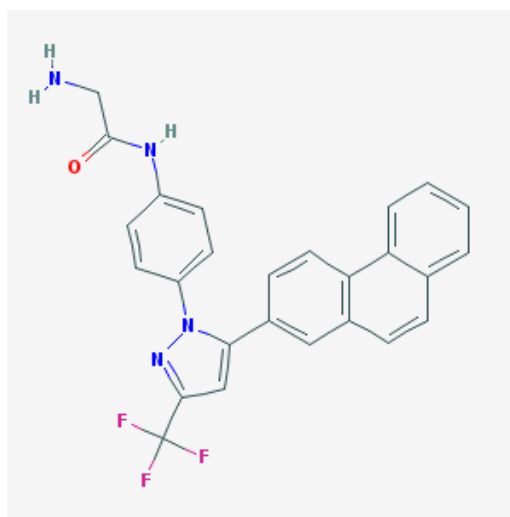


Figure 3.4: This figure shows the chemical structure of OSU-03012 with Molecular Formula: $C_{26}H_{19}F_3N_4O$. (Source of the figure: <http://PubChem.nlm.nih.gov>).

Nelfinivir, commercially known as Viracept (Pfizer, Groton, CT, USA), is an HIV-1 protease inhibitor that interferes with Akt activity downstream of EGFR and upstream of VEGF, and induces cell cycle arrest via autophagy, apoptosis and necrosis (Bruning, Friese et al. 2010; Bruning, Rahmeh et al. 2010) (Fig. 3.5). The mechanism of action for Nelfinivir is thought to occur via either one of two pathways; the first being the cross-reaction of the protease with the cytoplasmic proteasomal protein degradation machinery; the second with Endoplasmic reticulum resident proteases (Bruning, Friese et al. 2010). In both cases, Nelfinivir can lead to the accumulation of misfolded proteins that cause the unfolded protein response or the ER stress response. If there is a prolonged or irreparable stress reaction to Nelfinivir, the cell switches from a repair and survival mechanism to cell death by apoptosis. In addition, the swelling of the ER by the accumulation of misfolded proteins due to the ER stress response appears to be a central mechanism in Nelfinivir induced death in several cancer types, including lung cancer, gliomas, and ovarian cancer cells and precedes the activation of apoptosis (Bruning, Friese et al. 2010; Bruning, Rahmeh et al. 2010; Xie, Evangelidis et al. 2011). When apoptosis is induced, this can occur via one of two pathways to include the extrinsic pathway mediated by cell membrane bound death receptors or the intrinsic pathway mediated by the activation of pro-apoptotic intracellular mechanisms (Bruning, Friese et al. 2010; Bruning, Rahmeh et al. 2010; Xie, Evangelidis et al. 2011).

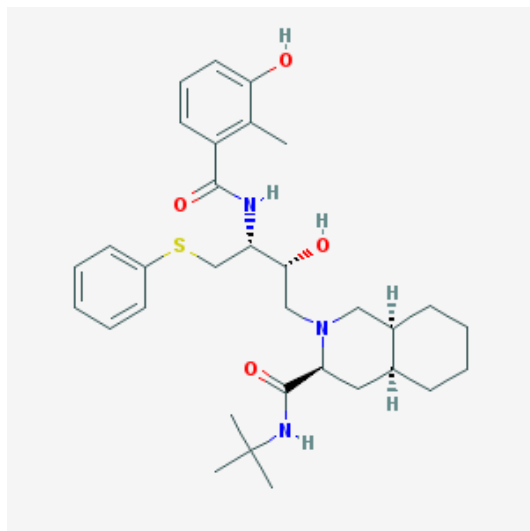


Figure 3.5: This figure shows the chemical structure of Nelfinivir with Molecular Formula: $C_{32}H_{45}N_3O_4S$. (Source of the figure: <http://PubChem.nlm.nih.gov>).

Nelfinivir has also been implicated in decreasing VEGF/HIF-1 alpha expression and angiogenesis in glioblastoma cells, and inhibiting the growth of more than 60 cancer cell lines from 9 different tumor types in the NCI-60 panel (Pyrko, Kardosh et al. 2007; Gills, Lopiccolo et al. 2008).

The prospect of utilizing Nelfinivir as a multipotent cytoprotective agent with selective anti-cancer activity should be considered with caution as the concentration of Nelfinivir is important in determining whether or not it functions as a cytoprotective drug or cell death inducing agent. Specifically, Nelfinivir has shown to be cytoprotective in murine liver cells, neurons, retina cells, pancreas cells, and cell death-inducing in leukemia cells (Bruning, Friese et al. 2010; Bruning, Rahmeh et al. 2010; Xie, Evangelidis et al. 2011).

Table 3.1: The five inhibitors used in the Alamar Blue metabolic assay with mouse and human cell lines. Data obtained from www.clinicaltrials.gov.

Inhibitor	Targets (Primary, Secondary, Off-targets)	Phase	Condition	Identifier	Miscellaneous
Chloroquine	AKT	Phase III	GBM	NCT00224978	Study completed
Nelfinivir	Unknown Implicated in AKT, MAPK, JNK, EGFR, NF-KB, mTOR,	Phase I-II	GBM Grade IV gliomas	NCT00694837 NCT01020292	HIV-1 PI Combination with TMZ, Radiation
Perifosine	AKT, RAS, GS3K3-beta	Phase II	Malignant gliomas	NCT00590954	
PIA-6	PI3K/AKT	NEVER TESTED IN GLIOMA PATIENTS			
OSU-03012	PKD/AKT, PERK				

Table 3.2: Selected Chemical and Physical Properties of OSU, Perifosine, Chloroquine, Nelfinivir and PIA-6 that contribute to characteristics of good drug candidates.

Name/ ID of Compound	Molecular Weight	Hydrogen bond donor	Hydrogen bond acceptor	Rotatable bond count	Topological surface area	Predicted oral availability
OSU/03012/CID10027278	460 g/mol	2	6	4	72.9 A ⁰	Yes
PER/CID 148177	461 g/mol	0	4	20	58.6 A ⁰	Yes
CLQ/CID 2719	319 g/mol	1	3	NA	NA	Yes
NFV/CID 64143	567 g/mol	4	6	10	127 A ⁰	NA
PIA-6/CID 93205	385 g/mol	4	4	6	126 A ⁰	Yes

All five compounds shortlisted here have the potential to impact the PI3K/Akt/mTOR pathway, and thus, the ability to be repurposed for BBB permeability. Chloroquine, Nelfinivir and Perifosine are already FDA approved for non-malignant diseases, some are already in clinical Phase I/II (Nelfinivir) or Phase III (Chloroquine) clinical trials as monotherapy; some were tested in combination and multimodality

therapy for other solid cancers (Perifosine, Chloroquine); and some are being used for GBM therapy (Chloroquine).

Specifically, the HIV-1 protease inhibitor Nelfinivir is in a Phase I/II human clinical trial study (NCT-00694837) in GBM patients, to determine primarily the safety, tolerability, and activity of Nelfinivir in newly diagnosed GBM patients. The expected clinical outcome of this trial is to determine if Nelfinivir can block the *in vivo* activity of AKT in the PI3K/Akt/mTOR pathway in GBM patients. Chloroquine was used in a human Phase III clinical trial study (NCT-00224978) to determine its efficacy as additive therapy in GBM patients after surgical resection. At the conclusion of the study, it was unclear whether or not the addition of Chloroquine offered an Overall Survival or Progression Free Survival when compared to the control, placebo, or carmustine wafer study groups. Perifosine is currently being studied in a human Phase II clinical trial (NCT-00590954) in patients with recurrent or malignant gliomas. In another clinical trial (NCT-01051957), Perifosine was used as an AKT inhibitor, in combination with Temsirolimus, an mTOR inhibitor, to target the PI3K/AKT/mTOR pathway in glioma patients.

The rationale to test these compounds in our NPcis mouse model system was that the three inhibitors (Chloroquine, Nelfinivir, Perifosine) that are already in the FDA glioma pipeline could be compared side-by-side to the two non-FDA approved inhibitors (PIA-6, OSU-03012). Moreover, Chloroquine, Nelfinivir, and Perifosine have shown limited efficacy as monotherapies in human clinical trials, while the compounds PIA6 and OSU-03012 have yet to be established as drug candidates. It is hoped that by

establishing a base line for future combination therapy, it can lead to the approval of the first Akt inhibitor which can be used either in monotherapy or combination therapy.

PRE-CLINICAL AND CLINICAL STUDIES OF NELFINIVIR

Nelfinivir has been utilized as a potential therapeutic in both infectious and non-infectious diseases, notably, HIV, and tumors. In combination with radiochemotherapy, Nelfinivir entered Phase I/II clinical trial (NCT 00694837) in newly diagnosed GBM patients. This trial is expected to find whether *in vivo* inhibition of the PI3K/Akt signaling pathways by Nelfinivir depends upon BBB penetration and tumor saturation.

Nelfinivir has been suggested for therapy to treat breast cancer, in combination with Tamoxifen, an estrogen receptor antagonist. Experiments using two estrogen-receptor positive cell lines T47D and MCF-7, and two estrogen-receptor negative cell lines MDA-MB-453 and MDA-MB-435 indicated that low doses of Nelfinivir (5 ug/mL) has a cytostatic effect, while higher doses of Nelfinivir demonstrate cytotoxic effects. Nelfinivir reduced the phosphorylation of Akt in the breast cancer cells which increased the radiosensitivity of these cells. The combination of Nelfinivir and Tamoxifen had no effect on Akt or Erk phosphorylation in the ER+ cells (TD47 & MCF-7), while in the ER-cells (MDA-MB-453 & MDA-MB-435) the changes in the phosphorylation status of these targets were observed. Despite these data, in analyzed breast cancer cells, the cytotoxic effects of a Tamoxifen and Nelfinivir combination were independent of the ER status, suggesting that a combination of these two drugs may be beneficial for patients with ER-negative tumors (Bruning, Friese et al. 2010).

Nelfinivir has also been evaluated in a pre-clinical study of leukemia cell lines HL-60 (acute promyelotic leukemia), IM-9 (EBV-transformed b-lymphoblastoid cells) and Jurkat (acute T-cell leukemia) where it was shown to induce cell death at concentrations between 4-10 ug/mL. However, the reduction in cell proliferation and cell death was not autophagy, but apoptosis. This was evaluated by the significant increase in the number of cells in the sub-G1 phase of the cell cycle, which was later confirmed by PARP cleavage and the substrate effector caspases 3 and 7 (Bruning, Rahmeh et al. 2010; Ikezoe, 2004).

PRE-CLINICAL AND CLINICAL STUDIES OF PERIFOSINE

Perifosine (PER) is currently in clinical trials for a number of human malignancies, as well as a potential therapeutic for a number of diseases (Momota, Nerio et al. 2005), such as hepatocellular carcinoma (HCC), neuroblastoma (NB), and prostate cancer, as well as in clinical trials for GBMs.

Perifosine inhibited the cell growth of HCC cell lines HepG2 and BEL7402 in a dose-dependent manner, resulting in apoptotic cell death. This suggests that Perifosine has the potential to be a good anti-tumor agent in the treatment of HCC and warrants further investigating, especially in combination therapy (Fei, Chen et al. 2010).

Perifosine as monotherapy, also caused the inhibition of cell growth in four neuroblastoma (NB) cells lines, as well as a dose-dependent decrease in the phosphorylation of Akt in the four NB cell lines, compared to control Akt which was unchanged. Results obtained from the *in vivo* tumor assays, demonstrated that Perifosine

caused a decrease in tumor burden in the mice as treated. Taken together, the data suggests that Perifosine may be a good candidate for patients with NB disease based on the preceding *in vitro* and *in vivo* assays (Li, Tan et al. 2010).

As tested either in monotherapy or in combination therapy in *in vitro* assays, Perifosine caused the inhibition of cell proliferation in prostate cancer cells CW1222Rv1, with the concomitant increase in apoptosis and the dose-dependent decrease in phosphorylation of Akt at Thr308 and Ser473. Furthermore, in *in vivo* assays, Perifosine in combination with radiation therapy delayed the start of prostate cancer formation. This data, when taken altogether, supports the continued use of Perifosine in pre-clinical *in vitro* and *in vivo* assays as a potential therapeutic for prostate cancer (Gao, Ishiyama et al. 2011).

Finally, Perifosine has been utilized in a human Phase II clinical trial, NCT00590954 (www.clinicaltrials.gov) with the goal of testing the efficacy of Perifosine in patients with recurrent or progressive malignant gliomas. A secondary objective of this clinical trial was to determine if Perifosine can inhibit the growth and proliferation of tumor cells. In this study, Perifosine was administered to 31 patients enrolled in the clinical trial, 5-10 days before cytoreductive surgery of the tumor was performed. The objective of this pattern was to determine if the Perifosine penetrates the tumor tissue and if it does, whether it is effective *in vivo*, possibly by reducing tumor burden. This study is ongoing so results are not yet available.

THE USE OF CHLOROQUINE IN PRE-CLINICAL AND CLINICAL STUDIES

The first example of the use of Chloroquine as a potential anti-tumor drug is in lung cancer. The A549 lung cancer cell line treated with Chloroquine as monotherapy, were sensitized such that in combination with Topotecan (TPT), the cells apoptosed. The authors suggest that Chloroquine is active against lung cancer cells, because it increased the toxicity of TPT by inhibiting or interfering with autophagy, with the concomitant death of lung cancer cells via apoptosis. Therefore, Chloroquine as combination therapy has the potential to increase the toxicity of the secondary compounds used, the result of which is apoptotic cell death (Wang, Peng et al. 2011), and the possible addition of autophagic cell death as well.

Another instance of the use of Chloroquine as a potential anti-tumor drug is in breast cancer cells. The mouse breast cancer cell lines 67NR and 4T1 in the presence of Rapamycin, an mTOR inhibitor, LY294002, a PI3K inhibitor and cisplatin, a chemotherapeutic drug, underwent autophagic cell death. When these cells were treated with Chloroquine in combination with other inhibitors such as Rapamycin, LY294002 and cisplatin, the mouse breast cancer cells were more sensitive to cell death, independent of autophagy. This suggests that Chloroquine can sensitize mouse breast cancer cell lines to increased tumor cell death other than autophagy (Maycotte, Aryal et al. 2012), and possibly to include apoptosis.

The third example of the use of Chloroquine as a potential anti-tumor drug is in GBM. In a human Phase III clinical trial, Study # NCT 00224978 (www.clinicaltrials.gov), Chloroquine was used after surgical resection to determine its

effects as an additive therapy in GBM treatment. The primary purpose of the study was to determine if there is a difference in progression-free survival or in overall survival of patients after two years of treatment. The study enrolled seven GBM patients and seven control patients; both arms of the study received extensive surgery, carmustine wafer therapy and standard radiation therapy. However, once the study began, patients were further stratified into the control arm of the study to receive placebo or carmustine wafer, or the treatment arm to receive Chloroquine. At the close of the study it was unclear if Chloroquine offered an overall survival advantage or progression free survival when compared to control placebo or carmustine wafer group. Therefore, it is important that Chloroquine be considered in the context of combination therapy rather than monotherapy.

PRE-CLINICAL STUDIES OF OSU-03012

The inhibitor OSU-03012 has been previously studied in *in vitro* assays to determine its efficacy against breast cancer (To, Zhao et al. 2007), myeloma, rhabdomyosarcoma, HCC, VSB, and GBM tumor cell lines (Yacoub, Park et al. 2006). It was proposed that OSU-03012 promotes cell death through a variety of tissue-specific pathways (Zhang, Suvannasankha et al. 2007). However, in glioma cells, OSU-03012 seems to be specific to the PDK1/Akt signaling pathway as it shows no effect on the phosphorylation status of ERK 1/2; JNK 1/2; or P38 MAPK (Zhang, Suvannasankha et al. 2007).

The overexpression of EGFR in breast cancer is often due to enhanced transcription from its promoter by YB-1 or Y-box binding protein. In a study by Zhao et al, the authors used two breast cancer cell lines: MDA-MB-435, a *HER-2* over-expressing cell line and MCF-7, an estrogen receptor positive breast cancer cell line. Both cell lines responded to OSU-03012 by a dose-dependent decrease of phosphorylated Akt at Thr 308 followed by the decrease of Akt at the Ser 473. This suggests that OSU-03012 targets only transformed cells with activated PDK1/Akt and over-expressed transcription factor YB-1 (To, Zhao et al. 2007), and may have clinical utility for the treatment of breast carcinoma with these features.

OSU-03012 was also pre-clinically evaluated as a therapy for multiple myeloma (MM). In MM cells, OSU-03012 caused the deactivation of PDK1/Akt, which was possible because of its cytostatic effect. Additionally, OSU-03012 also down-regulated survivin and X-linked inhibitor of apoptosis (XIAP), and also induced G2 cell cycle arrest with associated reductions in cyclins A and B (Zhang S, Suvannasankha A, et al. 2007). In Rhabdomyosarcoma (RMS), the most common soft tissue sarcoma of childhood (Cen, Hsieh et al. 2007), the PI3K/Akt/mTOR signaling pathway is often activated constitutively. In two RMS cell lines, RH-30 and SMS-CTR, exposure to 10 μ M of OSU-03012 for 8 hours led to a decrease in the activation or phosphorylation of PDK1 at the Thr308 activation site with IC_{50} of 5-6 μ M. In contrast, normal, untransformed control cells, human skeletal muscle myoblasts (HSMM) and human fibroblasts (HFF) were resistant to OSU-03012 (Cen, Hsieh et al. 2007). Two tested *PTEN*-negative GBM cell lines, U251 GBM and U87-MG, reacted to OSU-03012 in very different ways.

Specifically, the U251 GBM cell line was sensitive to the OSU-03012, while U87-MG cell line showed resistance.

THE USE OF PIAs IN PRE-CLINICAL STUDIES

PIAs, a series of AKT inhibitors, have been investigated as a potential treatment for leukemia. A panel of human leukemia cell lines namely the parental human leukemia cell line HL-60PT, apoptosis resistant HL-60AR, and the human K562 erythroleukemia red blood cell line containing the bcr/abl oncogene were used. These cell lines are characterized by high levels of activated Akt and were treated with 5 μ M and 10 μ M of PIAs Sh5 and Sh6 for 24 hours before evaluation. The PIAs Sh5 and Sh6 were designed such that they cannot be phosphorylated by PI3K on the 3' position of the myo-inositol ring, thus limiting the downstream Akt activation. The PIA Sh6 at 10 μ M was more potent in inhibiting the *in vitro* Akt kinase activity in the HL-60AR cell lines as compared to the PIA Sh5 at the same concentration of 10 μ M.

Furthermore, in the HL-60 AR leukemia cell lines, there were no significant differences in the dose-dependent dephosphorylation of p-Akt in the HL-60 AR cell lines with the PIAs as compared to the PI3K inhibitor LY294002 (Tabellini, Tazzari et al. 2004). One possible reason for this lack of response may be due to the fact that PI3K inhibitors are often cytostatic in nature and tend to induce G1 arrest in cell lines. It is believed that treatment with these PI3K inhibitors, in combination with chemotherapy agents *in vitro* and *in vivo*, may result in cytotoxicity via apoptosis (Tabellini, Tazzari et al. 2004).

We hypothesized that the five selected inhibitors (Chloroquine, Nelfinivir, Perifosine, PIA6 and OSU-03012) may inhibit the cell viability of mouse and human glioma cell lines and modify the phosphorylation of AKT substrates or effectors in its pathway.

3.2 MATERIALS AND METHODS

CULTURING OF WILD TYPE MOUSE PRIMARY ASTROCYTES

Primary astrocytes were collected grown and characterized essentially as described in Chapter 2.2

INHIBITORS NELFINIVIR, CHLOROQUINE, PERIFOSINE, PIA-6 AND OSU-03012

The compounds were a generous gift from the laboratory of Dr. Phillip Dennis, The Sidney Kimmel Comprehensive Cancer Center at Johns Hopkins Bayview.

ALAMAR BLUE METABOLIC ASSAYS AND IC₅₀ AND GI₅₀ CALCULATIONS

The human astrocytoma cell lines SF295 and U87MG, the mouse astrocytoma cell lines K1861-10, KR158, and KR130G#3 and primary murine astrocytes, were grown and tested essentially as described in Chapter 2.2.

3.3 RESULTS

To determine the effect of Nelfinivir, Chloroquine, Perifosine, PIA6 and OSU-03012 on the cell viability of mouse and human astrocytoma cell lines and primary astrocytes, the Alamar blue cell viability assays were utilized in a 96-well format.

The effects of OSU-03012 are described in Table 3.3. As shown in Fig. 3.6, OSU-03012 inhibits the cell viability of the cell lines tested in a similar dose-dependent manner, with IC_{50} values ranging from 5 μ M to 8 μ M.

Table 3.3: The calculated IC_{50} values for the five inhibitors tested with mouse and human cell lines.

Inhibitor		Astrocytes	K1861	KR158	KR130	SF295	U87MG
		Mouse Normal	Mouse Grade II	Mouse Grade III	Mouse Grade IV	Human Grade IV	Human Grade IV
Chloroquine	IC_{50} μ M	15 μ M	21 μ M	11 μ M	12 μ M	13 μ M	20 μ M
Nelfinivir	IC_{50} μ M	25 μ M	17 μ M	13 μ M	15 μ M	11 μ M	23 μ M
OSU-03012	IC_{50} μ M	5 μ M	6 μ M	5 μ M	6 μ M	5 μ M	8 μ M
Perifosine	IC_{50} μ M	39 μ M	34 μ M	31 μ M	21 μ M	17 μ M	12 μ M
PIA6	IC_{50} μ M	43 μ M	89 μ M	34 μ M	67 μ M	63 μ M	17 μ M

IC_{50} values are represented as means \pm SD and were calculated from a minimum of 3 independent experiments performed in triplicate with the Alamar blue cell viability metabolic assay.

Normal control mouse primary astrocytes had an IC₅₀ value of 5 μM while mouse astrocytoma cell line K1861-10 grade II, had an IC₅₀ value of 6 μM, KR158 grade III astrocytoma cell line IC₅₀ of 5 μM, and KR130G#3 astrocytoma cell line grade III had an IC₅₀ value of 6 μM. Similarly, human astrocytoma cell lines SF295 grade IV had an IC₅₀ value of 5 μM and U87MG grade IV had an IC₅₀ value of 8 μM (Table 3.3). In both instances, the mouse and human astrocytoma cell lines and control mouse primary astrocytes showed greater than 80% maximum inhibition with similar IC₅₀ values (Fig. 3.6). These results are in close agreement with the published reports in which OSU-03012 inhibited the phosphorylation of the PDK1/Akt target in the PI3K/Akt/mTOR signaling pathway in the 5-50 μM range as measured *in vitro* (Park, Yacoub et al. 2008).

The OSU-03012 inhibitor had no effect on the dose-dependent dephosphorylation of Akt in the KR158 mouse astrocytoma grade III cell line. This was demonstrated by the lack of distinction between p-PDK1 and p-Akt, from total PDK1 and total Akt as measured by Western blot analysis, using specific antibodies to the downstream molecules. Therefore, it is possible that OSU suppresses human and mouse astrocytoma cell lines independently of the PI3K/Akt pathway. Evidently, OSU-03012 inhibitor does not discriminate between rapidly proliferating mouse and human astrocytoma tumor cell types, and normal, control mouse primary astrocytes.

Normal mouse primary astrocytes were similarly sensitive to inhibition by OSU-03012 as compared to tumor cell lines. These results suggest that OSU-03012 is not a specific inhibitor in mouse and human astrocytoma cell lines as compared to control cells.

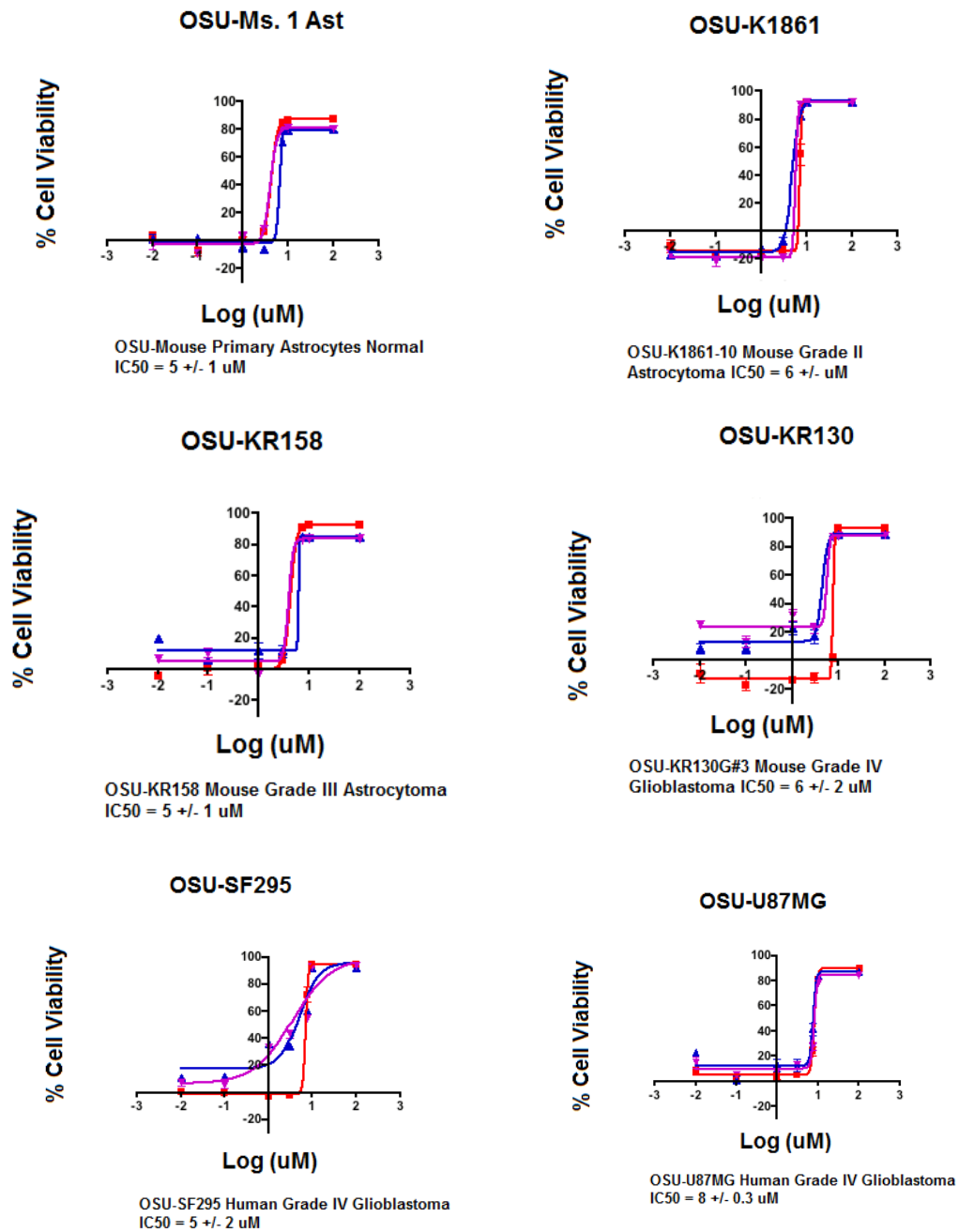


Figure 3.6: Effects of OSU-03012 on cell viability.

Mouse and human cells were plated in a 96-well plate in complete growth media at 37°C for 24 hours and then treated with OSU-03012 inhibitor for 72 hours (day 3). Cell viability was determined using the Alamar blue metabolic assay in triplicate and a representative experiment is shown from multiple experiments. The percentage of inhibition of cell viability was plotted against the logarithm dose of OSU-03012. The IC₅₀ value was shown as the means + standard deviation.

The anti-glioma activities of Perifosine are presented in Table 3.3. As shown in Fig 3.7, Perifosine inhibited cell viability, with IC₅₀ values ranging from 12 μM to 39 μM. Normal control mouse primary astrocytes had highest IC₅₀ value (39 μM), followed by mouse astrocytoma cell lines K1861-10, IC₅₀ of 34 μM, KR158, IC₅₀ of 31 μM, and KR130G#3, IC₅₀ of 21 μM. Similarly, the human astrocytoma cell lines SF295 had IC₅₀ values of 17 μM and U87MG, IC₅₀ of 12 μM. Taken altogether, all the mouse and human astrocytoma cell lines were sensitive to Perifosine at the concentrations used and by the methods tested, when compared to normal proliferating mouse primary astrocytes with IC₅₀ of 39 μM (Table 3.3). Furthermore, both mouse and human astrocytoma cell lines cells showed greater than 90% inhibition of cell viability in the presence of Perifosine (Fig. 3.7). These results suggest that further pre-clinical evaluation of Perifosine in combination with other known Akt kinase inhibitors may be warranted.

The effects of Chloroquine in human and mouse astrocytoma cells lines are presented in Table 3.3 and at Figure 3.8. Chloroquine inhibited the cell viability of all tested cells, in a dose-dependent manner, with IC₅₀ values ranging from 11 μM to 21 μM. Normal proliferating control mouse primary astrocytes had an IC₅₀ value of 15 μM, compared to the more rapidly proliferating mouse astrocytoma cell lines K1861-10, IC₅₀ of 21 μM, KR158, IC₅₀ of 11 μM, KR130G#3, IC₅₀ of 12 μM which suggests very little differential sensitivity to the inhibitor as tested. Similarly, the human astrocytoma cell lines SF295 had an IC₅₀ value of 13 μM, while U87MG had an IC₅₀ value of 20 μM. In addition, in all the cell lines tested, Chloroquine showed a greater than 80% decrease in cell viability.

In Table 3.3 and Figure 3.9, IC₅₀ values of Nelfinavir in mouse and human astrocytoma cell lines are shown. For normal mouse primary astrocytes IC₅₀ values were at 25 μM, for rapidly proliferating mouse astrocytoma cell lines such as K1861-10 grade II IC₅₀ at 17 μM, KR158, grade III IC₅₀ at 13 μM, K130G#3 grade IV IC₅₀ at 15 μM, and human astrocytoma cell line of SF295 had IC₅₀ of 11 μM. These results suggest that both mouse and human astrocytoma cell lines are sensitive to Nelfinavir, with greater than 80% inhibition of cell viability.

A study of PIA6 effects in mouse and human glioma cell line and primary astrocytes are shown in Table 3.3 and Fig 3.10. Rapidly proliferating mouse astrocytoma cell line KR158, grade III (IC₅₀ of 34 μM) and human GBM cell line, U87MG (IC₅₀ of 17 μM) were more sensitive to PIA-6 as compared to normal mouse primary astrocytes (IC₅₀ of 43 μM). Cell lines K1861-10 grade II (IC₅₀ of 89 μM), K130G#3 grade IV (IC₅₀ of 67 μM), and human astrocytoma cell line of SF295 (IC₅₀ of 63 μM) were resistant to PIA-6. All cell lines showed greater than 80% inhibition of cell viability.

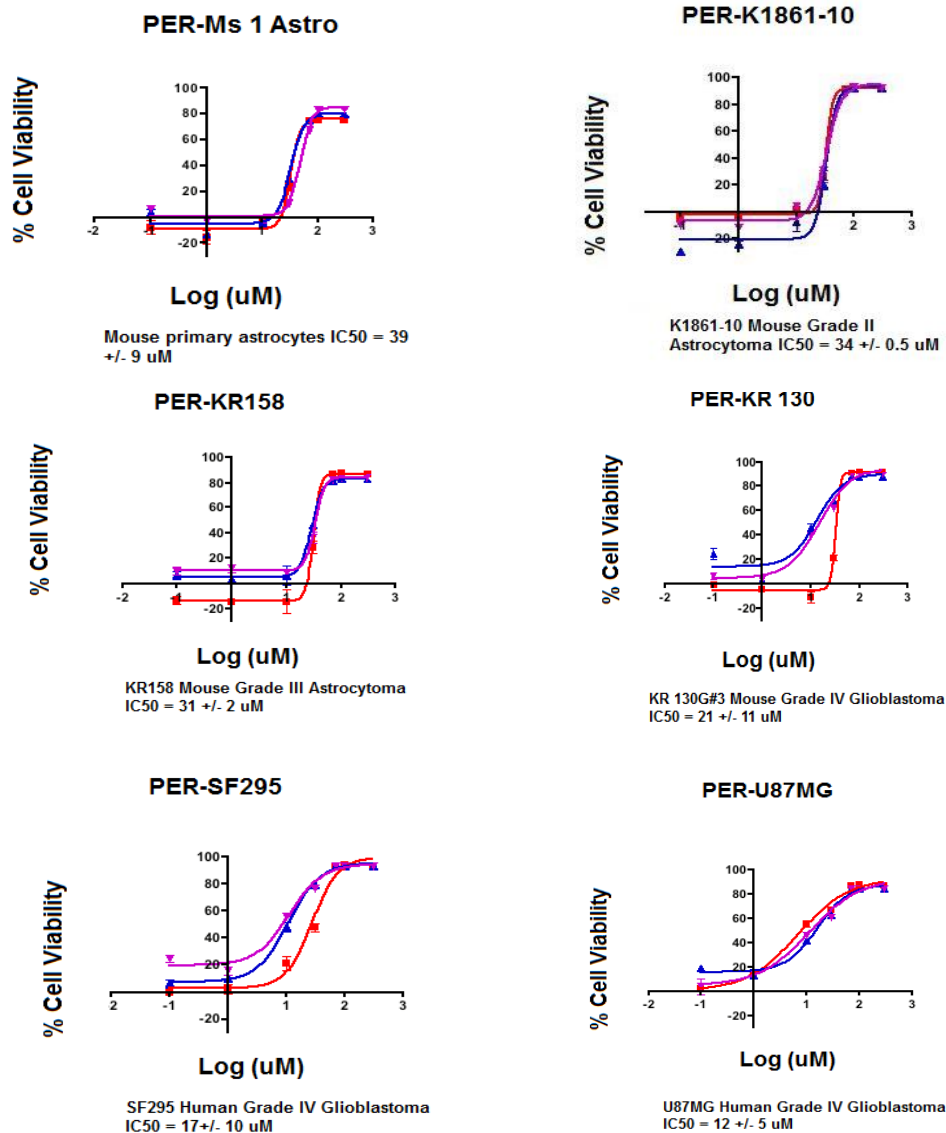


Figure 3.7: Effects of Perifosine on cell viability.

Effects of Perifosine (PER) on the cell viability of mouse and human astrocytoma cell lines compared to controls. Mouse and human cells were plated in a 96-well plate in complete growth media at 37°C for 24 hours and then treated with 300, 100, 70, 30, 10, 1, 0.1, 0 μMol/L Perifosine (PER) inhibitor for 72 hours(day3). Cell viability was determined using the Alamar blue metabolic assay in triplicate and a representative experiment is shown from multiple experiments. The percentage of inhibition of cell viability was plotted against the logarithm dose of Perifosine. The IC₅₀ value was defined as the concentration at which cell viability decreased by 50% and was calculated using GraphPad Prism. The IC₅₀ value was shown as the means + standard deviation.

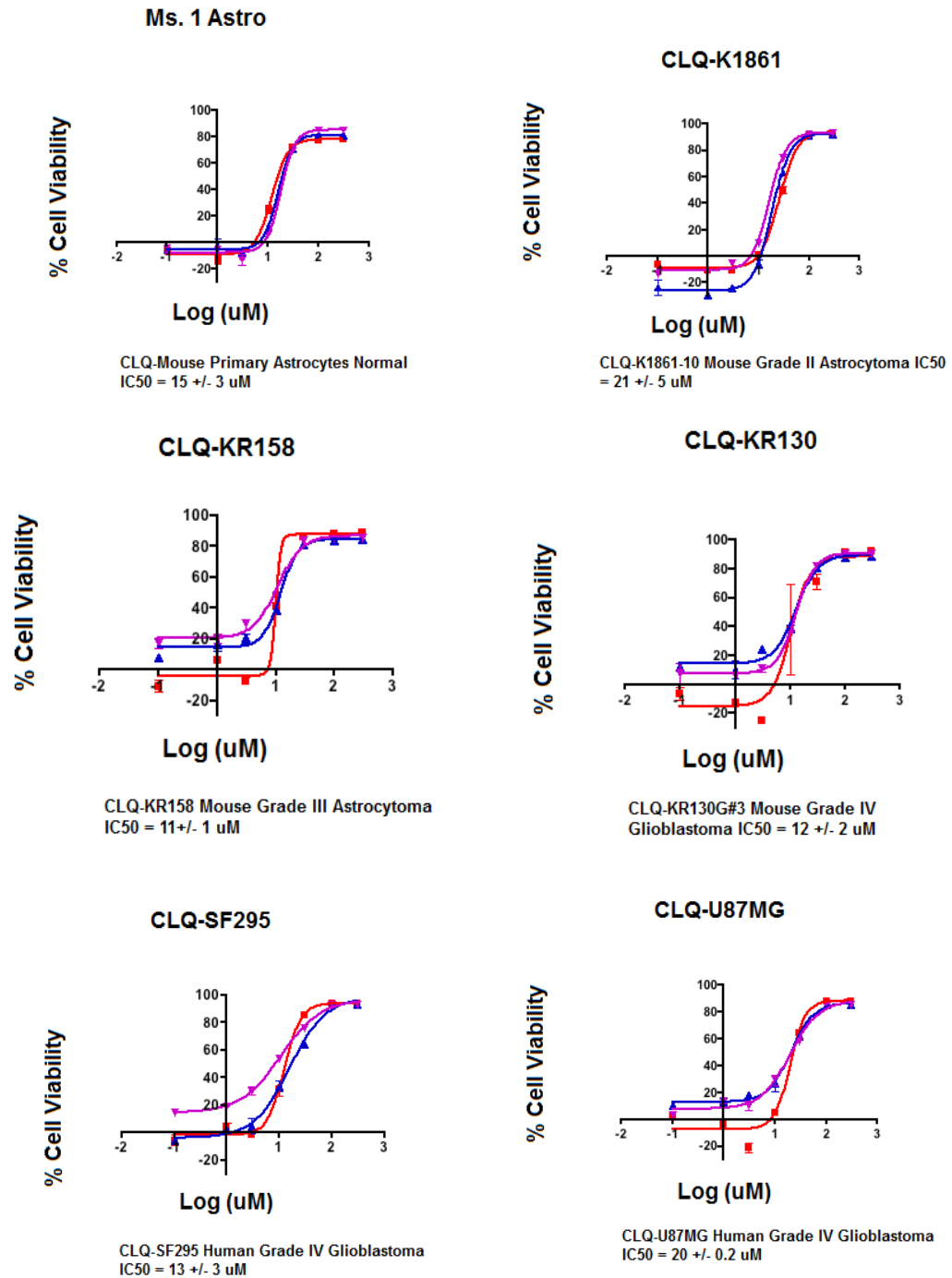


Figure 3.8: Effects of Chloroquine on cell viability. Mouse and human cells were plated in a 96-well plate in complete growth media at 37°C for 24 hours and then treated with 300, 100, 30, 10, 3, 1, 0.1, 0 μM/L Chloroquine inhibitor for 72 hours (day 3). Cell viability was determined using the Alamar blue metabolic assay in triplicate and a representative experiment is shown from multiple experiments. The percentage of inhibition of cell viability was plotted against the logarithm dose of Chloroquine. The IC₅₀ value was defined as the concentration at which cell viability decreased by 50% and was calculated using GraphPad Prism. The IC₅₀ value was shown as the means +/- standard deviation.

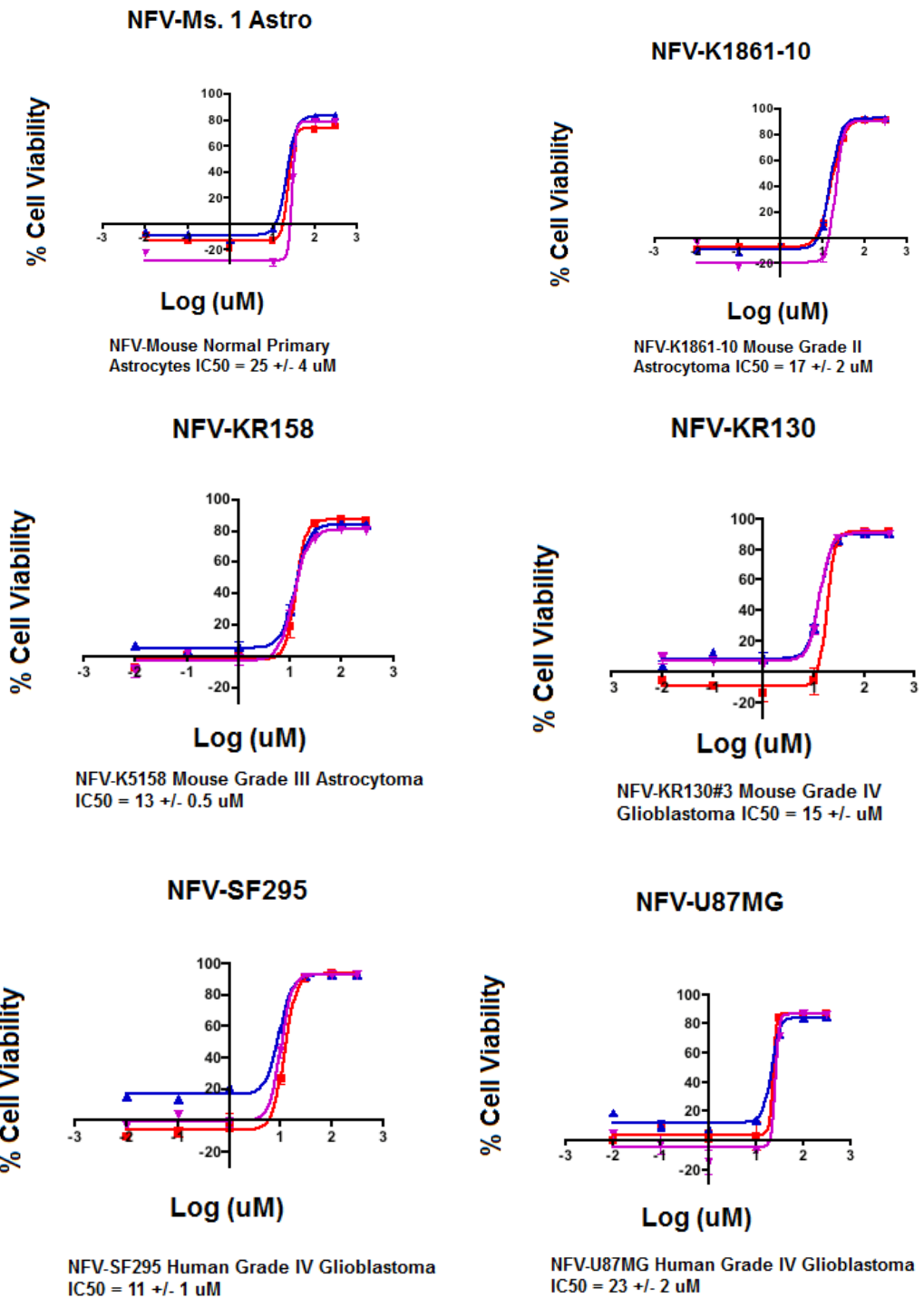


Figure 3.9: Effects of Nelfinivir on cell viability. Mouse and human cells treated with Nelfinivir inhibitor for 72 hours (D3). Cell viability was determined using the Alamar blue metabolic assay in triplicate and a representative experiment is shown from multiple experiments. The percentage of inhibition of cell viability was plotted against the logarithm dose of Nelfinavir. The IC₅₀ value was shown as the means + standard deviation.

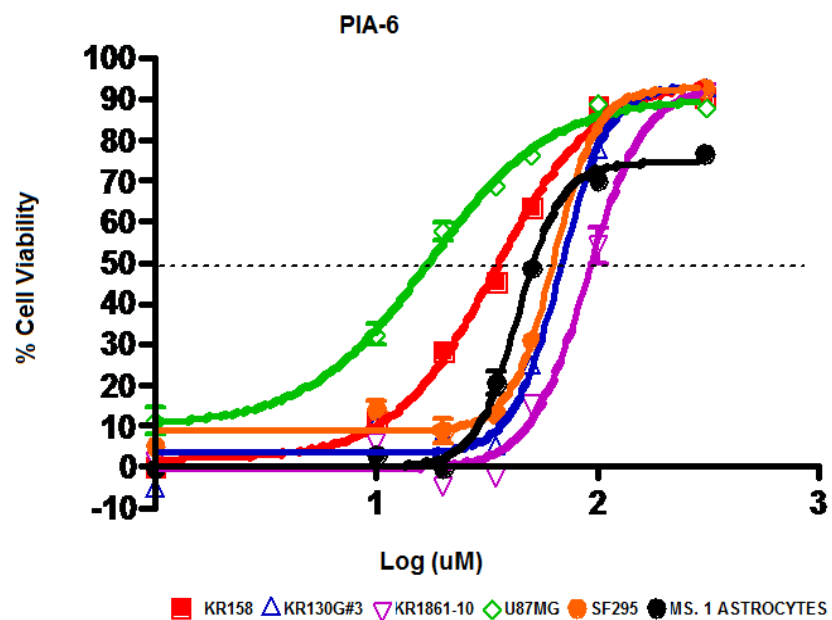


Figure 3.10: Effects of PIA6 on cell viability.

Effects of PIA-6 on cell viability of mouse and human astrocytoma cell lines as compared to control mouse primary astrocytes. Mouse and human cells were plated in a 96-well plate in complete growth media at 37°C for 24 hours and then treated with 300, 100, 30, 10, 3, 1, 0.1, 0 $\mu\text{Mol/L}$ PIA-6 inhibitor for 72 hours(D3). Cell viability was determined using the Alamar blue metabolic assay in triplicate and a representative experiment is shown from multiple experiments. The percentage of inhibition of cell viability was plotted against the logarithm dose of PIA-6. The IC_{50} value was defined as the concentration at which cell viability decreased by 50% and was calculated using GraphPad Prism. The IC_{50} value was shown as the means + standard deviation.

DISCUSSION

Our study of Perifosine, Chloroquine, Nelfinivir, PIA-6, and OSU-03012 demonstrate that these drugs are capable of inhibiting cell viability in mouse and human astrocytoma cell lines in a dose-dependent manner. Tested inhibitors varied in their ability to differentiate between astrocytoma cell lines and the non-proliferating control mouse primary astrocytes.

Some inhibitors were cytotoxic to some astrocytoma cell lines, but not others. This observation demonstrates the challenges of glioma therapy that has roots in the heterogeneity of gliomas. Importantly, the mouse astrocytoma cell lines tested have similar, defined genomic imbalance, a loss of heterozygosity of *Trp53* and *Nf1*. It may be expected that in the presence of a specific inhibitor these cell lines will respond to the inhibitor in a grade dependent manner. However, that was not the case, as tested astrocytoma cell lines were either sensitive or resistant (less sensitive) to an inhibitor, regardless of its tumor grade. Some reasons for this variability may include the acquired heterogeneity of the cell lines due to different secondary mutations present or the different pathways activated or deactivated in the cell lines, or the variance in drug metabolism.

One limitation of this study is that dysregulated pathways are subject to positive and negative feedback loops, cross talk and multiple nodes of interactions. This means that targeting a specific pathway known to be dysregulated in gliomas such as the PI3K/Akt pathway may activate feedback loops. This also implies that inhibiting one node or branch of the pathway with an inhibitor to shut down proliferation may actually

activate an effector molecule that causes increased activity in proliferation which can enhance tumor growth (Won, Yang et al. 2012). One possible way to overcome this limitation is to use combination therapy. This method of combination therapy will increase the chances of success in moving away from a cytostatic response to a cytotoxic response to include necrosis, apoptosis or autophagy, when inhibitors are combined *in vitro* and *in vivo* with other chemotherapy agents or with other modalities such as radiation and surgery.

CONCLUSION

In summary we have shown that Chloroquine, Nelfinivir, Perfosine, PIA-6, and OSU-03012 inhibit the cell viability of mouse and human astrocytoma cell lines *in vitro*. Relatively high concentrations required for cytotoxic effects of these compounds suggest that their effects on PI3K/Akt/mTOR signaling pathway are rather indirect. However, these five compounds may have further pre-clinical utility if assayed in combination therapies *in vitro*, as potential therapeutics in the arsenal to extend the life of GBM patients.

CHAPTER 4: PRE-CLINICAL EVALUATION OF SCHEINWEINFURTHIN AND ITS ANALOGUES

4.1 INTRODUCTION

Most brain tumor therapies to date have focused on molecularly targeted inhibitors of pathways known to be dysregulated in astrocytomas and glioblastomas (Chaplan, Eckert et al. 2010). However, in addition to the molecularly targeted inhibitors, there is interest in the use of natural products as antiglioma therapeutics. Natural products are the indigenous chemical compounds produced by plants, animals, and microbes or microorganism used to treat diseases (Koehn and Carter 2005; Gullo, McAlpine et al. 2006). Natural products tend to be very complex and vary in their biological activity (Beutler 2006). One main reason why natural products are important in the drug discovery process is that natural products may serve as the foundation for developing new drugs (Beutler 2006; Topczewski, Kuder et al. 2010). Of the 46 new molecular products approved by the FDA (Food and Drug Administration) in 2009-2010, twelve were of natural product origin (Zhu, Shi et al. 2012). In fact 60% of all new cancer drugs originate from natural sources (Gullo, McAlpine et al. 2006).

Some of the well-known plants that served as a source of anti-cancer compounds are *Catharanthus roseus*, *Camptothecin acuminata*, and *Taxus Brevifoila* (Kuder, Neighbors et al. 2009). For example, vincristine and vinblastine are the alkaloids from the

plant *Catharanthus roseus*. These drugs are important in treating Hodgkin's lymphoma, Ewing sarcoma, anaplastic large cell lymphoma and ependymomas in young children. Camptothecin was isolated from the plant *Camptothecin acuminata*. Two of its analogues, Topotecan and Irinotecan, are currently used in treating advanced ovarian, stomach, colorectal cancer and lung cancer as well as GBMs (Jeansonne, Koh et al. 2011). Camptothecin and its analogues inhibit DNA topoisomerase I, which results in blocking the DNA ligation step after the DNA strands have separated; hence, promoting cell death via apoptosis (Jeansonne, Koh et al. 2011). Paclitaxel, known by its trade name Taxol, was isolated from the bark of the Pacific yew tree *Taxus Brevifolia* (Kuder, Neighbors et al. 2009). Paclitaxel is used to treat cancers such as Kaposi's sarcoma, breast, lung, and non-small lung cell cancer (Beutler 2006), head, neck and ovarian cancer (Jeansonne, Koh et al. 2011). Paclitaxel and its analogues work by blocking cell mitosis, which stabilizes the microtubules, and which leads to cell cycle arrest, followed eventually by apoptosis (Jeansonne, Koh et al. 2011) (Topczewski, Kuder et al. 2010).

ORIGIN OF SCHWEINFURTHIN A

Schweinfurthin A (See Fig. 4.1) was identified from an organic extract obtained from the leaves of the plant *Macaranga schweinfurthin*, native to Cameroon, West Africa. In the *in vitro* NCI-60 cell line panel assay, the human glioblastoma cell line SF-295 showed sensitivity towards Schweinfurthin A with a GI₅₀ of 11 nM, and in the human glioblastoma cell line SF-539 with a GI₅₀ of 10 nM. However, the human lung adenocarcinoma cancer cell line A549 upon similar treatment with Schweinfurthin A was

resistant, with a GI_{50} of 2.2 $\mu\text{g/mL}$ (Rogers, Craker et al. 2006; Kuder 2009), or a calculated molarity of 4 μM .

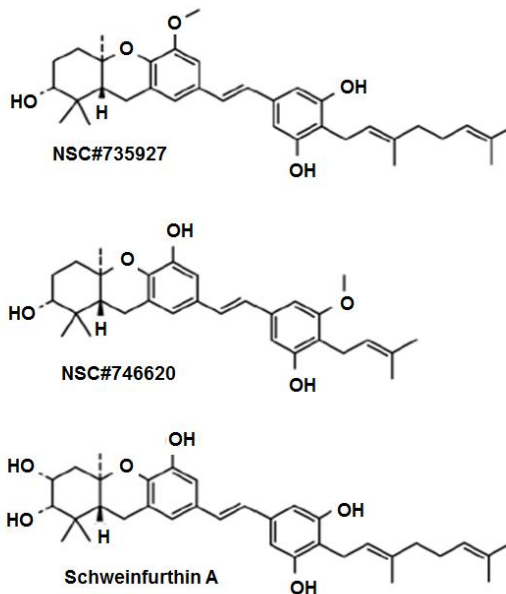


Figure 4.1: Diagram showing the structure of Schweinfurthin A. Top: NSC#735927-3dSB-Schweinfurthin B analogue. Middle: NSC#746620-Schweinfurthin analogue. Bottom: Schweinfurthin A.

The genus *Macaranga* is a large genus in the *Euphorbiaceae* family, located in many other parts of the world such as Loyalty Islands, New Caledonia native to *M. vedeliana*; *M. mappa* from Hawaii; and *M. alnifoila* from Madagascar (Beutler 2006; Rogers, Craker et al. 2006; Yoder, Cao et al. 2007). To date, the most famous family member, *Macaranga schweinfurthin* contains 9 natural plant members and approximately 50-75 Schweinfurthin analogues which have been developed or are being developed for use as potential chemotherapeutic agents in the fight against cancer (Kuder, Neighbors et al. 2009; Topczewski, Kuder et al. 2010). The three geranyl stilbenes originally extracted

from the leaves of the *Macaranga schweinfurthii* plant were named Schweinfurthin A, Schweinfurthin B, and Schweinfurthin C (Kuder, Neighbors et al. 2009). Schweinfurthins isolated from the *Macaranga alnifoila* native to Madagascar include the prenylated stilbenes Schweinfurthin-E, Schweinfurthin-F, Schweinfurthin-G and Schweinfurthin-H (Yoder and Cao 2007) . More recently, two additional stilbenes were isolated and purified from the leaves of the original Cameroonian *Macaranga schweinfurthin*, termed Schweinfurthin-I and Schweinfurthin-J (Klausmeyer, Van et al. 2010) (See Table 4.1). This source of Schweinfurthins A-J is not perpetual, and there is a legitimate concern that this natural product will someday become scarce (Beutler 2006; Rogers, Craker et al. 2006; Topczewski, Kuder et al. 2010). Therefore, there is an ongoing need to synthesize schweinfurthins in the lab and develop corresponding analogues (Topczewski, Kuder et al. 2010).

Table 4.1: Natural Schweinfurthin compounds and their analogues.

<i>Macaranga schweinfurthin</i>	<i>Macaranga alnifoila</i>	<i>Macaranga schweinfurthin</i>	Analogues of Schweinfurthin A
Schweinfurthin A	Schweinfurthin-E	Schweinfurthin -I	3dSB-NSC735927
Schweinfurthin B	Schweinfurthin-F	Schweinfurthin -J	NSC#746620
Schweinfurthin C	Schweinfurthin-G		
Schweinfurthin D	Schweinfurthin-H		

SCHWEINFURTHIN ANALOGUES

There are several reasons why it is important to synthesize analogues of natural schweinfurthins. These analogues can be used to determine the mechanism of action, toxicity and identify potential novel targets (Kuder, Neighbors et al. 2009), (Turbyville, Gursel et al. 2010), (Beutler 2006; Gullo, McAlpine et al. 2006; Rogers, Craker et al. 2006; Topczewski, Kuder et al. 2010). Additionally, analogues may serve as alternatives to natural products in cases of scarcity or increased demand. For example, analogues are indispensable when the supply of the natural product is limited due to scarcity at the source (Kuder, Neighbors et al. 2009; Topczewski, Kuder et al. 2010).

The University of Iowa (UI) has led the process of developing synthetic analogues of schweinfurthins, resulting in the successful production of approximately 75 synthetic analogues which are currently being used to (1) develop an understanding structure activity relationship for schweinfurthins, (2) to prepare materials on a 100 mg scale and (3) to examine the MTD or maximum tolerated dose in an *in vivo* assay (Reilly, Beutler et al. 2011). These noteworthy goals and projects may not have been amenable if SA and analogues were impossible to synthesize in the laboratory. Furthermore, analogues can be used to reduce the cost of the manufacturing process, by alleviating the need for collection and organic extraction of novel compounds from the natural product (Koehn and Carter 2005; Kuder 2009). Development and study of analogues also allows alteration of natural products aimed at increasing their potency, efficacy, and specificity, for instance, by the addition of select side groups and their modifications (Rogers, Craker et al. 2006; Kuder, Neighbors et al. 2009; Topczewski, Kuder et al. 2010). For example,

the addition of A-ring diol in the synthesized Schweinfurthin A analogues 35 and 37 resulted in an increase in their potency in SF-295 cells, as compared to the 3-deoxy synthesized compounds/ analogues 25 and 27 (Topczewski, Kuder et al. 2010).

In summary, it is vitally important to synthesize analogues of natural schweinfurthins and continue the ongoing efforts to develop and study analogues to further enhance the drug discovery process.

SCHWEINFURTHIN AS AN ATTRACTIVE DRUG CANDIDATE

Both the natural product Schweinfurthin A and its analogues have the potential as drug candidates due to their solubility in water (Koehn and Carter 2005; Chaplan, Eckert et al. 2010), chemical stability, ability to be absorbed from the digestive tract and biodistributed (Koehn and Carter 2005; Chaplan, Eckert et al. 2010), favorable molecular weight (less than 600) (Koehn and Carter 2005), total number of hydrogen donor/acceptor bonds (Koehn and Carter 2005), low number of rotatable bonds (Koehn and Carter 2005), a reduced polar surface area of 110.38\AA^2 (Veber, Johnson et al. 2002), acceptable toxicity/safety profile (Chaplan, Eckert et al. 2010) and scalability potential of its synthesis (Chaplan, Eckert et al. 2010). However, a molecular weight of 550 Da limits its use as an oral bioactive drug (Lipinski 2000). Also, for blood-brain barrier (BBB) permeability, a size of approximately 400 Da or less is recommended (Madsen and Hirschberg 2010). These features may limit possible applications of Schweinfurthin A as antiangioma therapy.

It was previously shown that Schweinfurthin A is selectively active towards SF-295 human glioblastoma cell lines and KR-158 mouse astrocytoma cell lines, as compared to normal mouse primary astrocytes (Turbyville, Gursel et al. 2010). In particular, Schweinfurthin A inhibits growth factor-stimulated Rho signaling (Turbyville, Gursel et al. 2010). In SF-295 cells, the treatment with 3dSB (Schweinfurthin A analogue) results in the cleavage of poly-ADP-ribose polymerase (PARP) and caspase-9, both markers of apoptosis (Kuder, Sheehy et al. 2012). Additionally, the phosphorylation of eukaryotic initiation factor 2 α , a known feature of cellular stress, occurs in response to 3dSB along with the upregulation of endoplasmic reticulum chaperones glucose-regulated protein 78 and protein disulfide isomerase (Kuder, Sheehy et al. 2012). The cytotoxic effects of 3dSB are enhanced in lipid depleted conditions (Holstein, Kuder et al. 2011). Moreover, 3dSB was found to enhance the lovastatin-induced decrease in protein prenylation, a known requirement for Ras-dependent proliferation of tumor cells. 3dSB decreases intracellular farnesyl pyrophosphate and geranylgeranyl pyrophosphate levels and modulates the homeostasis of isoprenoids (Holstein, Kuder et al. 2011).

In athymic nude mice subcutaneously injected with human SF-295 glioblastoma cells to form xenografts, the oral administration of Schweinfurthin A at a dose of 9.3 mg/kg lead to formation of smaller tumors in Schweinfurthin A-treated animals as compared to vehicle treated animals (Beutler et al, 2006). Recently, Schweinfurthin A and its analogues 3dSB (NSC#735927) and 620 (NSC#746620) were shown to traverse the BBB in a mouse pharmacokinetic study (Reilly, Beutler et al. 2011). Following intraperitoneal (IP) administration of 3dSB or Schweinfurthin A at 1 ug/mL, at 120 minutes

post-injection, peak concentrations of tested compounds in the mice brain decreased to approximately 0.01 ug/mL (1% starting level) and 0.1 ug/ml (10% starting level), for 3dSB and for Schweinfurthin A, respectively. In contrast, injection with analogue 620 led to peak plasma concentrations in the brain and increased up to 10 ug/mL (10-fold), suggestive of selective accumulation in the brain (unpublished data of Dr.Reilly lab).

4.2 MATERIALS AND METHODS

CULTURING OF WILD TYPE MOUSE PRIMARY ASTROCYTES

Primary astrocytes were collected grown and characterized essentially as described in Chapter 2.2

SCHWEINFURTHIN A AND ITS ANALOGUES

Schweinfurthin A and its analogues 3dSB (NSC#735927) and 620 (NSC#746620) were a generous gift.

ALAMAR BLUE METABOLIC ASSAYS AND IC50 AND GI50

CALCULATIONS

The human astrocytoma cell lines SF295, LN-18, U251,U118-MG and U87MG, the mouse astrocytoma cell lines K1861-10, KR158, and KR130G#3, and primary murine astrocytes were grown and tested essentially as described in Chapter 2.2.

4.2 RESULTS

SCHWEINFURTHIN A AFFECTS CELL VIABILITY IN SELECT MOUSE AND HUMAN ASTROCYTOMA CELL LINES

In Alamar blue cell viability assay, the mouse and human astrocytoma cell lines showed varying degrees of sensitivity toward Schweinfurthin A and its analogues. The activity of Schweinfurthin A in the mouse and human astrocytoma cell lines is presented in Table 4.2 and Fig. 4.2. Normal control mouse primary astrocytes had a GI₅₀ of 4.10 μM, while mouse astrocytoma cell line K130G#3 had a GI₅₀ value of 2.5 μM, suggesting that astrocytoma cell line was relatively more sensitive to Schweinfurthin A than normal astrocyte. The GI₅₀ was not achieved in mouse astrocytoma cell lines K1861-10 and KR158. Human astrocytoma cell line SF-295 was sensitive to Schweinfurthin A as indicated by its GI₅₀ value of 1.45. In contrast, human astrocytoma cell lines U251 with GI₅₀ value of 5.14 μM, LN-18 with GI₅₀ value of 7.38 μM and U118 MG with a GI₅₀ value of 9.24 μM were not sensitive to Schweinfurthin A a compared to both normal mouse primary astrocyte control with GI₅₀ of 4.10 μM. For the human U87-MG astrocytoma cell line, GI₅₀ was not achieved. Therefore, Schweinfurthin A showed the expected differential sensitivity towards the human SF-295 astrocytoma cell line as tested, and is in accordance with other published results (Rogers, Craker et al. 2006; Neighbors and Mente 2008), with GI₅₀ cytotoxicity values less than 1 μM. Statistical analyses were done using the one-way analysis of variance with Dunnett post-hoc test.

Table 4.2: The calculated IC₅₀, GI₅₀, and maximum percent inhibition of SA and select analogues tested with cell lines.

Inhibitor		Astrocytes	K1861	KR158	KR130	SF295	U87MG	LN-18	U251	U118-MG
		Mouse	Mouse	Mouse	Mouse	Human	Human	Human	Human	Human
		Normal	Grade II	Grade III	Grade IV					
Schweinfurthin-A	IC ₅₀	8.10µM	NA	5.64µM	NA	NA	4.04µM	7.41µM	8.25µM	8.79µM
	GI ₅₀	4.10µM	NA	NA	2.5µM	1.45µM	NA	7.38 µM	5.14µM	9.24µM
	Max%	83.89%	NA	63.7 %	NA	NA	NA	84.64%	94.37 %	85.44 %
3dSB SA analogue	IC ₅₀	NA	3.90µM	NA	10.02µM	4.31µM	NA	NA	NA	NA
	GI ₅₀	14.84µM	2.90µM	20.49µM	6.43µM	2.85µM	4.20µM	17.25µM	11.65µM	38.57µM
	Max%	NA	NA	NA	NA	NA	NA	NA	NA	NA
NSC#746620 SA analogue	IC ₅₀	NA	NA	NA	NA	NA	NA	NA	NA	NA
	GI ₅₀	10.75µM	7.07µM	NA	4.77µM	4.89µM	NA	10.61µM	9.48µM	NA
	Max%	NA	NA	84.67%	NA	NA	NA	NA	NA	NA

GI₅₀ values are represented as means and were calculated from a minimum of 3 independent experiments performed in triplicate with the Alamar blue cell viability metabolic assay. 2. NA-not available.

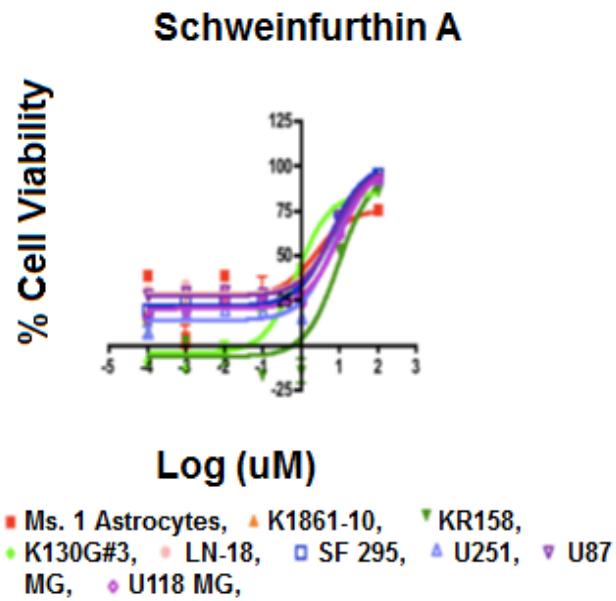


Figure 4.2: Effects of Schweinfurthin A on cell lines.

Schweinfurthin-A inhibits cell viability in mouse and human astrocytoma cell lines as compared to control mouse primary astrocytes. Cells were treated with 100, 10, 1, 0.1, 0.01, 0.001, 0.0001 μM SA inhibitor for 72 hours (D3).

EFFECTS OF SCHWEINFURTHIN ANALOGUE 3DSB ON SELECT MOUSE AND HUMAN ASTROCYTOMA CELL LINES

The data describing the activity of Schweinfurthin A analogue 3dSB (NSC#735927) in murine astrocytes and the mouse and human astrocytoma cell lines are presented in Table 4.2 and Fig. 4.3. In murine primary astrocytes, 3dSB demonstrated a GI₅₀ value of 14.84 μM, while in the mouse astrocytoma cell lines K1861-10 it demonstrated a GI₅₀ value of 2.90 μM and in K130G#3, a GI₅₀ value of 6.43 μM, showing glioma-specific differential sensitivity to the 3dSB analogue. Both human astrocytoma cell lines SF-295 and U87-MG were sensitive to the 3dSB analogue with a GI₅₀ value of 2.85 μM and 4.20 μM, respectively. The human astrocytoma cell line U251 with a GI₅₀ of 11.65 μM was also sensitive to 3dSB.

Importantly, the mouse astrocytoma cell line KR158 was substantially less sensitive to the 3dSB analogue with a GI₅₀ of 20.94 μM. Similarly, the human astrocytoma cell lines LN-18 with GI₅₀ of 17.25 μM and U118-MG with GI₅₀ of 38.57 μM, were even less sensitive to the 3dSB analogue than the mouse primary astrocyte control cells (GI₅₀ of 14.84 μM).

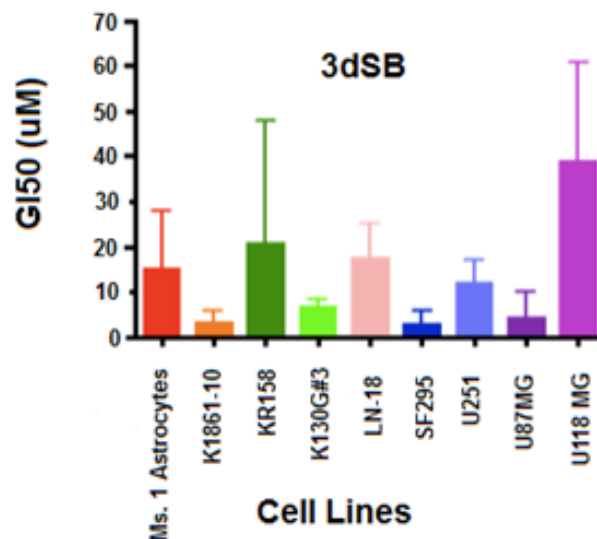


Figure 4.3: Calculated GI₅₀ values for 3dSB treated cell lines.

3dSB inhibits cell viability in mouse and human astrocytoma cell lines. Cells were treated with 100, 10, 1, 0.1, 0.01, 0.001, 0.0001 µM 3dSB inhibitor for 72 hours (D3). GI₅₀ values are represented as means±SD and were calculated from 3 independent experiments performed in triplicate with the Alamar blue cell viability metabolic assay.

EFFECTS OF SCHWEINFURTHIN ANALOGUE 620 (NSC#746620) ON MOUSE AND HUMAN ASTROCYTOMA CELL LINES

The data describing the activity of Schweinfurthin A analogue 620 (NSC#735927) in murine astrocytes and the mouse and human astrocytoma cell lines are presented in Table 4.2 and Fig. 4.4. In murine primary astrocytes, 620 demonstrated a GI₅₀ value of 10.75 µM, while in the mouse astrocytoma cell lines K1861-10 it demonstrated a GI₅₀ value of 7.1 µM and in K130G#3 a GI₅₀ value of 4.8 µM, showing glioma-specific differential sensitivity to the 620 analogue. In KR158 mouse astrocytoma cell line and in human astrocytoma cell lines U87-MG and U118-MG, GI₅₀ was not achieved. Human astrocytoma cell lines SF-295 was sensitive to the 620 analogue with a GI₅₀ value of 4.89 µM. The human astrocytoma cell line LN-18 with a

GI₅₀ of 10.61 μM was not sensitive to Schweinfurthin A analogue 620 (NSC#735927), and the human astrocytoma cell line U251 with GI₅₀ value of 9.48 μM demonstrated borderline sensitivity as compared to primary astrocytes (GI₅₀ value of 10.75 μM).

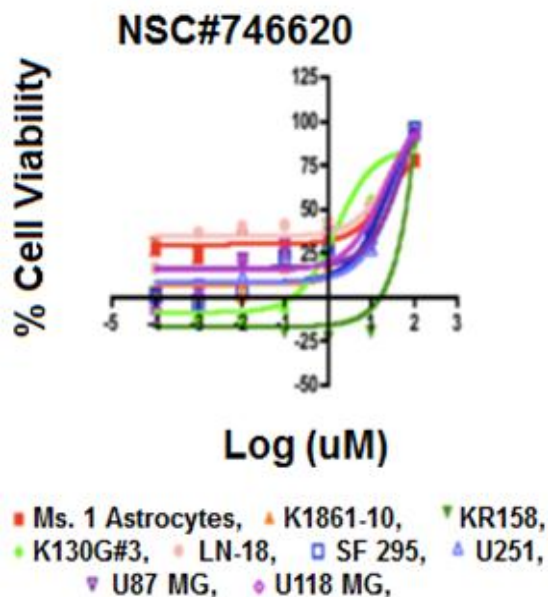


Figure 4.4: Effects of analogue NSC#746620 on cell viability.

NSC#746620 inhibits cell viability in mouse and human astrocytoma cell lines as compared to control mouse primary astrocytes. Cells were treated with 100, 10, 1, 0.1, 0.01, 0.001, 0.0001 μM NSC#746620 inhibitor for 72 hours (D3).

4.4 DISCUSSION

The natural plant product Schweinfurthin A and its analogues 3dSB (NSC#735927) and 620 (NSC#746620) demonstrate differential effects on cell viability in some of the mouse and human astrocytoma cell lines tested in Alamar blue cell viability metabolic assay. The Schweinfurthin A product was previously identified in the NCI-60 cell line panel as being cytostatic and cytotoxic in the CNS derived human

glioblastoma cell lines SF-295 and SF-539, while the lung cancer cell line A549 was resistant (Rogers, Craker et al. 2006; Beutler et al, 2006). Schweinfurthin A seems to be the more effective in inhibiting cell viability as compared to its analogues 3dSB (NSC#735927) and 620 (NSC#746620).

Among human and murine astrocytomas, SF-295 cells appears to be most sensitive to the the Schweinfurthin A and its analogues. Two mouse astrocytoma cell lines, K130G#3 and K1861-10, were also sensitive to all three inhibitors tested. Importantly, the observed effects of Schweinfurthin A in the mouse astrocytoma KR158 cell line were different from these previously reported by (Turbyville, Gursel et al. 2010). A possible explanation for this is the accumulation of the molecular changes in KR158 cell line or the difference in its substrains or that the fact that experimentation with this cell line was performed at different confluency. Any of these factors or their combination may have contributed to the differences in experimental results described in the current work versus the published study of Turbyville et al (Turbyville, Gursel et al. 2010).

One limitation of this study is that instead of human primary astrocytes we used primary murine astrocytes as controls. Obviously, species-specific differences in astrocyte sensitivities to Schweinfurthin and its analogues might be present. Further pre-clinical evaluations are necessary in order to ascertain the effects of Schweinfurthin A and its analogues as potential glioma therapeutics.

CONCLUSION

Schweinfurthin A and its analogues 3dSB (NSC#735927) and 620 (NSC#746620) are capable of inhibiting cell viability in some mouse and human astrocytoma cell lines. Whether this inhibition is mediated by direct cell killing (cytotoxic) or cytostatic effects remain unknown. Further pre-clinical *in vitro* and *in vivo* evaluations of Schweinfurthin A and its derivatives are warranted.

BIBLIOGRAPHY

Affronti, M. L., C. R. Heery, et al. (2009). "Overall survival of newly diagnosed glioblastoma patients receiving carmustine wafers followed by radiation and concurrent temozolomide plus rotational multiagent chemotherapy." Cancer **115**(15): 3501-3511.

Akhavan, D., T. F. Cloughesy, et al. (2010). "mTOR signaling in glioblastoma: lessons learned from bench to bedside." Neuro-oncology **12**(8): 882-889.

Al-Nasiry, S., N. Geusens, et al. (2007). "The use of Alamar Blue assay for quantitative analysis of viability, migration and invasion of choriocarcinoma cells." Human reproduction **22**(5): 1304-1309.

Ang, C., M. C. Guiot, et al. (2010). "Clinical significance of molecular biomarkers in glioblastoma." The Canadian journal of neurological sciences. Le journal canadien des sciences neurologiques **37**(5): 625-630.

Beutler, J. J., JG; Cragg, G; Wiemer, DF; Neighbors, JD; Salnikova, M; Hollingshead, M; Scudiero, DA; and McCloud, TG (2006). The Schweinfurthins. Medicinal and Aromatic Plants. R. J. B. L. E. C. a. D. Lange: 301-309.

Brennan, C., H. Momota, et al. (2009). "Glioblastoma subclasses can be defined by activity among signal transduction pathways and associated genomic alterations." PloS one **4**(11): e7752.

Bruning, A., K. Friese, et al. (2010). "Tamoxifen enhances the cytotoxic effects of nelfinavir in breast cancer cells." Breast cancer research : BCR **12**(4): R45.

Bruning, A., M. Rahmeh, et al. (2010). "The mitochondria-independent cytotoxic effect of nelfinavir on leukemia cells can be enhanced by sorafenib-mediated mcl-1 downregulation and mitochondrial membrane destabilization." Molecular cancer **9**: 19.

Cen, L., F. C. Hsieh, et al. (2007). "PDK-1/AKT pathway as a novel therapeutic target in rhabdomyosarcoma cells using OSU-03012 compound." British journal of cancer **97**(6): 785-791.

Chaplan, S. R., I. W. Eckert, et al. (2010). Drug Discovery and Development for Pain. Translational Pain Research: From Mouse to Man. L. Kruger and A. R. Light. Boca Raton, FL.

Choe, G., S. Horvath, et al. (2003). "Analysis of the phosphatidylinositol 3'-kinase signaling pathway in glioblastoma patients in vivo." Cancer research **63**(11): 2742-2746.

Cloughesy, T. F., K. Yoshimoto, et al. (2008). "Antitumor activity of rapamycin in a Phase I trial for patients with recurrent PTEN-deficient glioblastoma." PLoS medicine **5**(1): e8.

Daginakatte, G. C. and D. H. Gutmann (2007). "Neurofibromatosis-1 (Nf1) heterozygous brain microglia elaborate paracrine factors that promote Nf1-deficient astrocyte and glioma growth." Human molecular genetics **16**(9): 1098-1112.

David N. Louis, H. O., Otmar D. Wiesler, Webster K. Cavenee (2007). World Health Organization Classification of Tumors of the Central Nervous System Lyon, International Agency for Research on Cancer.

Ding, Q., R. Gu, et al. (2013). "PI-103 sensitizes acute myeloid leukemia stem cells to daunorubicin-induced cytotoxicity." Medical oncology **30**(1): 395.

Fayard, E., G. Xue, et al. (2010). "Protein kinase B (PKB/Akt), a key mediator of the PI3K signaling pathway." Current topics in microbiology and immunology **346**: 31-56.

Fei, H. R., G. Chen, et al. (2010). "Perifosine induces cell cycle arrest and apoptosis in human hepatocellular carcinoma cell lines by blockade of Akt phosphorylation." Cytotechnology **62**(5): 449-460.

Fortin, D., A. Desjardins, et al. (2005). "Enhanced chemotherapy delivery by intraarterial infusion and blood-brain barrier disruption in malignant brain tumors: the Sherbrooke experience." Cancer **103**(12): 2606-2615.

Fu, L., Y. A. Kim, et al. (2009). "Perifosine inhibits mammalian target of rapamycin signaling through facilitating degradation of major components in the mTOR axis and induces autophagy." Cancer research **69**(23): 8967-8976.

Gallia, G. L., B. M. Tyler, et al. (2009). "Inhibition of Akt inhibits growth of glioblastoma and glioblastoma stem-like cells." Molecular cancer therapeutics **8**(2): 386-393.

Gao, M., P. Y. Yeh, et al. (2008). "OSU-03012, a novel celecoxib derivative, induces reactive oxygen species-related autophagy in hepatocellular carcinoma." Cancer research **68**(22): 9348-9357.

Gao, Y., H. Ishiyama, et al. (2011). "The alkylphospholipid, perifosine, radiosensitizes prostate cancer cells both in vitro and in vivo." Radiation oncology **6**: 39.

Garrett, J. T., A. Chakrabarty, et al. (2011). "Will PI3K pathway inhibitors be effective as single agents in patients with cancer?" Oncotarget **2**(12): 1314-1321.

Gavilan, M. P., A. Castano, et al. (2009). "Age-related increase in the immunoproteasome content in rat hippocampus: molecular and functional aspects." Journal of neurochemistry **108**(1): 260-272.

Gills, J. J., J. Lopiccio, et al. (2008). "Nelfinavir, a new anti-cancer drug with pleiotropic effects and many paths to autophagy." Autophagy **4**(1): 107-109.

Gloesenkamp, C. R., B. Nitzsche, et al. (2012). "AKT inhibition by triciribine alone or as combination therapy for growth control of gastroenteropancreatic neuroendocrine tumors." International journal of oncology **40**(3): 876-888.

Goellner, E. M., B. Grimme, et al. (2011). "Overcoming temozolomide resistance in glioblastoma via dual inhibition of NAD⁺ biosynthesis and base excision repair." Cancer research **71**(6): 2308-2317.

Grzmił, M. and B. A. Hemmings (2010). "Deregulated signalling networks in human brain tumours." Biochim Biophys Acta **1804**(3): 476-483.

Gschwind, A., O. M. Fischer, et al. (2004). "The discovery of receptor tyrosine kinases: targets for cancer therapy." Nat Rev Cancer **4**(5): 361-370.

Gullo, V. P., J. McAlpine, et al. (2006). "Drug discovery from natural products." Journal of industrial microbiology & biotechnology **33**(7): 523-531.

Gursel, D. B., Y. S. Connell-Albert, et al. (2011). "Control of proliferation in astrocytoma cells by the receptor tyrosine kinase/PI3K/AKT signaling axis and the use of PI-103 and TCN as potential anti-astrocytoma therapies." Neuro-oncology **13**(6): 610-621.

Hamid, R., Y. Rotshteyn, et al. (2004). "Comparison of alamar blue and MTT assays for high through-put screening." Toxicology in vitro : an international journal published in association with BIBRA **18**(5): 703-710.

Harrison, C. (2011). "Signatures for drug repositioning." Nature reviews. Genetics **12**(10): 668.

Hawes, J. J. and K. M. Reilly (2010). "Bioluminescent approaches for measuring tumor growth in a mouse model of neurofibromatosis." Toxicologic pathology **38**(1): 123-130.

He, Z., L. Qin, et al. (2008). "Synergy of human immunodeficiency virus protease inhibitors with chloroquine against Plasmodium falciparum in vitro and Plasmodium chabaudi in vivo." Antimicrobial agents and chemotherapy **52**(7): 2653-2656.

Hegedus, B., D. Banerjee, et al. (2008). "Preclinical cancer therapy in a mouse model of neurofibromatosis-1 optic glioma." Cancer research **68**(5): 1520-1528.

Hoffman, K., F. A. Holmes, et al. (1996). "Phase I-II study: triciribine (tricyclic nucleoside phosphate) for metastatic breast cancer." Cancer chemotherapy and pharmacology **37**(3): 254-258.

Holstein, S. A., C. H. Kuder, et al. (2011). "Pleiotropic effects of a schweinfurthin on isoprenoid homeostasis." Lipids **46**(10): 907-921.

Hu, J., C. Jiang, et al. (2003). "Genome-wide allelotype study of primary glioblastoma multiforme." Chin Med J (Engl) **116**(4): 577-583.

Huse, J. T. and E. C. Holland (2009). "Genetically engineered mouse models of brain cancer and the promise of preclinical testing." Brain pathology **19**(1): 132-143.

Inda, M. M., R. Bonavia, et al. (2010). "Tumor heterogeneity is an active process maintained by a mutant EGFR-induced cytokine circuit in glioblastoma." Genes & development **24**(16): 1731-1745.

Ino, Y., J. S. Silver, et al. (1999). "Common regions of deletion on chromosome 22q12.3-q13.1 and 22q13.2 in human astrocytomas appear related to malignancy grade." J Neuropathol Exp Neurol **58**(8): 881-885.

Jeansonne, D. P., G. Y. Koh, et al. (2011). "Paclitaxel-induced apoptosis is blocked by camptothecin in human breast and pancreatic cancer cells." Oncol Rep **25**(5): 1473-1480.

Jimenez, S., D. Baglietto-Vargas, et al. (2008). "Inflammatory response in the hippocampus of PS1M146L/APP751SL mouse model of Alzheimer's disease: age-dependent switch in the microglial phenotype from alternative to classic." The Journal of neuroscience : the official journal of the Society for Neuroscience **28**(45): 11650-11661.

Kapoor, G. S., A. Christie, et al. (2007). "EGFR inhibition in glioblastoma cells induces G2/M arrest and is independent of p53." Cancer Biol Ther **6**(4): 571-579.

Karkan, D., C. Pfeifer, et al. (2008). "A unique carrier for delivery of therapeutic compounds beyond the blood-brain barrier." PloS one **3**(6): e2469.

Kim, Y. W., T. J. Liu, et al. (2011). "Identification of novel synergistic targets for rational drug combinations with PI3 kinase inhibitors using siRNA synthetic lethality screening against GBM." Neuro-oncology **13**(4): 367-375.

Klausmeyer, P., Q. N. Van, et al. (2010). "Schweinfurthins I and J from *Macaranga schweinfurthii*." J Nat Prod **73**(3): 479-481.

Koehn, F. E. and G. T. Carter (2005). "Rediscovering natural products as a source of new drugs." Discovery medicine **5**(26): 159-164.

Krakstad, C. and M. Chekenya (2010). "Survival signalling and apoptosis resistance in glioblastomas: opportunities for targeted therapeutics." Molecular cancer **9**: 135.

Kreisberg, J. I., S. N. Malik, et al. (2004). "Phosphorylation of Akt (Ser473) is an excellent predictor of poor clinical outcome in prostate cancer." Cancer research **64**(15): 5232-5236.

Kucab, J. E., C. Lee, et al. (2005). "Celecoxib analogues disrupt Akt signaling, which is commonly activated in primary breast tumours." Breast cancer research : BCR **7**(5): R796-807.

Kuder, C. H. (2009). Schweinfurthins as novel anticancer agents. PhD, University of Iowa.

Kuder, C. H., J. D. Neighbors, et al. (2009). "Synthesis and biological activity of a fluorescent schweinfurthin analogue." Bioorganic & medicinal chemistry **17**(13): 4718-4723.

Kuder, C. H., R. M. Sheehy, et al. (2012). "Functional evaluation of a fluorescent schweinfurthin: mechanism of cytotoxicity and intracellular quantification." Molecular pharmacology **82**(1): 9-16.

Kunwar, S., S. Chang, et al. (2010). "Phase III randomized trial of CED of IL13-PE38QQR vs Gliadel wafers for recurrent glioblastoma." Neuro-oncology **12**(8): 871-881.

Kyritsis, A. P., M. L. Bondy, et al. (2010). "Inherited predisposition to glioma." Neuro Oncol **12**(1): 104-113.

Larjavaara, S., R. Mantyla, et al. (2007). "Incidence of gliomas by anatomic location." Neuro-oncology **9**(3): 319-325.

Lathia, J. D., J. Gallagher, et al. (2010). "Integrin alpha 6 regulates glioblastoma stem cells." Cell stem cell **6**(5): 421-432.

Lei, L., A. M. Sonabend, et al. (2011). "Glioblastoma models reveal the connection between adult glial progenitors and the proneural phenotype." PloS one **6**(5): e20041.

Li, Z., F. Tan, et al. (2010). "In vitro and in vivo inhibition of neuroblastoma tumor cell growth by AKT inhibitor perifosine." Journal of the National Cancer Institute **102**(11): 758-770.

Lim, S. K., S. R. Llaguno, et al. (2011). "Glioblastoma multiforme: a perspective on recent findings in human cancer and mouse models." BMB reports **44**(3): 158-164.

Lipinski, C. A. (2000). "Drug-like properties and the causes of poor solubility and poor permeability." Journal of pharmacological and toxicological methods **44**(1): 235-249.

Lipinski, C. A., F. Lombardo, et al. (2001). "Experimental and computational approaches to estimate solubility and permeability in drug discovery and development settings." Advanced drug delivery reviews **46**(1-3): 3-26.

LoRusso, P. M. (2013). "Mammalian target of rapamycin as a rational therapeutic target for breast cancer treatment." Oncology **84**(1): 43-56.

LoRusso, P. M., A. B. Anderson, et al. (2010). "Making the investigational oncology pipeline more efficient and effective: are we headed in the right direction?" Clinical cancer research : an official journal of the American Association for Cancer Research **16**(24): 5956-5962.

Ma, W., H. Hui, et al. (2009). "Pharmacological characterization of pannexin-1 currents expressed in mammalian cells." J Pharmacol Exp Ther **328**(2): 409-418.

Madsen, S. J. and H. Hirschberg (2010). "Site-specific opening of the blood-brain barrier." Journal of biophotonics **3**(5-6): 356-367.

Maher, E. A., C. Brennan, et al. (2006). "Marked genomic differences characterize primary and secondary glioblastoma subtypes and identify two distinct molecular and clinical secondary glioblastoma entities." Cancer research **66**(23): 11502-11513.

Maycotte, P., S. Aryal, et al. (2012). "Chloroquine sensitizes breast cancer cells to chemotherapy independent of autophagy." Autophagy **8**(2): 200-212.

McBride, S. M., D. A. Perez, et al. (2010). "Activation of PI3K/mTOR pathway occurs in most adult low-grade gliomas and predicts patient survival." Journal of neuro-oncology **97**(1): 33-40.

McGillicuddy, L. T., J. A. Fromm, et al. (2009). "Proteasomal and genetic inactivation of the NF1 tumor suppressor in gliomagenesis." Cancer cell **16**(1): 44-54.

Mercer, R. W., M. A. Tyler, et al. (2009). "Targeted therapies for malignant glioma: progress and potential." BioDrugs : clinical immunotherapeutics, biopharmaceuticals and gene therapy **23**(1): 25-35.

Molina, J. R., Y. Hayashi, et al., Eds. (2010). Invasive glioblastoma cells acquire stemness and increased Akt activation. Neoplasia.

Momota, H., E. Nerio, et al. (2005). "Perifosine inhibits multiple signaling pathways in glial progenitors and cooperates with temozolomide to arrest cell proliferation in gliomas in vivo." Cancer research **65**(16): 7429-7435.

Mueller, S., M. Y. Polley, et al. (2011). "Effect of imaging and catheter characteristics on clinical outcome for patients in the PRECISE study." Journal of neuro-oncology **101**(2): 267-277.

Neighbors, J. D. and N. R. Mente (2008). "Synthesis of the Schweinfurthin hexahydroxanthene core through Shi epoxidation." Tetrahedron Letters **49**: 516-519.

Ohka, F., A. Natsume, et al. (2012). "Current trends in targeted therapies for glioblastoma multiforme." Neurology research international **2012**: 878425.

Ozawa, T., C. W. Brennan, et al. (2010). "PDGFRA gene rearrangements are frequent genetic events in PDGFRA-amplified glioblastomas." Genes & development **24**(19): 2205-2218.

Park, M. A., A. Yacoub, et al. (2008). "OSU-03012 stimulates PKR-like endoplasmic reticulum-dependent increases in 70-kDa heat shock protein expression, attenuating its lethal actions in transformed cells." Molecular pharmacology **73**(4): 1168-1184.

Park, S., N. Chapuis, et al. (2008). "PI-103, a dual inhibitor of Class IA phosphatidylinositide 3-kinase and mTOR, has antileukemic activity in AML." Leukemia : official journal of the Leukemia Society of America, Leukemia Research Fund, U.K **22**(9): 1698-1706.

Parsons, D. W., S. Jones, et al. (2008). "An integrated genomic analysis of human glioblastoma multiforme." Science **321**(5897): 1807-1812.

Patel, M., M. A. Vogelbaum, et al. (2012). "Molecular targeted therapy in recurrent glioblastoma: current challenges and future directions." Expert opinion on investigational drugs **21**(9): 1247-1266.

Paternot, S. and P. P. Roger (2009). "Combined inhibition of MEK and mammalian target of rapamycin abolishes phosphorylation of cyclin-dependent kinase 4 in glioblastoma cell lines and prevents their proliferation." Cancer research **69**(11): 4577-4581.

Pruilla, M., A. Calastretti, et al. (2007). "Preferential chemosensitization of PTEN-mutated prostate cells by silencing the Akt kinase." Prostate **67**(7): 782-789.

Puli, S., A. Jain, et al. (2010). "Effect of combination treatment of rapamycin and isoflavones on mTOR pathway in human glioblastoma (U87) cells." Neurochemical research **35**(7): 986-993.

Pyrko, P., A. Kardosh, et al. (2007). "HIV-1 protease inhibitors nelfinavir and atazanavir induce malignant glioma death by triggering endoplasmic reticulum stress." Cancer research **67**(22): 10920-10928.

Rainov, N. G. and V. Heidecke (2011). "Clinical development of experimental virus-mediated gene therapy for malignant glioma." Anti-cancer agents in medicinal chemistry **11**(8): 739-747.

Rascher, G., A. Fischmann, et al. (2002). "Extracellular matrix and the blood-brain barrier in glioblastoma multiforme: spatial segregation of tenascin and agrin." Acta neuropathologica **104**(1): 85-91.

Reilly, K. M., J. A. Beutler, et al. (2011). Schweinfurthin Analogs PK in mice brain concentrations.

Reilly, K. M., R. G. Tuskan, et al. (2004). "Susceptibility to astrocytoma in mice mutant for Nf1 and Trp53 is linked to chromosome 11 and subject to epigenetic effects." Proceedings of the National Academy of Sciences of the United States of America **101**(35): 13008-13013.

Rey, J. A., M. J. Bello, et al. (1993). "Abnormalities of chromosome 22 in human brain tumors determined by combined cytogenetic and molecular genetic approaches." Cancer Genet Cytogenet **66**(1): 1-10.

Riddick, G., H. Song, et al. (2011). "Predicting in vitro drug sensitivity using Random Forests." Bioinformatics **27**(2): 220-224.

Riemenschneider, M. J. and G. Reifenberger (2009). "Molecular neuropathology of gliomas." Int J Mol Sci **10**(1): 184-212.

Rivera, A. L. and C. E. Pelloski (2010). "Diagnostic and prognostic molecular markers in common adult gliomas." Expert review of molecular diagnostics **10**(5): 637-649.

Rivera, A. L. and C. E. Pelloski (2010). "Diagnostic and prognostic molecular markers in common adult gliomas." Expert Rev Mol Diagn **10**(5): 637-649.

Rogers, B. J., L. E. Craker, et al., Eds. (2006). Medicinal and Aromatic Plants. The Schweinfurthins.

Ruano, Y., M. Mollejo, et al. (2008). "Identification of survival-related genes of the phosphatidylinositol 3'-kinase signaling pathway in glioblastoma multiforme." Cancer **112**(7): 1575-1584.

Sathornsumetee, S., D. A. Reardon, et al. (2007). "Molecularly targeted therapy for malignant glioma." Cancer **110**(1): 13-24.

Schilcher, R. B., C. D. Haas, et al. (1986). "Phase I evaluation and clinical pharmacology of tricyclic nucleoside 5'-phosphate using a weekly intravenous regimen." Cancer research **46**(6): 3147-3151.

Staunton, J. E., D. K. Slonim, et al. (2001). "Chemosensitivity prediction by transcriptional profiling." Proceedings of the National Academy of Sciences of the United States of America **98**(19): 10787-10792.

Stiles, C. D. and D. H. Rowitch (2008). "Glioma stem cells: a midterm exam." Neuron **58**(6): 832-846.

Swamidass, S. J. (2011). "Mining small-molecule screens to repurpose drugs." Briefings in bioinformatics **12**(4): 327-335.

Tabellini, G., P. L. Tazzari, et al. (2004). "Novel 2'-substituted, 3'-deoxy-phosphatidyl-myo-inositol analogues reduce drug resistance in human leukaemia cell lines with an activated phosphoinositide 3-kinase/Akt pathway." British journal of haematology **126**(4): 574-582.

Theeler, B. J. and M. D. Groves (2011). "High-grade gliomas." Current treatment options in neurology **13**(4): 386-399.

Thumma, S. R., R. K. Fairbanks, et al. (2012). "Effect of pretreatment clinical factors on overall survival in glioblastoma multiforme: a Surveillance Epidemiology and End Results (SEER) population analysis." World journal of surgical oncology **10**(1): 75.

To, K., Y. Zhao, et al. (2007). "The phosphoinositide-dependent kinase-1 inhibitor 2-amino-N-[4-[5-(2-phenanthrenyl)-3-(trifluoromethyl)-1H-pyrazol-1-yl]phenyl]-ace tamide (OSU-03012) prevents Y-box binding protein-1 from inducing epidermal growth factor receptor." Molecular pharmacology **72**(3): 641-652.

Topczewski, J. J., C. H. Kuder, et al. (2010). "Fluorescent schweinfurthin B and F analogs with anti-proliferative activity." Bioorganic & medicinal chemistry **18**(18): 6734-6741.

Turbyville, T. J., D. B. Gursel, et al. (2010). "Schweinfurthin A selectively inhibits proliferation and Rho signaling in glioma and neurofibromatosis type 1 tumor cells in a NF1-GRD-dependent manner." Molecular cancer therapeutics **9**(5): 1234-1243.

Van Meir, E. G., C. G. Hadjipanayis, et al. (2010). "Exciting new advances in neuro-oncology: the avenue to a cure for malignant glioma." CA: a cancer journal for clinicians **60**(3): 166-193.

Veber, D. F., S. R. Johnson, et al. (2002). "Molecular properties that influence the oral bioavailability of drug candidates." Journal of medicinal chemistry **45**(12): 2615-2623.

Vitucci, M., D. N. Hayes, et al. (2011). "Gene expression profiling of gliomas: merging genomic and histopathological classification for personalised therapy." British journal of cancer **104**(4): 545-553.

Wang, Y., R. Q. Peng, et al. (2011). "Chloroquine enhances the cytotoxicity of topotecan by inhibiting autophagy in lung cancer cells." Chinese journal of cancer **30**(10): 690-700.

Wei, Q., L. Clarke, et al. (2006). "High-grade glioma formation results from postnatal pten loss or mutant epidermal growth factor receptor expression in a transgenic mouse glioma model." Cancer research **66**(15): 7429-7437.

Westhoff, M. A., J. A. Kandenwein, et al. (2009). "The pyridinylfuranopyrimidine inhibitor, PI-103, chemosensitizes glioblastoma cells for apoptosis by inhibiting DNA repair." Oncogene **28**(40): 3586-3596.

Wiencke, J. K., S. Zheng, et al. (2007). "Methylation of the PTEN promoter defines low-grade gliomas and secondary glioblastoma." Neuro-oncology **9**(3): 271-279.

Won, J.-K., H. W. Yang, et al. (2012). "The crossregulation between ERK and PI3K signaling pathways determines the tumoricidal efficacy of MEK inhibitor." Journal of Molecular Cell Biology **4**: 153-163.

Xie, L., T. Evangelidis, et al. (2011). "Drug discovery using chemical systems biology: weak inhibition of multiple kinases may contribute to the anti-cancer effect of nelfinavir." PLoS computational biology **7**(4): e1002037.

Yacoub, A., M. A. Park, et al. (2006). "OSU-03012 promotes caspase-independent but PERK-, cathepsin B-, BID-, and AIF-dependent killing of transformed cells." Molecular pharmacology **70**(2): 589-603.

Yoder, B. J., S. Cao, et al. (2007). "Antiproliferative prenylated stilbenes and flavonoids from *Macaranga alnifolia* from the Madagascar rainforest." J Nat Prod **70**(3): 342-346.

Yoder, B. J. and S. e. a. Cao (2007). "Cytotoxic prenylated stilbenes and flavonoids from *Macaranga alnifolia* from the Madagascar rainforest." J. Nat. Prod. **70**(3): 342-346.

Yuan, X., J. Curtin, et al. (2004). "Isolation of cancer stem cells from adult glioblastoma multiforme." Oncogene **23**(58): 9392-9400.

Zhang, C., A. G. Elkahloun, et al. (2011). "Expression signatures of the lipid-based Akt inhibitors phosphatidylinositol ether lipid analogues in NSCLC cells." Molecular cancer therapeutics **10**(7): 1137-1148.

Zhang, H.Y., P.N. Zhang, et al. (2009). "Aberration of the PI3K/AKT/mTOR signaling in epithelial ovarian cancer and its implications in cisplatin-based chemotherapy." Eur J Obstet Gynecol Reprod Biol **146**(1): 81-6.

Zhang, J. H., T. D. Chung, et al. (1999). "A Simple Statistical Parameter for Use in Evaluation and Validation of High Throughput Screening Assays." Journal of biomolecular screening **4**(2): 67-73.

Zhang, L., X. Mu, et al. (2007). "In vitro cytotoxicity assay with selected chemicals using human cells to predict target-organ toxicity of liver and kidney." Toxicology in vitro : an international journal published in association with BIBRA **21**(4): 734-740.

Zhang, M., R. L. Atkinson, et al. (2010). "Selective targeting of radiation-resistant tumor-initiating cells." Proceedings of the National Academy of Sciences of the United States of America **107**(8): 3522-3527.

Zhang, S., A. Suvannasankha, et al. (2007). "OSU-03012, a novel celecoxib derivative, is cytotoxic to myeloma cells and acts through multiple mechanisms." Clinical cancer research : an official journal of the American Association for Cancer Research **13**(16): 4750-4758.

Zhu, F., Z. Shi, et al. (2012). "Therapeutic target database update 2012: a resource for facilitating target-oriented drug discovery." Nucleic acids research **40**(Database issue): D1128-1136.

Zou, Z. Q., X. H. Zhang, et al. (2009). "A novel dual PI3K α /mTOR inhibitor PI-103 with high antitumor activity in non-small cell lung cancer cells." International journal of molecular medicine **24**(1): 97-101.

<http://www.unmc.edu/biochemistry>

<http://www.chemspider.com/>

<http://www.graphpadprism.com>

<http://www.NetPhos.com>

<http://www.rembrandt.nci.nih.gov/>

<http://PubChem.ncbi.nlm.nih.gov>

<http://www.clinicaltrials.gov>

<http://genome.ucsc.edu>

<http://www.Qiagen.com>

<http://www.Invitrogen.com>

APPENDIX

THE ROLE OF PANNEXINS IN INTERCELLULAR COMMUNICATION AND THE IMPLICATIONS FOR GLIOMAGENESIS

A1. INTRODUCTION

Intercellular communication is important in signal transduction, survival and death processes, and occurs via two distinct mechanisms, by the release of molecules such as neurotransmitters, hormones or ATP into the synaptic cleft, termed paracrine intercellular communication (PIC), or by gap junction intercellular communication (GJIC) (Boassa, Ambrosi et al. 2007). Gap junctions are intercellular channels that allow the passage of small ions and molecules between the adjacent cells (Musil and Goodenough 1991). These channels are formed by the docking of two hemi-channels in contacting plasma membranes, resulting in conduits between the cytoplasmic compartments (Asklund, Appelskog et al. 2004). Gap junction channels mediate the exchange of both the ions such as Na⁺, K⁺, Ca²⁺, and the small hydrophilic molecules such as glucose, glutamate, glutathione, IP₃ (inositol triphosphate or 1,4, 5-triphosphate), cyclic AMP (cyclic adenosine monophosphate), and ATP (adenosine triphosphate). The mechanism of this is speculated to be dependent upon passive diffusion along a concentration gradient (Nagasawa, Chiba et al. 2006).

The pioneering work by W.R. Loewenstein (Loewenstein 1979) observed that hepatic tumor cells are deficient in intercellular ionic exchange, as compared to electrically coupled normal cells. This led to the hypothesis that the absence or

suppression of gap junctions is a pre-requisite for uncontrolled cell growth. A number of tumorigenic cell lines do not communicate with normal cells, and tumorigenic cells also lack intercellular communication, thereby supporting Loewenstein's hypothesis (Mesnil, Crespin et al. 2005; Taberner, Medina et al. 2006). Gap junction intercellular communication propagates cell death in cancerous cells (Krutovskikh, Piccoli et al. 2002). In breast cancer, the metastatic potential correlates with a breakdown in gap junction intercellular communication (Saunders, Seraj et al. 2001). In fact, the great majority of the disseminated cancer cells fail to develop heterotypic cell adhesion in distant organs, and remain metastatically dormant as single cells (Rubin 2008).

Importantly, gap junction channels (GJC) are downregulated in gliomas and several other tumor types. For example, the expression of astrocytic gap junction protein connexin43 (Cx43), is often reduced in astrocytomas and is advantageous for the growth of glioma cells (Mesnil, Crespin et al. 2005; Sin, Crespin et al. 2012).

FAMILIES OF GAP JUNCTION PROTEINS

There are two unrelated gene families that encode gap junction forming proteins, termed the innexins and the connexins. Innexins, or **Invertebrate connexin** analogs, are found in Protostomes, including all invertebrates. Genome sequencing projects have identified 8 innexin genes in the fruit fly, *Drosophila*; approximately 25 innexin genes in the nematode *C. elegans* and several innexin genes in other invertebrate species (Lehmann, Lechner et al. 2006; Scemes, Suadicani et al. 2007).

The connexins family code for the closely related integral membrane proteins involved in gap junction formation in Deuterostomes (Musil and Goodenough 1991). There are 20 connexin genes in mice and 21 connexin genes in humans (Lehmann, Lechner et al. 2006; Scemes, Suadicani et al. 2007).

The pannexins, named from the Greek word pan, “throughout” or “all” and the Latin nexus, “connection”, have sequence homology to the invertebrate gap junction proteins, the innexins, and structural homology to the vertebrate family of gap junction proteins, the connexins (Panchin, Kelmanson et al. 2000; Litvin, Tiunova et al. 2006; Swayne, Sorbara et al. 2010) . Pannexins are found in both vertebrates and invertebrates (Lehmann, Lechner et al. 2006; Boassa, Ambrosi et al. 2007; Scemes, Suadicani et al. 2007). In both human and rodent genomes, the pannexin gene family consists of 3 members and are extremely conservative. In humans, these proteins are termed PANX1 (426 amino acids and MW of 47.6), PANX2 (664 amino acids and MW of 73.3 kDa), and PANX3 (392 amino acids and MW of 44.7 kDa) (See Figure A-1).

Pannexins are abundantly expressed in both mouse and human tissues. For example, Panx1 is abundantly expressed in skin, heart, muscle, ovary, brain and erythrocytes; Panx3 is expressed in and plays a role in the differentiation of osteoblasts and hypertrophic chondrocytes, and the maturation and transport of sperms; while Panx2 is abundantly expressed in the CNS, its function is still not clear (Litvin, Tiunova et al. 2006; Celetti, Cowan et al. 2010; Bond, Lau et al. 2011; Penuela, Gehi et al. 2013). Details on the size and genomic structure of human and murine pannexin-encoding genes are summarized in Table A1.

PANNEXINS STRUCTURE IS SIMILAR TO THAT OF OTHER GAP JUNCTION PROTEINS

Both innexins and connexins contain four trans-membrane domains, with two extracellular loops, one cytoplasmic loop and cytoplasmic N and C termini (Lehmann, Lechner et al. 2006; Huang, Maruyama et al. 2007). (See Figure A-2).

The extracellular loops of the connexins contain three conserved cysteine residues, while extracellular loops of innexins and pannexins contain two conserved cysteine residues (See Figure A-1, closed circles). The cysteine residues are important as they form and maintain strong interactions between the hemi-channels, and contribute to the integrity of the gap junction by preventing the leakage of molecules and currents into the extracellular space (Scemes, Suadicani et al. 2007).

Table A.1A: Comparison of the genomic structure of mouse and human Pannexin genes.

	Pannexin 1	Pannexin 2	Pannexin 3
Mouse ID	UC009ofi.1	UC007hez.1	UC0090vi.1
RNA Accession	NM-019482	NM-001002005	NM-172454
Chromosome	9	15	9
Exon count	5	4	4
Protein length	426 aa	607 aa	392 aa
Genomic size	39694 bp	9775 bp	9321 bp
RNA size	2112 bp	1922 bp	2518 bp
Human ID	Q96RD7	Q96RD6	Q96QZ0
RNA Accession	NM-015368	AF-398511	NM-052959
Chromosome#	11	22	11
Exon count	5	4	4
Protein length	426 aa	633 aa	392 aa
Genomic size	60045 bp	9565 bp	8800 bp
RNA size	2782 bp	2984 bp	1609 bp

Data were compiled using <http://genome.ucsc.edu>

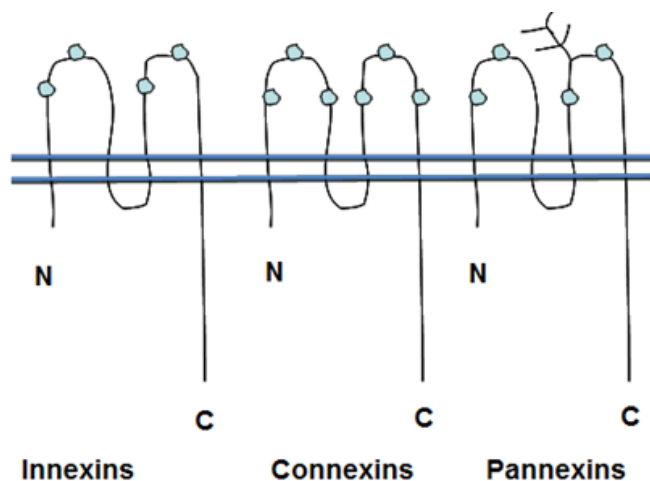


Figure A.1: This diagram represents the innexin, connexin and pannexin channel forming proteins in invertebrates and vertebrates.

Closed circles represent conserved cysteine residues. Branched lines on pannexins represent glycosylated residues on the second intercellular loop. Figure adapted from Pflugers Arch 2009 April; 457(6): 1207-1226.

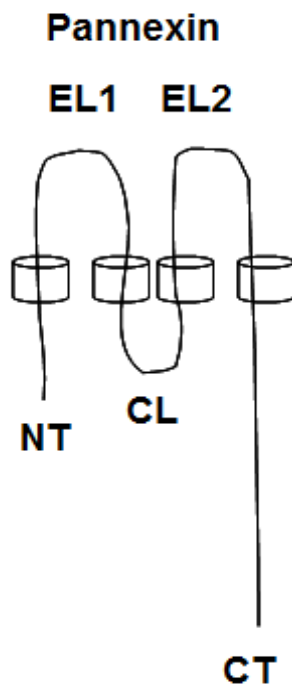


Figure A.2: This diagram represents the typical structure of the pannexin.

Pannexin proteins, which resemble gap junction proteins, have 4 trans-membrane domains, labeled 1-4; 2 extracellular loops labeled E1 and E2; 1 cytoplasmic loop labeled CL; the NH₂ terminal labeled NT and the COOH terminal labeled CT; both termini reside in the cytoplasm. Figure adapted from www.unmc.edu/biochemistry.

The hemi-channels that form the connexin and innexin gap junction protein channels are each composed of six individual subunits. These individual subunits are referred to as connexons and innexons, respectively (Scemes, Suadicani et al. 2007). The pannexons, or pannexin subunits, are composed of six individual subunits in Panx1, and eight individual subunits in Panx2 (Ambrosi, Gassmann et al. 2010). The numbers of subunits in the Panx3 channel has not been experimentally determined yet. However, that number is expected to be six, similar to Panx1, based on the sequence similarity of Panx3 to Panx1 (Boassa, Ambrosi et al. 2007; Penuela, Bhalla et al. 2007; Penuela, Celetti et al. 2008; Penuela, Bhalla et al. 2009; Ambrosi, Gassmann et al. 2010).

Importantly, pannexins do not readily form intercellular gap junction channels when expressed in mammalian cells (Boassa, Qiu et al. 2008; Iglesias, Dahl et al. 2009; Ma, Hui et al. 2009). In fact, pannexin oligomers have repeatedly been shown to be channels that are functional in single membranes, but not as intercellular channels bringing together two adjacent membranes (Sosinsky, Boassa et al. 2011).

Panx1 is often glycosylated in the lumen of the endoplasmic reticulum at its second extracellular loop at Asn254; while an N-linked glycosylation site is present at N71 in Panx3. Additionally, a glycosylation site was also predicted at N86 in Panx2 (Boassa, Ambrosi et al. 2007; Penuela, Bhalla et al. 2007). The bulky carbohydrate moieties at the extracellular domain may introduce steric hindrances to prevent the pannexin channels from coming into close proximity with each other to dock, thus interfering with intercellular channel formation. However, deglycosylated pannexins, at least Panx1, could form transient gap junctions (Boassa, Ambrosi et al. 2007; Penuela,

Bhalla et al. 2007). It seems that glycosylation is a necessary event to promote the traffic of Panx1 to the cell surface. Specifically, glycosylated Panx1 is targeted to the plasma membrane while non-glycosylated Panx1 is retained in the intracellular compartments (Boassa, Qiu et al. 2008). Therefore, it is possible that Panx1, being glycosylated and incapable to dock, is not functional as an intercellular channel. It is important to note that Panx 1 subunits may form unopposed hemichannels, not incorporated into gap junctions.

PANNEXINS IN PARACRINE INTERCELLULAR COMMUNICATION

In contrast to (GJIC) gap junction intercellular communication that requires the direct cell-to-cell intercellular channels that allow the passage of small ions and molecules between the cytoplasm of nearby cells, paracrine intercellular communication (PIC) relies on the release of extracellular messengers into the extracellular space. These messengers which are incapable of crossing the plasma membrane of the nearby cell, bind as ligands to receptor proteins that are present in the plasma membrane, which then transduce the message across the membrane into the inside of the nearby cell (D'Hondt, Ponsaerts et al. 2009).

Both pannexin 1 and pannexin 3 are capable of forming unopposed hemichannels that may open in response to a variety of signals, electrical and chemical, thereby forming a conduit between the cytoplasm and the extracellular milieu. These hemichannels are bidirectional and allows the passage of ions and small metabolic or signaling molecules below 1-2kDa. Panx 1 hemichannels allow the diffusive release of a variety of paracrine messengers, including calcium, ATP, glutamate, prostaglandins, NAD(+) and glutathione

(Wang, De Bock et al. 2013). Panx1 hemichannels are anion-selective, with a rank order of permeability:

NO (3) (-)>I(-)>Br (-)>Cl (-) >F (-)>> aspartate (-)≈ glutamate (-)≈ gluconate(-)

(Ma, Compan et al. 2012).

Glutamate, a signal transduction molecule released by open Panx1 channels is of particular importance for this study as this molecule is implicated in glioma cell invasion and motility (Lyons, Chung et al. 2007). Malignant gliomas release glutamate, which is detrimental to the surrounding cells and promotes tumor growth, expansion and invasion. On nearby/neighborly glioma cells, glutamate activates calcium permeable AMPA-R receptors and induces intracellular calcium wave oscillations necessary for glioma cell migration and increases its invasiveness (Lyons, Chung et al. 2007). Furthermore, glioma cells release glutamate to activate their own AMPA-Rs in an autocrine fashion. It is possible that Panx1 channels may act as a conduit for glutamate release in gliomas.

Another signal transduction molecule released through Panx1 hemichannels is ATP. When released into the extracellular space, ATP is enzymatically hydrolyzed by the ectonucleotidase to produce ADP and AMP. Both products may bind to the purinogenic receptors, P2X7 and P2Y located on nearby cells (D'Hondt, Ponsaerts et al. 2009; Iwabuchi and Kawahara 2011; Kim and Kang 2011; Kim, Liu et al. 2011). Activation of astroglial P2Y receptors triggers a rise in intracellular calcium, which increases astroglial excitability and promotes intercellular communication (Butt 2011). In ischemic astroglia, the binding of ATP to P2X7, in turn, suppresses further release of ATP through Panx1 channels (Iwabuchi and Kawahara 2011). However, this self-limiting mechanism

does not work in every condition or type of cells. Under stimulation with ATP, both the metabotropic P2Y receptors (Locovei, Wang et al. 2006) and the ionotropic P2X7 receptors (Locovei, Wang et al. 2006) are capable of activating Panx1 channels.

Importantly, ATP-dependent activation of P2X7 receptors involves a set of proteins collectively called the inflammasome that is usually activated as a last resort defense mechanism against intracellular bacterial infections and viruses (Vladimer, Marty-Roix et al. 2013). Inflammasome-dependent autophagy is also implicated in chronic inflammatory disease and autoimmune disorders (Deretic, Jiang et al. 2012). However, inflammasome-mediated cell death has also been observed in astrocytes and neurons (de Rivero Vaccari, Bastien et al. 2012; Zou and Crews 2012). It is likely that a deficiency of Panx1 may serve to prevent inflammasome activation.

Panx1 hemichannels also release intracellular calcium. When Panx1 channels are opened, IP3 is released, calcium is released as well, resulting in a calcium wave propagation; ATP is also released which causes activation of the purinogenic P2X7R receptors (Iglesias, Dahl et al. 2009).

The Panx3 channel also participates in transporting ATP into the extracellular space and in calcium wave propagation (Ishikawa, Iwamoto et al. 2011). In osteoblasts, these events lead to subsequent activation of PI3K-AKt signaling, promote cell differentiation, bone formation and prevent apoptosis (Ishikawa, Iwamoto et al. 2011).

PANNEXINS IN GLIOMAGENESIS

There is compelling evidence that pannexins may be involved in glioma cell proliferation and migration.

In humans, PANX2 is located in chromosomal region 22q13.3, a site that is often deleted in human astrocytomas and ependymomas (Rey, Bello et al. 1993; Ino, Silver et al. 1999; Oskam, Bijleveld et al. 2000; Oskam, Bijleveld et al. 2000; Hu, Jiang et al. 2003; Modena, Lualdi et al. 2006). A search for PANX2 encoding genes and data in the Repository of Molecular Brain Neoplasia Data (REMBRANDT), (<http://rembrandt.nci.nih.gov/>) suggests that PANX2 is ubiquitously down-regulated in all types of brain tumors and that this downregulation is associated with poor prognosis (See Figures A-3A and A-3B.)

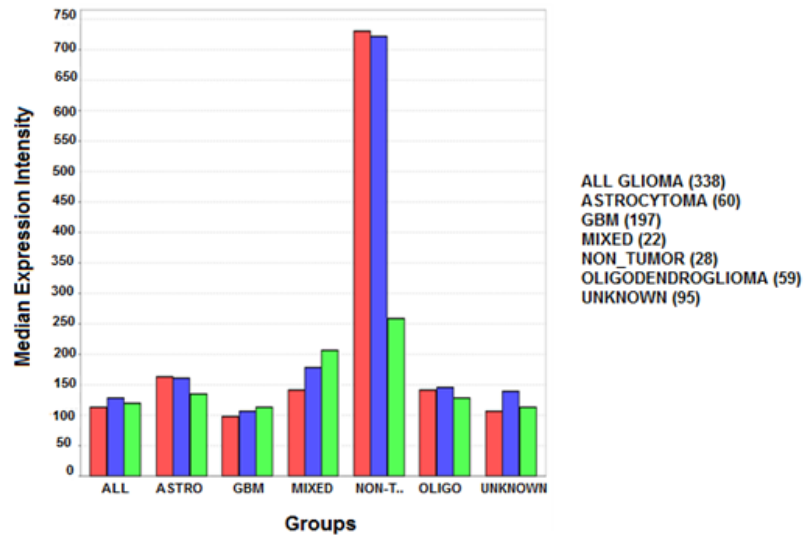


Figure A.3A: The Expression of PANX2 mRNA in human brain tumor samples.

Gene expression plots that displays average expression intensities for the PANX2 gene, based on Affymetrix GeneChip arrays (U133 Plus2.0 arrays) expression in human brain tumor samples.

Kaplan-Meier Survival Plot for Samples with Differential PANX2 Gene Expression

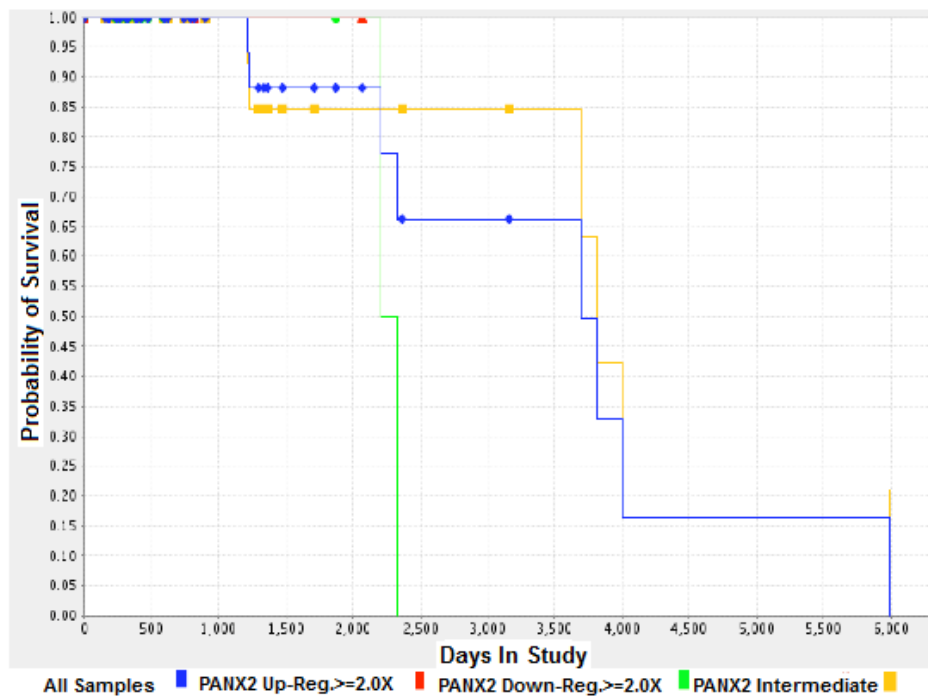


Figure A.3B: The Kaplan-Meier survival plot for samples with differential PANX2 gene expression.

The data also suggests that there are statistically significant Panx2 based predictions of post-diagnosis survival for patients with glial tumors. This data is provided by high-throughput studies revealing the differential expression of pannexin-encoding genes in tumor samples and in model systems.

Importantly, drugs that block pannexin channels are also able to inhibit glioma migration. Pannexins exhibit a remarkable sensitivity to blockade by carbenoxolone (with an IC_{50} of approximately 5 μ M), a classical inhibitor of gap junction communication (Bruzzone and Dermietzel 2006). As shown in the organotypic brain slice culture implantation model, carbenoxolone also inhibits cell migration of glioma cells in co-cultures with astrocytes (Oliveira, Christov et al. 2005), while the treatment with its inactive analogue glycyrrhizic acid (GZA) does not produce any effect.

In rat C6 gliomas, the tumor suppressive role of Panx1 was demonstrated experimentally. In C6 gliomas, the expression of connexins is reduced (Zhu, Caveney et al. 1991) and the expression of pannexins is lost. The stable expression of Panx1 significantly reduced cell proliferation in monolayers, anchorage-independent growth as well as growth of C6 tumors in athymic nude mice (Lai, Bechberger et al. 2007). In follow-up experiments, Panx1 was shown to dramatically accelerate formation of large multicellular aggregates, whereby thousands of monodispersed cells adhere and spontaneously compact further into a single multicellular unit within a short time, typically 24 hours (Bao, Lai et al. 2012). The most likely mediator of this phenomenon is ATP release, as the addition of exogenous ATP alone also accelerated the assembly of both wild-type and Panx1 aggregates. Exogenous ATP also reversed the inhibitive effects of CBX-mediated Panx1 channel closure (Bao, Lai et al. 2012). An immediate driver of aggregate assembly is the remodeling of intracellular contractile actomyosin network. Indeed, Panx1-positive glioma cell aggregates possess a significantly more robust F-actin network than their wild-type counterparts (Bao, Lai et al. 2012). As suggested by Bao and co-authors, the missing link between the Panx1/ATP/P2X7 signaling cascade and the actomyosin system is intracellular calcium. Indeed, Panx1/ATP/P2X7 stimulated calcium waves occur in direct parallel to actin microfilament organization in C6 cells (Cotrina, Lin et al. 1998; Bao, Lai et al. 2012).

In order to determine if there was a correlation between pannexin expression and tumor progression, we examined the expression levels of pannexins in mouse and human astrocytoma cell lines of different grades by Western blot analysis. Mouse primary

astrocytes cells were included as a normal control. Our data suggests that both Panx1 and Panx2 are expressed in mouse primary astrocytes, and are down-regulated or absent in tumorigenic cell lines (See Figures A-4 and A-5).

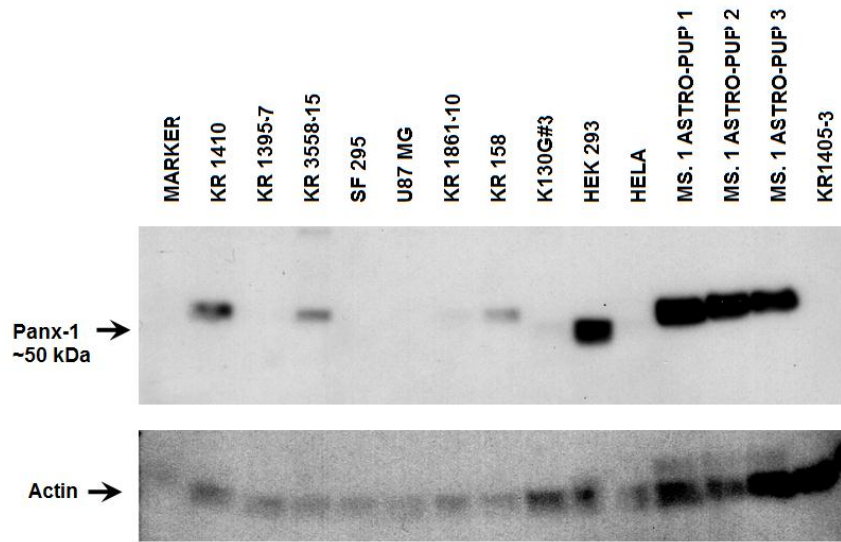


Figure A.4: The figure shows that Panx1 is abundantly expressed in mouse primary astrocytes, as well as HEK 293.

Using anti-Panx1 antibody, western blotting of total protein extracted from a panel of human and mouse astrocytoma cell lines show differential expression of Panx1 expression as compared to control mouse primary astrocytes. The actin loading control is suggestive of inaccurate protein loading.

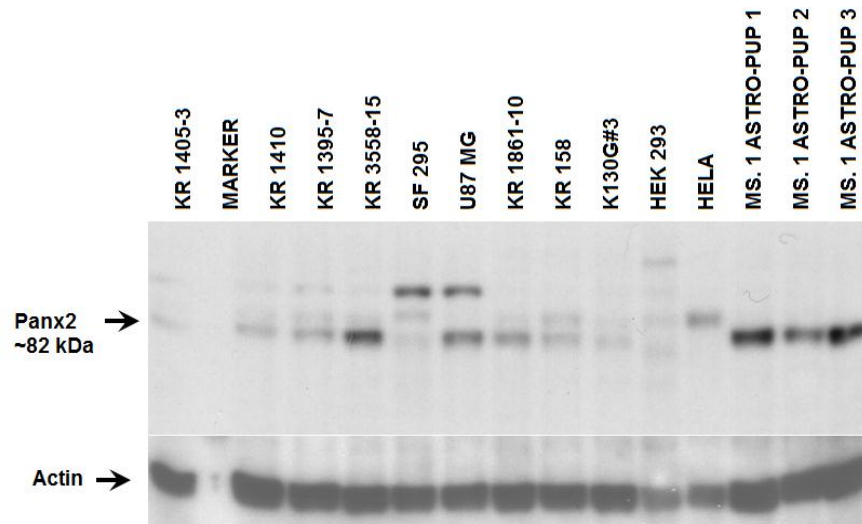


Figure A.5: The figure shows that Panx2 is abundantly expressed in mouse primary astrocytes and reduced in some other human and mouse tumorigenic cell lines.

The human and mouse astrocytoma cell lines show differential expression of Panx2 expression as compared to control mouse primary astrocytes. Actin was used as a loading control to ensure equal protein loading.

To characterize the function of Panx2 in gliomagenesis, a number of *in vitro* and *in vivo* experiments were attempted, including (1) Biotinylation assay to determine if Panx2 formed hemi-channels or gap junction channels; (2) Phosphatase assay to determine the post-translational modification or phosphorylation status of Panx2 protein; (3) Western blot analysis to determine the protein expression levels of Pannexin in normal and transformed mouse and human cell lines; (4) Epitope tagging assay; (5) shRNA knock-down assay; and (6) Panx2 conditional knock-out mouse construct to determine the *in vivo* physiological function of Panx2.

A2. MATERIALS AND METHODS

BIOTINYLATION ASSAY

Normal mouse primary astrocytes and the transformed KR158 mouse astrocytoma cell line (Grade III) were each plated at a density of 2.5×10^5 - 5×10^5 cells per 2 ml DMEM (High glucose, 12430-104, GIBCO BRL, Carlsbad, CA) complete medium and incubated overnight. The next day, the cells were washed 3 times in ice-cold PBS (Cat#14109-169, GIBCO BRL, Carlsbad, CA). Confluent monolayers were incubated at 4°C for 30 minutes, with rocking, in sterile water with 300 ug/ml of EZ-Link Sulfo-NHS-LC-Biotin Reagents (Cat#21335, Thermo Fisher Scientific Inc, Rockford, IL). To remove excess biotin and any unreacted biotinylation reagent, the reaction was quenched with 1 ml filter-sterilized (MCE 0.22 µM filter, Millex, Millipore, Cork, Ireland) TBS (Tris buffered saline) (BP24711, Fisher Scientific, Pittsburg, PA),. The cells were washed twice for 5 minutes each in 1 mL TBS, before harvesting in 250 µl cell lysis buffer with protease inhibitors as previously described.

To fractionate the biotinylated proteins, a Streptavidin-sepharose pull down step was performed by the addition of 300 µl of Sepharose beads (Cat#17-5113-01, Amersham Biosciences, Piscataway, NJ) equilibrated in 700 µl of cell lysis buffer. 100 µl of 50% Sepharose was added to the biotinylated cell lysate to a final volume of 1ml and incubated at 4°C overnight with rocking. Following the overnight incubation, the cells were pelleted by centrifugation, and washed in cell lysis buffer and PBS. The sepharose beads were re-suspended in 60 µl of 2X sample loading buffer, eluted by boiling for 5

minutes at 100°C and analyzed by SDS-PAGE 4-12% gels. The blots were probed for the presence of Pannexin 1 (ARP42783, Ativia Biosystems, San Diego, CA; Cat#48-800, Zymed Labs, Carlsbad, CA), Pannexin 2 (ARP42778, Ativia Biosystems, San Diego, CA; Cat#42-2900, Zymed Labs, Carlsbad, CA), and Pannexin 3 (K-16, sc-51386, Santa Cruz Biotech, Santa Cruz, CA) as well as internal control anti-actin (1-19, sc-1616, Santa Cruz Biotech), and loading control GAPDH (Clone 6C5, 2-RGM2, Advanced Immunochemical, Long Beach, CA), and Alpha-tubulin (32-2600, Zymed Labs, Carlsbad, CA; A-11126, Molecular Probes, Eugene, OR). Each antibody was used at 1:1000.

PHOSPHATASE ASSAY

Mouse primary astrocytes were plated at a density of 2.5×10^5 cells per 2 ml DMEM complete medium and allowed to adhere overnight. The next day, the medium was changed and the cells were washed once in 2 ml serum free DMEM medium (SFM) with 1% Penicillin-Streptomycin (CellGro/Mediatech, Manassas, VA) without FBS (HyClone, Logan, UT) and further incubated in 2 ml SFM until the next day. Following the SFM incubation, the medium was removed, and the cells washed and scraped from the dish in 1ml ice-cold PBS, and pelleted by centrifugation at 100 x g for 2 minutes in PBS/PMSF (2 ml ice-cold PBS, 10 ul PMSF (200mM)). The pelleted cells were lysed in 50 µl of Lambda Protein Phosphatase lysis buffer (50 mM HEPES, 150 mM NaCL, 10% v:v Glycerol, 1% TritonX-100) (Lambda Protein Phosphatase (20,000 U) (New England Biolabs) with protease inhibitors (5 µl/ml of PMSF (200mM) or 10 µl of PMSF in 2 ml

lambda PPase lysis buffer; 1 μ l/ml Aprotinin (10 μ g/mL) or 2 μ l/2 ml; 1 μ l/ml Leupeptin (5 μ g/mL) or 2 μ l /2ml) incubated on ice for 30 minutes, then centrifuged at 4°C for 15 minutes. The supernatants were transferred to a clean microfuge tube and the volumes combined and measured.

Ten microliters of 10X MnCl₂ were added to 100 μ l of supernatant, followed by 10 μ l of 10X PPase buffer and the volumes equally divided into 50 μ l each into separate microfuge tubes. As a negative control, 5 μ l of 0.5M EDTA, and 2.5 μ l of lambda PPase enzyme (20,000 units) (NEB, Ipswich, MA), were added to one 50 μ l tube of supernatant and the tube was placed at 65°C for 1 hour in a thermal cycler to inactivate the PPase. The inactivated lysate was stored at -80°C until protein assay.

To the other 50 μ l tube containing supernatant 2.5 μ l of lambda PPase enzyme was added and immediately incubated at 30°C for 2.5 hours in a thermal cycler, followed by the addition of 5 μ l of 0.5 M EDTA and inactivation at 65°C for 1 hour. The activated lysate was also stored at -80°C until protein assay.

Both protein lysates were resolved on an SDS-PAGE 4-12% protein gel, transferred to PVDF (Cat# IPVH00010, Millipore, Bedford, DA) membrane, and probed for Pannexin 2 (ARP42778, Ativia Biosystems, at 1: 1000. The blots were stripped and re-probed for Actin (1-19, sc-1616, Santa Cruz Biotech, Santa Cruz, CA), also at 1:1000.

Panx2 shRNA KNOCKDOWN ASSAYS

To knockdown the mRNA expression of Panx2 in mouse primary astrocytes and KR158 III astrocytoma cell line, we used shRNA technology, following the manufacturer's instructions. Briefly, WT mouse primary astrocytes and KR158 astrocytoma grade III cells were seeded at 250,000 cells/2 ml DMEM with FBS and without Pen/Strep antibiotic into 6 well plates, and grown to 80 % confluent monolayers. To transfect the shPanx2 plasmid into cells, the DMEM media was removed and cells were washed 2X with 500- μ l shRNA Plasmid Transfection medium (sc108062, Santa Cruz Biotechnology, Santa Cruz, CA). Each well received 0.8 ml Transfection medium and 0.2 ml of reagent mixture solutions A & B previously incubated for 45 minutes at room temperature. Solution A was comprised of 10 μ l of resuspended shRNA plasmid mouse Panx2 (sc152004 Santa Cruz Biotechnology, Santa Cruz, CA) and 90 μ l shRNA Plasmid Transfection Medium. Solution B contained 100 μ l of Transfection medium.

Control wells contained control plasmids only (control plasmid A, sc108060, Santa Cruz Biotechnology, Santa Cruz, CA); shRNA Plasmid transfection reagent only (sc108061, Santa Cruz Biotechnology, Santa Cruz, CA) or cells only control. All solutions and controls were made at 1:2; 1:4 or 1:8 ratios of shRNA plasmids and transfection reagents. The 6-well plates were incubated 5-7 hours, up to 18-hours, at 37°C. Following the 18- hour incubation, 1 ml of normal growth media containing 2X normal (FBS) serum and 2X normal Pen/Strep (CellGro/Mediatech, Manassas, VA) (enriched media) was added to each well, and the plates further incubated for an additional 18-24 hours at 37° C. Post-incubation, the media was again changed, fresh

media was added, and the plates incubated an additional 48 hours, before harvesting the cells. To harvest, cells were washed in 1 ml PBS, scraped and then transferred to a 1.5 ml eppendorf tube, and then lysed in 50 µl cell lysis buffer with protease inhibitors as described previously, and incubated on ice for 30 minutes before pelleting at 140,000 g for 15 minutes at 4°C. The supernatant was removed and transferred, and the lysates stored at -80°C until protein assay, before resolving by Western blot.

PANNEXIN 1-2-3 EPI TOPE TAGGING & TRANSFECTIONS ASSAYS

PCR primers were designed with MacVector to amplify each Pannexin for cloning into an expression vector. The “Reverse” primer of each Pannexin was designed so that the final Pannexin product would be a fusion protein expressing specific tags: Panx1-c-myc; Panx2-Flag-Tag and Panx3-His.

For Pannexin 1 the primers were Panx1-HindIII Forward Primer which contained the c-myc tag with Flanking sequence: GCGCGC; Restriction enzyme: HIND III (AAG CTT); Kozak initiation sequence (ACC); Start codon (ATG); and a Coding region of approximately 4-7 triplets to give the following:

Panx1-HindIII FORWARD PRIMER: (5' GCG CGC AAG CTT ACC ATG GCC ATC GCC CAC TT) and Panx1-EcoR1-c-MYC tag Reverse Primer was designed as follows:

Flanking sequence: GCG CGC; Restriction enzyme: EcoR1 (GAA TTC); Stop codon: TCA; Coding region of approximately 4-6 triplets, and the C-MYC TAG: (CAG ATC TTC TTC AGA AAT AAG TTT TTG TTC) to give the following: Panx1-EcoR1-

C-MYC TAG REVERSE PRIMER: (5' GCG CGC GAA TTC TCA CAG ATC TTC TTC AGA AAT AAG TTT TTG TTC).

The Pannexin 2 primers were designed to contain the Flanking sequence: GCGCGC; Restriction enzyme: HIND III (AAG CTT); Kozak initiation sequence (ACC); Start codon (ATG); and a Coding region of approximately 4-7 triplets to give the following: Panx2-HindIII FORWARD PRIMER: (5' GCG CGC AAG CTT ACC ATG CAC CAC CTC CTG GA). The Panx2-FLAG TAG REVERSE PRIMER was designed as follows: Flanking sequence: GCG CGC; Restriction enzyme: EcoR1 (GAA TTC); Stop codon: TCA; Coding region of approximately 4- 6 triplets and the FLAG TAG: (CTT ATC GTC GTC ATC CTT GTA ATC) to give the following Panx2-EcoR1-FLAG-TAG REVERSE PRIMER: (5' GCG CGC GAA TTC TCA CTT ATC GTC GTC ATC CTT GTA ATC).

The Pannexin 3 primers were designed to contain the Flanking sequence: GCGCGC; Restriction enzyme: HIND III (AAG CTT); Kozak initiation sequence (ACC); Start codon (ATG); and a Coding region of approximately 4-7 triplets to give the following: Panx3-HindIII FORWARD PRIMER: (5' GCG CGC AAG CTT ACC ATG TCG CTC GCA CAC AC). The Panx3-EcoR1-HIS TAG REVERSE PRIMER was designed as follows: Flanking sequence: GCG CGC; Restriction enzyme: EcoR1 (GAA TTC); Stop codon: TCA; Coding region of approximately 4-6 triplets and the HIS TAG: (CAT CAT CAC CAT CAC CAC) to give the following: Panx3-EcoR1-HIS TAG REVERSE PRIMER: (5' GCG CGC GAA TTC TCA CAT CAT CAC CAT CAC CAC).

PCR amplification was performed with Platinum High Fidelity kit (Cat#11304-029, Invitrogen, Carlsbad, CA). Briefly, the reaction mixture contained 1 μ l of 10X HF buffer; 0.4 μ l of $MgSO_4$ (50 mM); 0.2 μ l dNTP's (10 mM); 2 μ l Panx2 HindIII Forward Primer (10mM) (5' GCG CGC AAG CTT ACC ATG CAC CAC CTC CTG GA); 2 μ l Panx2 EcoR1 Flag-tag Reverse Primer (10mM) (5' GCG CGC GAA TTC TCA CTT ATC GTC GTC ATC CTT GTA ATC); 0.4 μ l Platinum Taq HF enzyme (1unit/mL); 90-100 ug Bac-Panx2 DNA; and dH₂O to a final volume of 10 μ l. The Bac-Panx2 plasmid DNA was purified by mini-prep or maxi-prep according to the manufacturer's instructions. (See appendix B for Qiagen mini-prep and maxi-prep protocols).

The cycling conditions were: 94°C for 2 min; 94°C or 15 sec; 68-75° C for 1 min; 68°C for 2 min; with 30 cycles total. The 2.3-3.4 KB product of the Panx2 PCR reaction was checked on a 0.7% TAE agarose gel, the bands of interest excised under UV illumination and column purified using Qiagen Qiaquick protocol, as previously described. The PCR fragments were eluted in 50 μ l Elution buffer (Cat#19086, Qiagen, Valencia, CA), and the gel-purified concentrations measured and noted. The PCR products and pcDNA3.1+ vector (1-2 ug) (Invitrogen, Carlsbad, CA) were each digested with HindIII and EcoR1 at 37°C overnight. Six μ l of 10X NEB2 buffer (New England Biolabs, Ipswich, MA) was added, followed by 0.6 μ l BSA ((10mg/mL) NEB, Ipswich, MA)); 1 μ l of HindIII (20,000 u/mL) restriction enzyme; 1 μ l of EcoR1 (20,000 u/mL) restriction enzyme; and dH₂O to a final volume of 60 μ l. All digested samples were run on a 0.7% TAE agarose gel; the bands or interest were excised under UV illumination; purified using the Qiagen-Qiaquick protocol according to the manufacturer's instructions;

and the DNA eluted with 10 µl EB buffer (Cat#19086, Qiagen, Valencia, CA) and the concentrations determined. The vector pcDNA3.1 (+) was further purified with Antarctic phosphatase (1,000 u/mL, NEB, Ipswich, MA), which catalyzes the removal of 5' phosphate groups from DNA, thereby preventing the vector from self-ligating.

The Panx2 insert was ligated into vector (pcDNA3.1 (+) (1-2 ug)) at 1:3, 1:5, or 1:7 ratios of vector. Ligation reactions were set up with pcDNA3.1 (+) (1-2 ug) vector with 1 µl of T4 DNA ligase enzyme (20,000 u/mL, NEB, Ipswich, MA); 2 µl of 10X T4 DNA ligation buffer (NEB, Ipswich, MA) and dH₂O to a final volume of 20 µl. The ligation reaction was incubated at 16°C overnight. The next day, 10 µl of the overnight ligation reaction mixture was transformed into TOP-10 cells as previously described, plated onto Ampicillin (50 ug/mL) plates and incubated at 37°C overnight until colony formation. Selected transformants were grown up overnight in Luria Broth with Ampicillin (50 ug/mL) at 37°C with shaking, followed by DNA mini-prep following the manufacturer's protocol (See appendix B for mini-prep protocol). The restriction enzymes HindIII (20,000 u/mL) and EcoR1 (20,000 u/mL) were used to digest and hence identify the presence of the appropriate Panx2-Flag-tag insert into vector pcDNA3.1 (+), in some of the clones.

For transfections the epitope tagged mouse Panx2-Flag-tagged vector was transfected into KR 158 grade III cell lines following the manufacturer's protocol for Lipofectamine 2000 (Invitrogen, Carlsbad, CA) or Fugene 6 (Roche Diagnostics Corporation, Indianapolis, IN) as previously described. Briefly, 250,000 KR 158 cells were seeded into 6-well plates and incubated at 37° C overnight. The next day, cells were

transfected with Panx2-Flag-tag in the presence of Fugene or Lipofectamine. After 48 hours, the KR158 cells were harvested and lysed in cell lysis buffer with protease inhibitors, as previously described. Following protein assay and resolution on 10% SDS-Page gels; transfer to 0.45 μ M nitrocellulose ((NC), LC2001, Invitrogen) or PVDF (Cat# IPVH00010, Millipore, Bedford, DA) membranes, the blots were probed with HRP conjugated Flag-tag antibody at 1:1000 (A8592, Sigma Aldrich, St. Louis, MO). *In these experiments, the absence of a positive band corresponding to Panx2 suggests that the transfection of Panx2-Flag-tag into KR158 grade III cells did not work as expected.*

Panx2 CKO TARGETING CONSTRUCT - BAC ISOLATION

The BAC DNA to be inserted into the targeting vector was retrieved from a BAC derived from C57BL/6 available from Children's Hospital and Research Center at Oakland, Oakland, CA) (CHORI) and was used to streak for single colonies before characterization by restriction enzyme digest analysis (Malureanu, LA, 2011).

Pannexin 2 BAC DNA (Clone RP23-458P6) was shipped to us as bacterial LB agar stab culture. The electro competent cells DH10B (Invitrogen, Carlsbad, CA) *E.coli* host harboring the plasmid contained 12.5 μ g /ml chloramphenicol for BAC clones. *E. Coli* was streaked onto an LB/chloramphenicol (25 μ g/mL) plate and 13 single colonies picked, grown up and glycerol stocked for storage at -80° C.

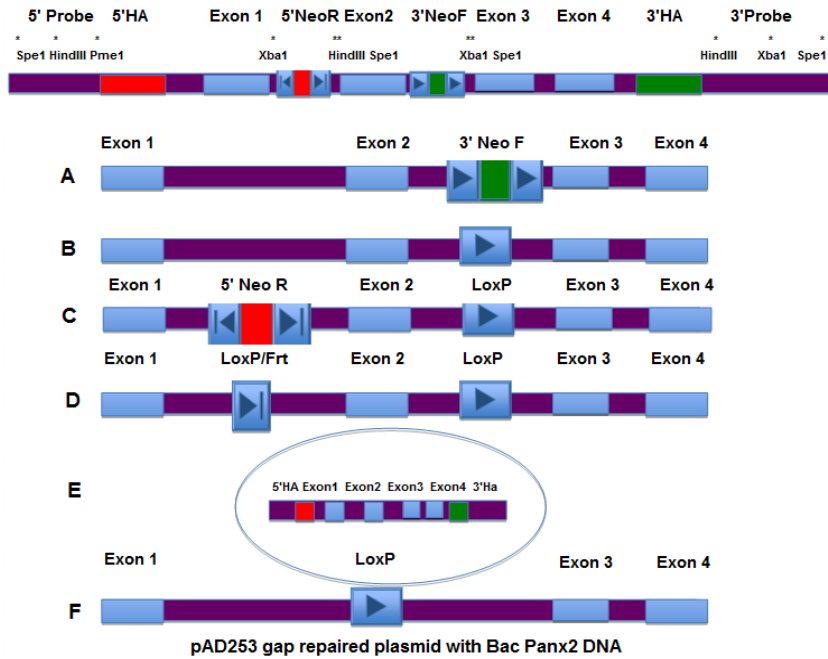


Figure A-6: Conditional knock-out vector construction.

This diagram shows the Panx2 gene with Exons 1-4; Exon 2 targeted for deletion in the CKO allele. The 5' end of the diagram shows the restriction enzyme sites used for Southern blot analysis; Spe1/HindIII, and Pme1 used for linearization. The 3' end shows RE sites Xba1/HindIII/Spe1; also for Southern blot analysis. Internal RE sites distal to the 3' end include Xba1/Spe1. The diagram also shows the location of the 5' and 3' Neo cassettes flanking Exon 2 for deletion; and the 5' and 3' Homology arms for homologous recombination. A. The Panx2 gene with Exon 2 flanked by 3' Neo Forward cassette for deletion. The 3'NeoF selection cassette (loxP-PGK-EM7-NeobpA-loxP) is targeted to the 3' side of Exon 2 for deletion. First targeting the 3' NeoF cassette in EL350 Cre-recombinase cells via Homologous recombination, is excised to leave a loxP site, 3' of Exon2 for deletion. B. The Panx2 gene with LoXP site after excision of 3' Neo F cassette. C. The Panx2 gene with Exon 2 flanked by 5' Neo Reverse cassette for deletion. The 5'NeoR selection cassette (FRT-loxP-PGK-EM7-NeobpA-FRT-loxP) is targeted to the 5' end of Exon 2 for deletion. Second targeting, the 5' NeoR loxP/FRT in EL250 Cre-Flpe recombinase cells via homologous recombination is excised to leave loxP and FRT sites, 5' of Exon 2 for deletion. D. The Panx2 gene with LoXP/Frt sites after excision of the 5' Neo Reverse cassette. E/F. The gap repaired plasmid containing one LoXP site and Exon 2 deleted, with Bac-Panx2 DNA is the CKO in the presence of Cre-Flpe recombinase mice and homologous recombination with genomic mouse DNA.

Table A.1B. Bacterial strains and genotype used for recombineering.

Strain	Genotype
EL 250	DY380[(cro-bioA)⟨>araC-PBADflpe]
EL 350	DY380[(cro-bioA)⟨> araC-PBADcre]
DH10B	F-mcrA Δ (mrr-hsdRMSmcrBC)O/ 80diacZ Δ M15 Δ lacX74deoRrecA1endA1araD139 Δ (ara,leu)7649ga/ Uga/KrspLnupG
DY380	DH10B[lambdacI857(cro-bioA⟨>tet)]
Cassette	
PLTM 260	Neomycin bpA driven by the pGK and pEM7 promoter
PLTM332	Neomycin bpA driven by the pGK and pEM7 promoter

(Data were compiled from Liu, P et al, 2003; Kuznetsov, S.G. et al, 2009).

TRANSFORMATION OF DNA INTO RECOMBINOGENIC STRAINS

DH10B *E. coli* cells containing BAC-Panx2 were cultured overnight in LB broth/chloramphenicol at 25ug/ml. The next day the cells were mini-prepped according to the manufacturer's protocol. Briefly, the cells were pelleted at 4000 rpm for 5 minutes, the supernatant removed, and the pellet resuspended in 200 μ l P1 buffer (Qiagen, Valencia, CA). Buffer P2 (200 μ l) (Qiagen, Valencia, CA) was added to the cells in suspension then the mixture incubated for 5 minutes at room temperature. Buffer N3 (350 μ l) was added to the mixture before centrifugation at 14,000 rpm for 10 minutes. The supernatant was transferred to a new microfuge tube and 525 μ l of isopropanol was added, then the tubes were spin at 14,000 rpm for 5 minutes. The pellet was washed with 100 μ l of 70% ethanol. The pellet was air-dried for 5 minutes and resuspended in 30 μ l dH₂O. One microgram (ug) of BAC-Panx2DNA was used for electroporation, while 15 μ l of BAC-Panx2 DNA was used for restriction enzyme digestion to characterize the BAC-Panx2 DNA.

A map of the Panx2 BAC genomic DNA with restriction enzyme (RE) sites showed that Not1 (10,000 u/mL) was a non-cutter and BamH1 (20,000 u/mL) would cut at several sites to give a detailed banding pattern. To confirm the presence of BAC-Panx2 DNA in the DH10.B recombinogenic strain, BAC-Panx2 DNA was digested with BamH1 and Not1 restriction enzymes. To 15 µl of eluted BAC-Panx2 DNA, 1.8 µl dH₂O, 2.0 µl 10X BamH1 buffer (NEB, Ipswich, MA), 0.2 µl 10 ug/mL BSA (NEB, Ipswich, MA), and 1.0 µl BamH1 enzyme (20,000 u/mL) were added. In an equivalent step 1.8 µl dH₂O, 1.0 µl Not1 enzyme, (10,000 u/mL) 2 µl 10X NEB 3 buffer (NEB, Ipswich, MA), and 0.2 µl 10 ug/mL BSA (NEB, Ipswich, MA), was added to 15 µl of eluted BAC-Panx2 DNA. Both the Not1 and BamH1 reactions were incubated at 37°C for 1 hour and samples run on a 0.5% Seakem LE (Lonza, Rockland, ME) agarose gel in 1X TAE (Tris-acetate-EDTA) buffer, at 25V, 4° C overnight (O/N).

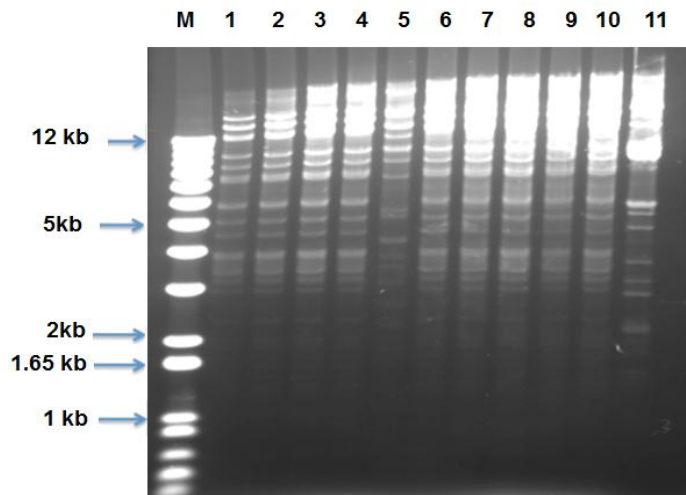


Figure A.7: Identification of correctly targeted Bac-Panx2 DNA clones.

This figure shows the molecular marker “M” with sizes identified on the left, followed by Bac-Panx2 DNA clones labeled 1-11. Based on the predicted RE digests of BamH1/Not1, the results indicate that the correctly targeted Bac-Panx2 DNA clones have the following sizes: 6, 3.9, 3.5, 1.5, 1.4, 3, 1.9-2 Kb. Clones 1-4, 6-10 are correctly targeted. Clone 5 is incorrect; and clone 11 is an internal control.

To prepare competent DY380 cells for electroporation of BAC-Panx DNA, one stab of glycerol-stocked DY380 cells was used to inoculate LB/chloramphenicol (25 ug/mL) cultured overnight at 32°C with agitation at 250 rpm. The next day, 900 µl of DY380 cell culture was placed in 30 ml LB broth and incubated at 32°C, with agitation at 250 rpm. Two, 10 ml cell cultures were transferred into cold 50 ml Oakridge tubes, incubated on ice for 5 minutes, and the cells pelleted by centrifugation at 6000 rpm at 4°C for 5 minutes. The pellet was resuspended in 1 ml ice-cold 10% glycerol/H₂O (v: v) and transferred to pre-chilled 1.5 ml microfuge tubes. The cells were pelleted at 14,000 rpm for 30 seconds, placed on ice, and resuspended in 1 ml ice-cold 10% glycerol/H₂O. After three more washes in 10% glycerol/H₂O, the pellet was resuspended in 50 µl ice cold H₂O and transferred to a pre-chilled electroporation cuvette (0.1-cm gap). Next, 600 ug and 1200 ug of BAC-Panx2 DNA was added to the 50 µl cell suspension and mixed. Controls contained equivalent volumes of H₂O/50 µl cell suspension. Cells were electroporated (1.8V, 25 uF, 200 ohms, 4.0 ms) and 1 ml of SOC medium was added to the cuvette, before transferring to a 14-ml Falcon tube (Becton-Dickson). The tube was incubated for 1.5 hours at 32°C with shaking. After incubation, the cells were spun 14,000 rpm, for 20 seconds at room temperature and the pellet resuspended in 100 µl LB broth. Aliquots of cell suspension in LB broth of 100 µl and 900 µl were plated on LB/Chloramphenicol plates (25 ug/mL), and incubated at 32°C overnight. *There were no colonies seen on the control plates; however, colonies were present on both the 600 ng and 1200 ng plates at both 100 µl and 900 µl volumes.*

To confirm the presence of BAC-Panx2 DNA in DY380 cells, transformed colonies, cultured in LB/Chloramphenicol (25 ug/mL) at 32°C overnight, were mini-prepped and the DNA eluted as previously described, were restriction enzyme digested with BamH1, along with a 2- 4 ug sample of control BAC-Panx2 DNA. To 15 µl each of BAC-Panx2 DNA from electroporated DY380 cells, or control BAC-Panx2 DNA, was added dH₂O 1.8 µl; BamH1 buffer 10X (NEB, Ipswich, MA) 2.0 µl; BSA (10 ug/mL) (NEB, Ipswich, MA) 0.2 µl; and BamH1 enzyme (20,000 u/mL) 1.0 µl. Following 1 hour of incubation at 37°C, the digests were run on a 0.5% -0.7% 1X TAE buffer (Tris-acetate-EDTA) and Seakem LE (Lonza, Rockland, ME) agarose gel at 150V, for 1 hour. The control BAC-Panx2 DNA was used to determine whether the transformed clones had a similar matching RE digest pattern. Glycerol stocks were made of the correct clones and stored at -80°C. *The results indicate that clones 1-3, 5-7, 9-10, 11, 13-19 have the correct digest pattern.*

RETRIEVAL OF THE BAC-PANX2 DNA FROM THE DY380 CELLS INTO THE PAD253 VECTOR CONTAINING 5'-3'HA

DY380 cells were grown in LB/chloramphenicol (25 ug/mL) at 32°C, overnight with shaking at 250 rpm. The next day, 1 ml of the overnight culture was added to 29 ml LB/chloramphenicol (25 ug/ml) and 15 ml of each overnight culture was added to two 50 ml baffled flasks: one labeled Induced and the other labeled Non-induced/Control. Both 50 ml flasks and contents were incubated at 32°C, for 2 hours with agitation at 250 rpm. Following incubation, 5 ml of culture from each flask was removed and discarded, and the remaining 10 ml of cell culture treated as indicated: The Non-induced/control flask was incubated at 32°C for 15 minutes, while the induced flask was placed in a 42°C water bath with shaking at 200 rpm for 15 minutes. After incubation, both flasks were placed on ice for another 10 minutes, and the cultures transferred to chilled 50 ml Oakridge tubes, spun at 6000 rpm, and 4°C for 5 minutes. The pellets were resuspended in 1 ml ice-cold 10% glycerol/dH₂O water, transferred to chilled 1.5 ml microfuge tubes on ice, and washed twice with 1 ml ice-cold water as described above. The cell pellet was resuspended in 100 µl ice-cold dH₂O and 50 µl of cells transferred to chilled microfuge tubes with or without 100 ng of retrieval plasmid DNA (pAD253-5'HA-3'HA). The labeled tubes contained the following: No DNA-Control/Non-induced; With DNA-Control/Non-induced; No DNA/Induced; With DNA/Induced. The contents (DY380 cells with/without retrieval plasmid) of the microfuge tubes were transferred to chilled electroporation cuvettes and electroporated under the same conditions described previously (1.8V, 25 uF, 200 ohms, 4.0 milliseconds). After electroporation, 1 ml SOC

media was added to the cuvette and the contents incubated for 1.5 hours at 32°C with shaking. After incubation, the cells were plated on LB plates supplemented with Ampicillin (50 ug/mL), and further incubated at 32°C overnight. The transformants selected from the Induced-DNA plate were grown in LB/Ampicillin at 32°C, mini-prepped, and digested with BamH1 restriction enzyme. After digestion, the samples were run on a 0.7% TAE Seakem LE agarose gel and the digest pattern of BAC-Panx2 DNA from the retrieval plasmid confirmed by comparison with the original control BAC-Panx2 DNA. *This confirmed the presence of the BAC Panx2 DNA into the pAD253-5'HA-3'HA vector complex.*

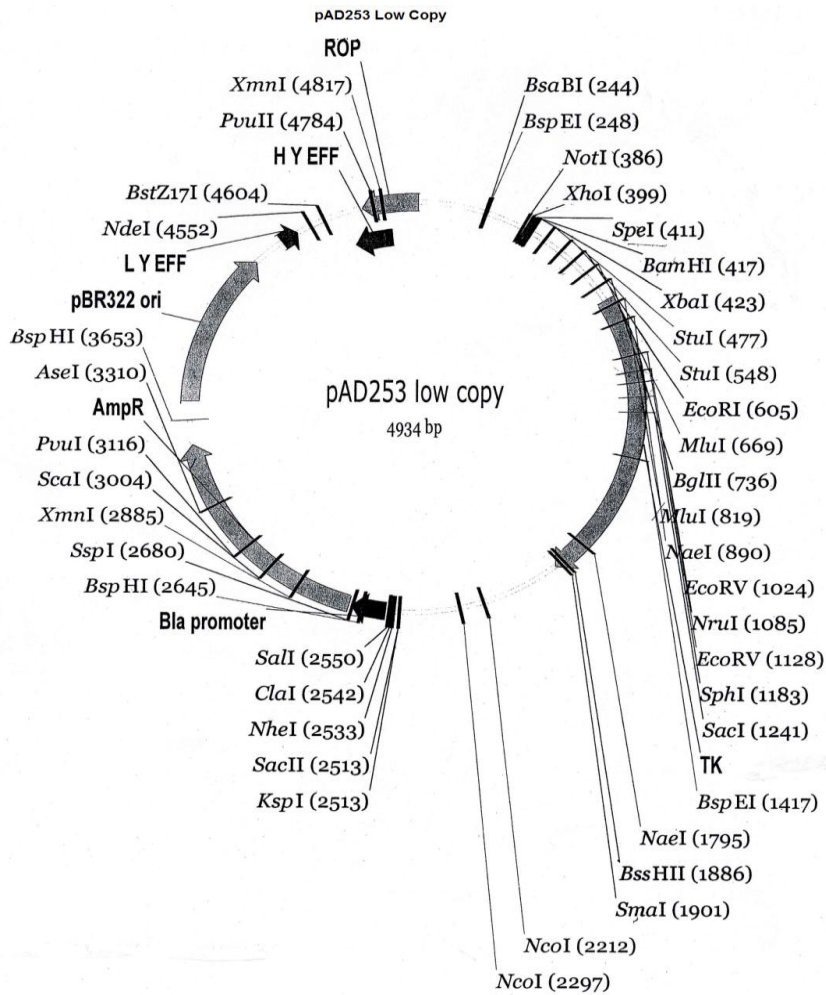


Figure A.8: Diagram to show the pAD253 retrieval vector.

The final gap-repaired plasmid with Bac-Panx2 DNA; the CKO construct, should have 5'HA and 3'HA; Bac-Panx2 DNA in pAD253; loxP/FRT sites 5' of Exon 2 introduced via PLTM260 NeoR cassette cloned in pcDNA3.1 and via HR. The loxP site 3' of Exon 2 introduced via PLTM332 NeoF cassette cloned into pcDNA3.1 and via HR. In the presence of Cre-Flpe recombinase mice and via homologous recombination with genomic DNA, Exon 2 excised to leave loxP site. This will generate the KO.

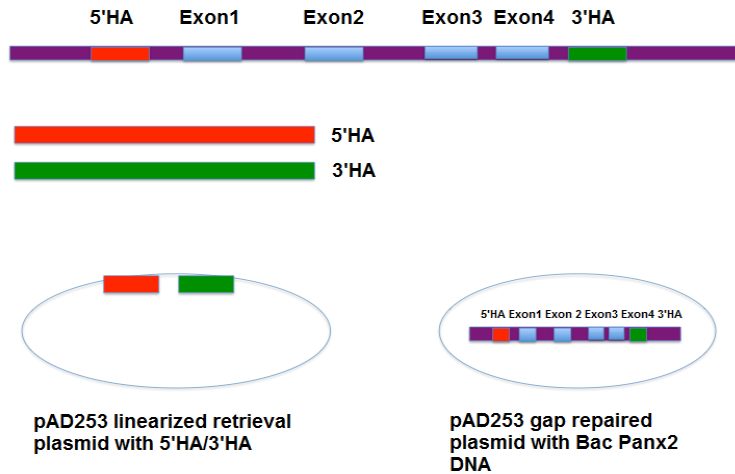


Figure A.9: Diagram showing pAD253 retrieval plasmid with homology arms and Bac-Panx2 DNA.

Top: This diagram shows the Panx2 gene with Exons 1-4; 5' and 3' Homology arms to Bac-Panx2 DNA. Middle: Diagram representing 5' and 3' HA with RE sites for Southern blot analysis and RE diagnostics. Bottom left: Diagram with pAD253 and 5' and 3' HA inserted. Bottom right: pAD253 gap-repaired plasmid or CKO; the final construct.

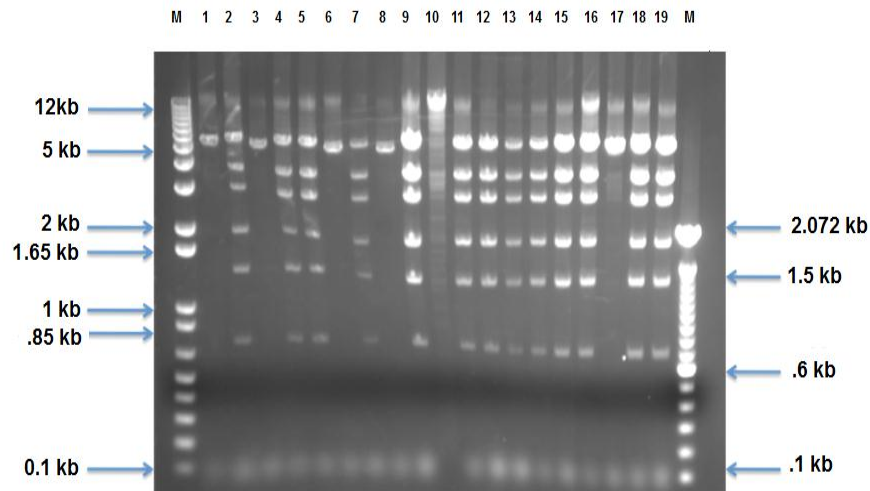


Figure A.10: Confirmation of Bac-Panx2 DNA in retrieval vector pAD253.

This picture shows that Bac-Panx2 DNA with 5' and 3' HA correctly inserted into the pAD253 retrieval vector. RE digests with BamH1/Not1 confirmed the identity of the Bac-Panx2 DNA based on the correct digest pattern as compared to control Bac-Panx2 DNA. Correct clones are #2, 4, 5, 7, 9, 11, 12, 13, 14, 15, 16, 18, 19; Clone 10 is a control DNA.

CONSTRUCTING THE PAD253 RETRIEVAL VECTOR/CASSETTE

Table A.2: Primer sets used for generating 5' and 3' Homology arms for Retrieving.

	Forward (5'-3')		Reverse (5'-3')
5'HA Probe 1 Forward with Not1/Pme1	AAG GAA AAA A GCG GCC GC <i>GTT TAA AC</i> CCC CTG TGC TTT CCC ACA GAC ATT TCC TAA GCC	5'HA Probe 2 Reverse with Xho1	CCG CCG CTC GAG GGA AAT CAG GGA GGG CAA AGG TTA GGA GTA
3'HA Probe Probe 4 Forward with Not1	CCG CCG GCG GCC CCC CTG ACT AGG AAC CTA GTC CCC TCT ATT	3'HA Probe 3 Reverse with BamH1	CGC CGC GGA TCC GCA TGG CCA GCT TGA GTT CTG CTT TCT AAC AGC

PCR primers were designed using MacVector, and ordered from Integrated DNA Technologies (IDT) Coralville, IA). Primer sequences used for constructing the 5'homology arms and 3' homology arms for the retrieval vector are listed in the table above. 5'HA-pAD253: Not1/Xho1 and these primers amplify a 300 bp size fragment. 3'HA-pAD253: Not1/BamH1 and these primers amplify a 300 bp size fragment.

PCR amplification was performed with Thermal Ace kit (Cat#45-0116, Invitrogen, Carlsbad, CA). The reaction mixture contained 1 µl of dNTP (10 mM), 100-150 ug of DNA (BAC-Panx2 DNA), 1 µl (10 mM) of each primer ((3'HA probe 4 Forward primer and 3'HA probe 3 Reverse primer for the 3'HA); (5'HA probe 1 Forward primer and 5'HA probe 2 Reverse primer for the 5'HA)); 5 µl of 10X Thermal Ace buffer, 1 µl of Thermal Ace DNA Polymerase enzyme (2 u/µl), and dH₂O to a final volume of 50 µl. PCR was performed using a PTC-225 Peltier Thermal Cycler (MJ Research) for 98°C for 3 min/ 98°C for 30 sec, 65.2°C for 30 sec, X 35 cycles, 72°C for 2.5 min/ 72°C for 10 min. To confirm the 300 bp product of the PCR reaction, 5 µl of the

50 µl PCR mixtures was loaded onto a 2.5% Seakem LE agarose gel/1X TAE buffer and run as previously described.

To column purify, the remaining 45 µl PCR product was mixed with 5 volumes or 225 µl of PB (Cat#19066, Qiagen, Valencia, CA) binding buffer and loaded onto a Qiaquick spin column placed in a 2ml collection tube. After a 60 second spin at 14,000 X G to bind the DNA to the column, the column was washed once with 750 µl of PE buffer (Cat#19065, Qiagen, Valencia, CA) and the flow through discarded. The column was spun once more to remove excess buffer then, transferred to a new 1.5 ml microfuge tube and the PCR fragments eluted using 50 µl of EB (Cat#19086, Qiagen, Valencia, CA) buffer.

To digest the 5'HA PCR fragments for cloning into the retrieval pAD253 vector, 6 µl of NEB 3 restriction buffer (10X), 1 µl each of restriction enzymes **Not1** (10,000 u/mL) and **Xho1** (20,000 u/mL); and 0.6 µl of 10 mg/mL BSA (Cat#B9001S, NEB, Ipswich, MA) were added to the 50 µl volume of PCR mixture, and dH₂O added to a final volume of 60 µl. The entire mixture was incubated at 37°C for 2 hours or overnight as needed.

The 3'HA PCR fragments were similarly digested for cloning into the retrieval pAD253 vector. To the 50 µl volume of 3'HA PCR mixture was added 6 µl of BamH1 restriction buffer (10X); 1 µl each of restriction enzymes **BamH1** (20,000 u/mL) and **Not1** (10,000 u/mL); 0.6 µl of BSA 10 mg/mL (NEB, Ipswich, MA), and dH₂O added to a final volume of 60 µl. The entire mixture was incubated at 37°C for 2 hours or overnight as needed.

The (1-2 ug) or 25 µl volume of pAD253 low-copy vector was digested with 5 µl of BamH1 restriction buffer (10X), 1 µl each of restriction enzymes **Xho1** (20,000 u/mL) and **BamH1** (20,000 u/mL), 0.5 µl BSA 10 mg/mL BSA (Cat#B9001S, NEB, Ipswich, MA), and dH₂O to a final volume of 50 µl. The mixture was incubated at 37°C for 2 hours or overnight as needed.

All digested samples were run on a 0.7-1% Seakem LE agarose gel/1X TAE at 100 V for 1 hour. The bands were excised from the gels, and the gel slices weighed and transferred to 6 ml round-bottom tubes.

The gel slices were purified using a Qiagen gel-extraction kit (Qiagen, Valencia, CA) and following the manufacturer's protocol. The DNA was eluted with 10 µl EB buffer and the concentration measured and noted. The 5'HA and 3' HA digested-gel-purified PCR fragments were ligation ready.

The gel-purified pAD253 retrieval vector was further purified by treating with phosphatase, which catalyzes the removal of 5' phosphate groups from DNA, thereby preventing the vector from self-ligating. Briefly, to 10 µl of the eluted retrieval vector, 1 µl of 10X Antarctic phosphatase buffer (NEB, Ipswich, MA) and 2 µl of Antarctic phosphatase enzyme (1,000 u/mL, NEB, Ipswich, MA) was added. The reaction was incubated for 1 hour before deactivating at 65°C to quench the enzymatic reaction.

The pAD253 retrieval vector containing the 5'HA and 3'HA was generated by triple ligation reaction at 1:3, 1:5, or 1:7 ratios of vector (pAD253 vector) to insert (5'HA /3'HA). It was generated by mixing the gel-purified PCR product of the 5'HA-Not1/Xho1, the gel-purified PCR product of the 3'HA-Not1/BamH1, and the gel-

purified-phosphatase-treated retrieval vector pAD253 digested with Xho1/BamH1, with 1 μ l of T4 DNA ligase enzyme (20,000 u/mL, M0202S, NEB, Ipswich, MA) and 2 μ l of 10X T4 DNA ligation buffer (B02025, NEB, Ipswich, MA), with dH₂O to a final volume of 20 μ l. The ligation reaction mixture was incubated at 16°C overnight.

The next day, 10 μ l of the ligation reaction mixture was transformed into OneShot chemically competent TOPO-10 cells (C4040-06, Invitrogen, Carlsbad, CA), following the manufacturer's protocols. Ten microliters (10 μ l) of ligation reaction mixture was added to 50 μ l TOPO-10 cells, incubated on ice 30 minutes, heat-shocked for 30 seconds in a 42°C water-bath, before adding 250 μ l SOC (Cat#15544-034, Invitrogen, Carlsbad, CA) media to the tube. The culture was then transferred to a 14-ml round bottom Falcon tube and incubated for 1 hour, at 37°C with shaking at 225 rpm. The ligation reaction mixture was plated onto LB/Ampicillin (50 ug/mL) plates and incubated at 37°C, overnight. The next day, transformants were selected and placed in 5 ml LB broth/Ampicillin (50 ug/mL) and incubated overnight at 37°C with shaking. The cultures were mini-prepped using Qiagen mini-prep kit as previously described. Plasmid DNA was eluted in 30 μ l dH₂O.

To confirm the identity of the pAD253 retrieval vector containing both the 5'HA and 3'HA inserts, 15 μ l of the eluted samples were double digested with **BamH1** (20,000 u/mL) and **Xho1** (20,000 u/mL) to confirm the presence of the 600 bp insert. The pAD253-5'HA-3'HA vector complex was linearized by digestion with the **Xho1** (20,000 u/mL) restriction enzyme to create a double strand break for gap repair.

To further purify the retrieval vector complex for retrieving into Bac-Panx2 DNA beta-agarase digest was performed. Linearized digests of pAD253-5'HA-3'HA were run on a low melting point beta-agarase gel at 4°C and bands excised, placed in 1.5 ml microfuge tubes and incubated at 65°C. The tubes were then incubated at 42°C and the volumes measured. 1/10 volume of 10X agarase buffer (Cat# B0392S, NEB, Ipswich, MA) and 1 ul agarase enzyme (1000 u/mL, M0392S, NEB, Ipswich, MA) was added per 100 µl volume, incubated at 40°C for 4 hours to overnight with shaking. This was followed by 20 minute incubation on ice, centrifugation at 12,000 rpm for 10 minutes and the supernatant removed. To precipitate the DNA, 1µl of glycogen, 1/10 volume of 3M NaOAc and 2.5 volumes of 100% EtOH was added to the supernatant, incubated at -20°C for a minimum of 30 minutes, and then spun at 14,000 rpm for 20 minutes. The pellet was washed with 100 µl 70% EtOH, air-dried for 5 minutes, and resuspended in 20 µl dH₂O to a final concentration of 100-300 ng/µl. The purified retrieval pAD253 plasmid containing 5'HA and 3'HA was ready for BAC-Panx2 DNA.

**CONSTRUCTION OF THE SECOND MINI-TARGETING VECTOR: TO
INSERT THE PLTM 260 NEO REVERSE CASSETTE INTO THE PCDNA3.1
VECTOR**

PCR primers were designed using MacVector. Primer sequences used for constructing the PLMT 260 Neo Reverse targeting vector are listed in the table below. These primers all amplify a 300 bp fragment and are reconstituted at 100 mM concentration in dH₂O.

Table A.3: Primer sets used for generating the 5' and 3' Homology arms for the Second Mini-targeting construct with pLTM260 5' Neo Reverse cassette.

	Forward (5'-3')		Reverse (5'-3')
5'HA pLTM260 Forward2 with Nhe1/AatII	GGC CTA GCT AGC GAC GTC CTC CAG CCC CTT TAT GAC TTT TCT AGA CC	5'HA pLTM260 Reverse2 with EcoR1/Kpn1	GGC CG GAA TTC GGT ACC ATG CAG AGA CTG CTG TTC CCC AAA CGG
3'HA pLTM260 Forward2 with EcoR1/HindIII/Spe1	GGC CG GAA TTC AAG CTT ACT AGT AAG GCA GGC AGC TCT ACC GGA GGG	3'HA pLTM260 Reverse2 with Not11/AatII	AAG GAA AAA A GCG GCC GC GAC GTC GAG GCT GGC ATC CAC GCC GGG CAG

PCR amplification was performed with Thermal Ace DNA Polymerase kit as described earlier, with the following modifications. The reaction mixture contained 10 mM dNTP, 100-150 ug of BAC-Panx2 DNA, 10 mM of each primer (3'HA Forward primer and 3'HA Reverse primer for the 3'HA), (5'HA Forward primer and 5'HA Reverse primer for the 5'HA), 5 µl of 10X Thermal Ace buffer, 1 µl of Thermal Ace DNA Polymerase enzyme (2 u/µl), and dH₂O to a final volume of 50 µl. PCR was performed with the settings: 98°C for 3 min/98°C for 30 sec, 69-77°C temperature gradient for 30 sec, 72°C for 1 min; for 35 cycles, 72°C for 10 min; and 4°C hold.

To check the 300 bp product of the PCR reaction, 5 µl each of the 5'HA and 3'HA PLTM260 Neo Reverse 50 µl PCR mixture was loaded onto a 2.5% Seakem LE agarose gel/1X TAE and resolved as previously described. The remaining 45 µl was loaded onto a Qiaquick column, and purified as described previously. Eluted PCR fragments were restriction enzyme digested with (Nhe1/EcoR1), (EcoR1/Not1) or

(Nhe1/Not1), gel purified, and pcDNA3.1 vector phosphatase-treated before setting up a triple ligation reaction at 1:3, 1:5, and 1:7 ratios of vector pcDNA3.1 to insert (5'HA/3'HA). The ligation mixture was transformed into TOPO-10 cells, plated onto LB/Ampicillin (50 ug/mL) plates and incubated at 37°C overnight. Colonies were cultured in LB/Ampicillin (50 ug/mL), and mini-prepped as previously described. To verify the presence of the 600 bp insert in the pcDNA3.1-5'HA-3'HA vector complex, the DNA was digested with the restriction enzymes Nhe1/Not1.

The second step in preparing the PLTM260 5'Neo reverse targeting construct involved digesting the pcDNA3.1-5'HA-3'HA vector complex with restriction enzymes Kpn1 and Hind III, followed by gel purification. Vector PLMT260 was similarly digested with Kpn1 and HindIII, to release the 5'Neo Reverse cassette from the PLTM260 vector. The PLTM260 5'Neo Reverse cassette was phosphatase treated and purified, before setting up a triple ligation reaction in the ratios 1:3, 1:5, and 1:7 for insert pcDNA3.1-5HA-3'HA, with vector PLTM260 5'Neo Reverse cassette.

The ligation reaction was transformed into TOPO-10 cells, and plated onto LB/Kanamycin (50 ug/mL) plates. Resultant colonies were cultured in LB/Kanamycin (50 ug/mL) at 32°C, overnight followed by mini-prep and digestion with restriction enzymes Kpn1 and HindIII, as described above. *The presence of the 1.9- 2kb insert of the PLTM260 5'Neo-reverse cassette in the pcDNA3.1-5'HA-3'HA complex confirms the identity of the second mini-targeting vector.* The pcDNA3.1-5'HA-3'HA-5'Neo-Reverse vector complex was linearized by digestion with the AatII restriction enzyme, and gel purified as described in detail above, with the following minor modifications. Notably,

the samples were run on a 0.8% low melt Seakem LE agarose (Cat#50004, Lonza, Rockland, ME) gel in 1X TBE (Tris-borate-EDTA), at 30V overnight at room temperature. Bands were excised, gel purified and stored at -20° C.

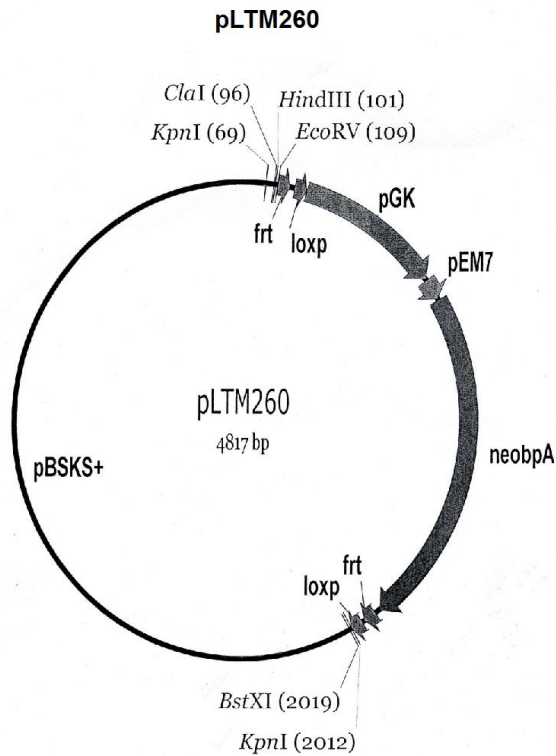


Figure A.11: Diagram showing the pLTM260 vector containing the Neomycin cassette.

This vector was used to make the second mini-targeting construct. The 5'NeoR selection cassette (FRT-loxP-PGK-EM7-NeobpA-FRT-loxP) was excised from the pLTM260 vector with RE HindIII/KpnI, for cloning into vector pcDNA3.1 with 5'HA and 3'HA to complete the second targeting construct.

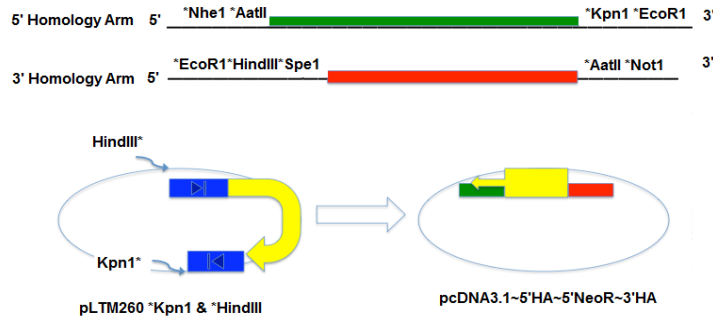


Figure A.12: Diagram to show the homology arms for the second targeting construct.

5'HA contains at the 5' end: RE NheI/AatII for linearization; and 3' end: RE KpnI/EcoRI for excising NeoR cassettes from vector/cloning into pcDNA3.1. 3' HA contains at the 5' end: RE EcoRI for cloning into pcDNA3.1; HindIII/SpeI for Southern blot analysis and 3' end: RE AatII for linearization and NotI for pcDNA3.1 cloning.

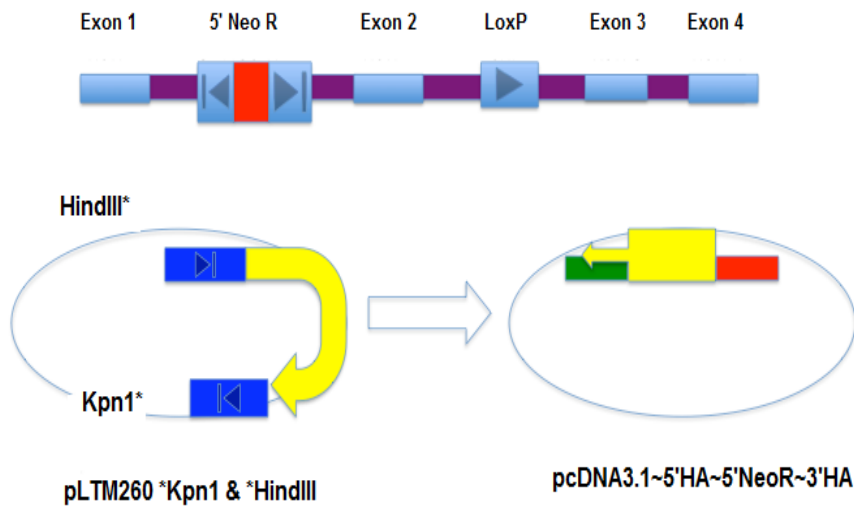


Figure A.13: Diagram showing the construction of the second mini-targeting vector.

The 5'NeoR selection cassette (FRT-loxP-PGK-EM7-NeobpA-FRT-loxP) is targeted to the 5' end of Exon2 for deletion. The 5'HA (green) 5': NheI-AatII and 3': EcoRI- Kpn1, and 3'HA (red), 5: EcoRI-HindIII-SpeI and 3': AatII-NotI, RE digested, ligated and cloned into pcDNA3.1 vector. The 5'NeoR selection cassette (FRT-loxP-PGK-EM7-NeobpA-FRT-loxP) is excised from the pLTM260 vector with RE HindIII/Kpn1, and present in the final second targeting construct to include pcDNA3.1-5'HA-5'NeoR-3'HA.

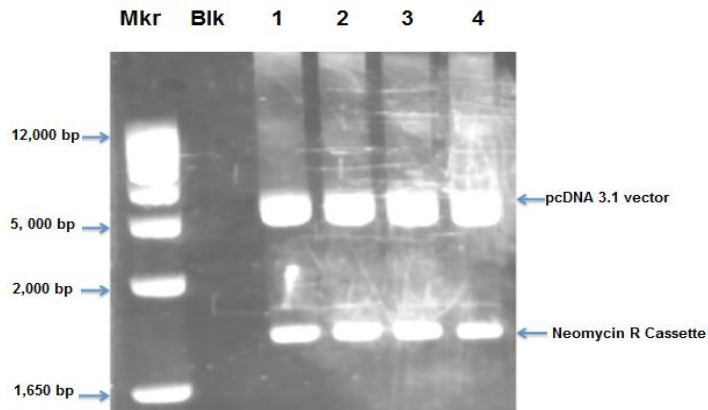


Figure A.14: The second mini-targeting vector containing homology arms and pLTM260 Neomycin cassette. This picture shows the 5'Neo Reverse cassette at 1.94 kB containing 5' and 3' homology arms inserted into pcDNA3.1 vector with size 5.4 kB and linearized by AatII RE. Molecular marker shows the relative sizes of the products.

CONSTRUCTION OF THE FIRST MINI-TARGETING VECTOR: TO INSERT THE PLTM 332 NEO FORWARD CASSETTE INTO THE PCDNA3.1 VECTOR

PCR primers were designed using MacVector. Primer sequences used for constructing the PLMT 332 Neo Forward targeting vector are listed below. These primers all amplify a 300 bp fragment and are reconstituted at 100 mM concentration in dH₂O.

Table A.4: Primer sets used for generating the 5' and 3' Homology arms for the First mini-targeting construct pLTM332 3' Neo Forward cassette.

	Forward (5'-3')		Reverse (5'-3')
5'HA pLTM332 Forward2 with Nhe1/AatII	GCG CG CTA GCT AGC GAC GTC GGC CAA GAC TGA GGC GGT ACC CCC	5'HA pLTM332 Reverse2 with EcoR1/HindIII/SpeI	GCG CCG GAA TTC AAG CTT ACT AGT TGC CCC TCA CTT TAG GAG CAA CCC
3'HA pLTM332 Forward2 with EcoR1/Bstx1/XbaI	CGC CCG GAA TTC CCA CCG CGG TGG TCT AGA GGT CTG ATA GGA GTC TGG ACA CTC CC	3'HA pLTM332 Reverse2 with Not1/AatII	GCC AAG GAA AAAA GCG GCC GC GAC GTC GGC GTT TCA CAA CCC AAC TCA CTT GCT GC

PCR amplification was performed with Thermal Ace DNA Polymerase kit as described earlier, with the following modifications. The reaction mixture contained 10 mM dNTP, 100-150 ug of BAC-Panx2 DNA, 10 mM of each primer ((3'HA Forward primer and 3'HA Reverse primer for the 3'HA), (5'HA Forward primer and 5'HA Reverse primer for the 5'HA)), 5 µl of 10X Thermal Ace buffer, 1 µl of Thermal Ace DNA Polymerase enzyme (2 u/µl), and dH₂O to a final volume of 50 µl. PCR was performed at 98°C for 3 min, 98°C for 30 sec, 69-77°C temperature gradient for 30 sec, 72°C for 1 min; x 35 cycles, 72°C for 10 min; 4°C hold.

To check the 300 bp product of the PCR reaction, 5 µl each of the 5'HA and 3'HA PLTM332 Neo Forward 50 µl PCR mixture was loaded onto a 2.5% Seakem LE agarose gel/1X TAE and resolved as previously described. The remaining 45 µl was loaded onto a Qiaquick column and purified as described previously. Eluted PCR fragments were restriction digested with **Nhe1/EcoR1** for 5'HA, **Not1/EcoR1** for 3'HA,

Nhe1/Not1 for vector pcDNA3.1, gel purified, and pcDNA3.1 vector phosphatase-treated before setting up a triple ligation reaction at 1:3, 1:5, and 1:7 ratios of vector pcDNA3.1 to insert (5'HA/3'HA). The ligation mixture was transformed into TOPO-10 cells plated onto LB/Ampicillin (50 ug/mL) and incubated at 37°C overnight. Colonies were cultured in LB/Ampicillin (50 ug/mL), and mini-prepped as previously described. To verify the presence of the 600 bp insert in the pcDNA3.1-5'HA-3'HA vector complex, the DNA was digested with the restriction enzymes **Nhe1/Not1**.

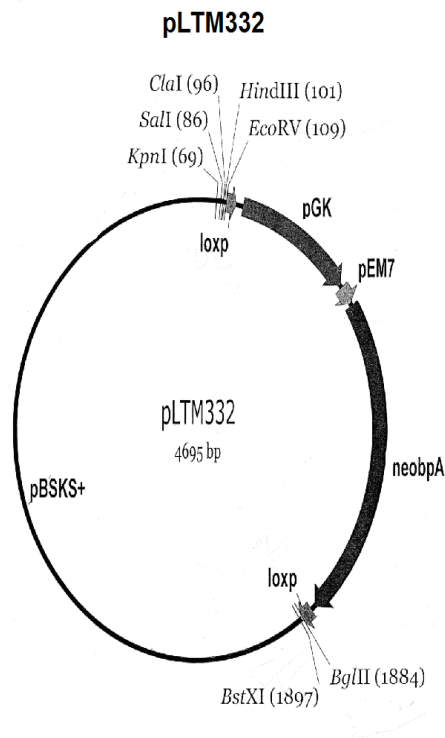


Figure A. 15: This diagram shows the pLTM332 vector containing Neomycin cassette.

This vector was used to construct the first mini-targeting vector. The 3'NeoF selection cassette (loxP-PGK-EM7-NeobpA-loxP) was excised from the vector pLTM332 with either RE HindIII/BglII or HindIII/BstXI for cloning into vector pcDNA3.1 with 5' HA and 3'HA; or before cloning into vector pcDNA3.1 with 3'HA, respectively.

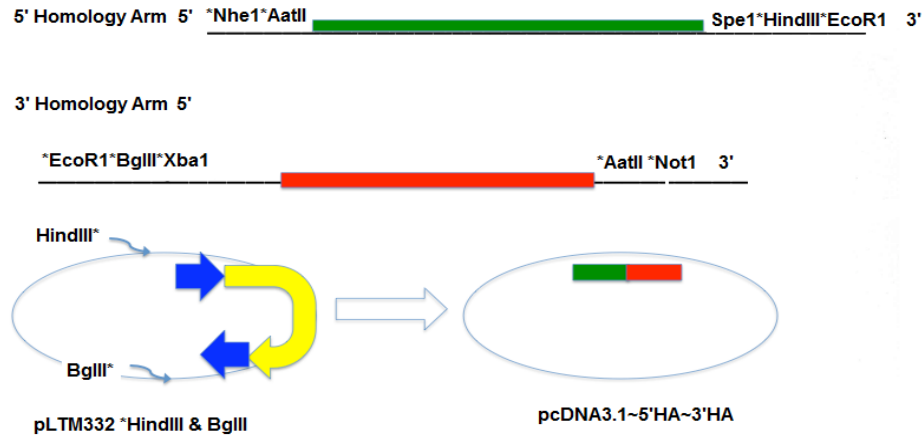


Figure A.16: Diagram to show the homology arms for first targeting construct.

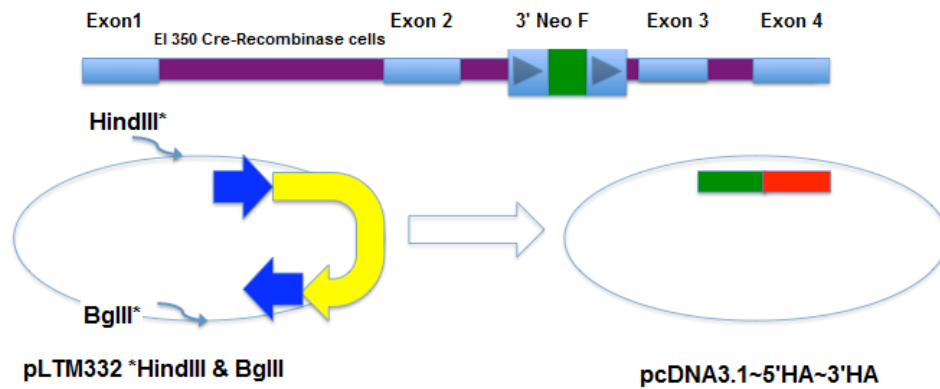


Figure A.17: Diagram to show the construction of the first targeting construct.

The 3'NeoF selection cassette (loxP-PGK-EM7-NeobpA-loxP) is targeted to the 3' side of Exon 2 for deletion. 5'HA (green) with 5':NheI-AatII and 3': SpeI-HindIII-EcoRI, RE digested, ligated and cloned into pcDNA3.1 vector. 3'HA (red) with 5': EcoRI-BglII-XbaI and 3': AatII-NotI. The 3'NeoF selection cassette (loxP-PGK-EM7-NeobpA-loxP) excised from the vector pLTM332 with HindIII/BglII is absent from the final construct.

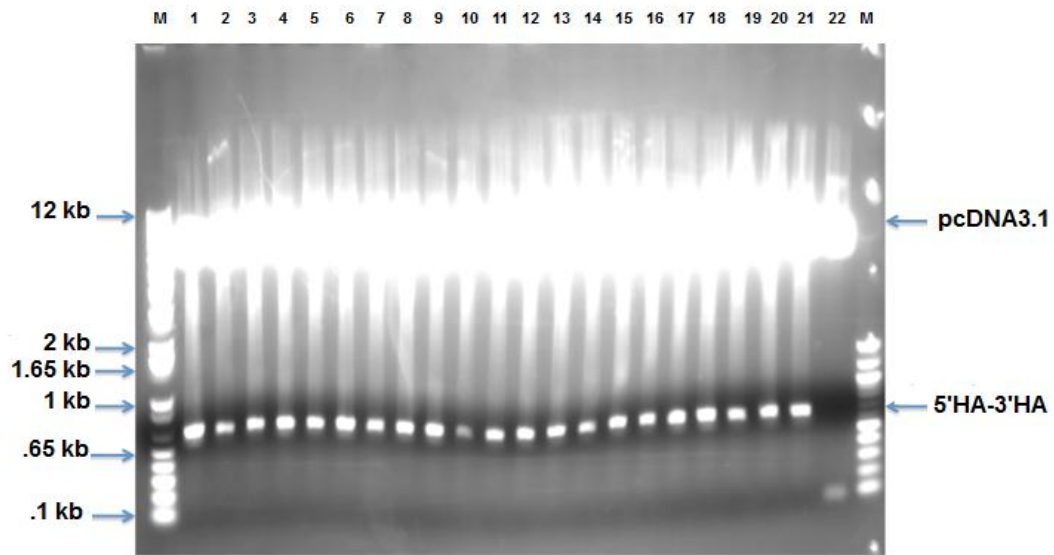


Figure A.18: Mini-targeting vector containing homology arms without Neomycin cassette.

This picture shows the First mini-targeting vector pcDNA 3.1 at approximately 5.4 kB containing the 5' and 3' HA at approximately 600 bp; without the 3 NeoF cassette. All clones 1-21 have the correctly targeted vector and insert, with the exception of clone #22.

An equivalent step in preparing the PLTM 332 3'Neo Forward mini-targeting construct involved digesting the pcDNA3.1-3'HA vector complex with restriction enzymes **HindIII** (37°C 1 hr digest) and **Bstx1** (55°C overnight digest) essentially as described above, including gel purification. In addition, vector PLMT332 containing the 3' Neo Forward cassette, was similarly digested with HindIII (37°C 1 hr digest) and Bstx1 (55°C overnight digest) followed by phosphatase treatment and purification before setting up a double ligation reaction in the ratios outlined above for insert of pcDNA3.1-3HA with vector PLTM332 containing 3' Neo Forward cassette.

The ligation reaction was transformed into TOPO-10 cells, plated onto LB/Kanamycin (50 ug/mL) and incubated at 32°C overnight. Colonies were cultured in LB/Kanamycin and mini-prepped as previously described. To verify the presence of the 1.9-2 kb insert of the 3'Neo-Forward cassette in the pcDNA3.1-3'HA complex, the DNA was digested with the restriction enzymes HindIII and Bstx1. *We were successful in cloning both the 3'HA and 3' NeoF cassette into the pcDNA3.1 vector; there was no evidence of the 5'HA. Data not shown.*

We were unsuccessful in obtaining the complete targeting vector to include: pcDNA3.1-5'HA-3'HA-PLTM332 Neo Forward vector, to complete the Panx2 targeting construct.

GENERATING 5' & 3' PROBES FOR SOUTHERN BLOT ANALYSIS

PCR primers were designed using MacVector. These primers all amplify a 1.8 kb fragment and are reconstituted at 100 mM concentration in dH₂O. Primer sequences used for constructing the 5' and 3' probes for genotyping by Southern blot analysis are listed as follows.

Table A.5: Primer sets used for generating the 5' and 3' Probes for Southern blot analysis.

	Forward (5'-3')		Reverse (5'-3')
5'Probe pcDNA3.1 Pan2Probe1 Forward EcoRV	CGC CGC GAT ATC TAC ATT AAT TCA ATT AAT CAG GAC TAT GTT C	5'probe pcDNA3.1 Pan2Probe2 Reverse Not1	AAG GAA AAA A GCG GCC GC CAA ACG AAC CGA GTT CAT ATT GAC CAT CCC
3'Probe pcDNA3.1 Pan2Probe3 Forward EcoRV	CGC GCG GAT ATC TGC AGG TGG GGA CTG CGA AGA CCA GGG TAT	3'probe pcDNA3.1 Pan2Probe4 Reverse Not1	AAG GAA AAAA GCG GCC GC GGT ACC CGG CAC TAT CAA ATC TAC ACA TTT

PCR amplification was performed with Thermal Ace DNA Polymerase kit. The reaction mixture contained 10 mM dNTP, 100-150 ug of Panx2-BAC DNA, 10mM each of (primer ((5' probe for pcDNA3.1 (+) = Pan2 Probe 1=Forward; Pan2 Probe2=Reverse); and 3'probe for pcDNA3.1 (+)=Pan2 Probe 4=Reverse); Pan2 Probe3=Forward)), 5 µl of 10X Thermal Ace buffer, 1 µl (2 u/µl) of Thermal Ace DNA Polymerase enzyme, and dH₂O to a final volume of 50 µl. PCR was performed at: 98°C for 3 min/98°C for 30 sec, 65.2°C for 30 sec, 72°C for 2.5 min x 35 cycles, 72°C for 10 min, 4°C hold. To check the product of the PCR reaction, 5 µl of the 50-µl PCR mixture was loaded onto a 1.2% Seakem LE agarose gel/1X TAE to confirm the presence of a 1.8 kb Panx-2 5' Probe and 1.8 kb Panx-2 3' Probe. The remaining 45 µl of PCR product was purified by Qiagen Qiaquick as previously described. PCR fragments were eluted using 50 µl of EB buffer (Cat#19086, Qiagen, Valencia, CA).

To digest the 5' and 3' Panx-2 probes for cloning into pcDNA.1 vector, restriction enzyme digests were performed as follows: For the 5' probe double digest, 6 µl NEB 3 restriction buffer (10X), 1 µl each of restriction enzymes Not1 (10,000 u/mL) and EcoRV (20,000 u/mL), and 0.6 µl of 10 mg/mL BSA (B9001S, NEB, Ipswich, MA) was added to the 50 µl volume of purified and eluted PCR product. dH₂O was added to a final volume of 60 µl. The entire mixture was incubated at 37°C for 1 hour or overnight as needed.

The 3' Panx-2 probe PCR product was similarly double digested with 6 µl NEB 3 restriction buffer (10X), 1 µl each of restriction enzymes EcoRV (20,000 u/mL) and Not1 (10,000 u/mL); and 0.6 µl BSA (10 mg/mL) was added to the 50 µl volume of purified and eluted PCR product. dH₂O was added to a final volume of 60 µl. The entire mixture was incubated at 37°C for 1 hour or overnight as needed.

The pcDNA3.1 (+) (1 or 2 ug) vector was double digested with 5 µl of 10X NEB 3 restriction buffer, 1 µl each of restriction enzymes Not1 (10,000 u/mL) and EcoRV (20,000 u/mL), 0.5 µl BSA (10 mg/mL), and dH₂O to a final volume of 50 µl. The entire mixture was incubated at 37°C for 1 hour to overnight as needed.

All digested samples were run on a 1.0% Seakem LE agarose gel/1X TAE until resolved and the bands of interest excised. Gel slices were purified using the Qiagen MinElute gel extraction kit. The DNA was eluted with 10 µl EB buffer. The 5' Panx-2 probe and 3' Panx-2 probe digested, gel-purified PCR fragments were ready for ligation.

The gel-purified pcDNA3.1 (+) vector was further purified by treating with Antarctic phosphatase enzyme (1000 u/mL, M0289S, NEB, Ipswich, MA) before the setting up the ligation reaction.

To determine the vector to insert ratio, 4 μ l each of 5' Panx2-probe, 3' Panx2-probe and pcDNA3.1 (+) vector were each loaded on a 1.2% Seakem LE agarose gel/1X TAE. After calculating the vector to insert ratio, the ligation reactions of pcDNA3.1 (+) containing 5'Panx-2 probe and 3'Panx-2 probe were generated by triple ligation reaction at 1:3, 1:5, or 1:7 ratios of vector pcDNA3.1 (+) to insert (5'Panx-2 probe/3'Panx-2 probe) as previously described.

The following day, the ligation mixture was transformed into One-Shot TOP10 cells as previously described and plated onto LB/Ampicillin (50 ug/mL) and incubated at 37°C overnight. The next day, the transformants were selected and cultured in 5 ml LB/Ampicillin (50 ug/mL) at 37°C overnight with shaking. The cultures were mini-prepped for DNA as previously described, and digested with diagnostic restriction enzymes Not1 and EcoRV to ensure the presence of the insert. To 15 μ l of eluted DNA was added 3 μ l NEB 3 restriction buffer (10X), 1 μ l each of restriction enzymes EcoRV (20,000 u/mL) and Not1 (10,000 u/mL), 0.3 μ l BSA (10 mg/mL), and dH₂O to a final volume of 30 μ l. The samples were digested at 37°C for 1 hour, run on a 0.7% Seakem LE agarose gel/1X TAE for 2 hours at 110-120 V, and visualized by UV illumination to confirm the presence of the pcDNA3.1 (+) vector at 5 kb and insert at 1.8 kb.

MAKING THE 5' AND 3' PROBE FOR THE SOUTHERN BLOT

The 5' probe was generated by adding 60 ng of 5'probe template DNA (pcDNA3.1 (+) and 1.8Kb 5'Panx-2 probe insert), 10 mM Random Primer (Thermal Ace DNA Polymerase kit, Cat# E0200, Invitrogen, Carlsbad, CA) and dH₂O to 36 µl final volumes. The samples were boiled at 100°C for 5 minutes, before the addition of 10 µl of 5X Dctp buffer, 6 µl ³²P dCTP (3000 Ci/mmol; 10mCi/mL, BLU513H250, Perkin Elmer, Waltham, MA) and 1 µl Klenow enzyme ((50, 000 u/mL) Cat# 0210M, NEB, Ipswich, MA)) with mixing. The samples were incubated at 37° C for 2 hours, transferred to spin columns, spun at 1000 X g for 4 minutes and separated as follows: Two microliters of the reaction mixture was placed in a counting vial and read on the scintillation counter to measure the activity of the probe. The remaining 5' Panx2-probe mixture was boiled at 100° C for 5 minutes, transferred to the blot containing hybridization buffer, and incubated at 65° C overnight in a water-bath. The pre-hybridization buffer was removed from the blot prior to the addition of the hybridization buffer. The following day, the blots were washed (15 minutes x 65° C for 4 washes) and exposed to autoradiography film kept at -80° C for 1 week before developing. The targeted ES clones were subsequently identified as being suitable for genotyping by Southern analysis.

The 3'Panx-2 probe PCR fragments were similarly digested with 60 ng of 3'Probe template DNA (pcDNA3.1 (+) and 1.8 kb 3'Panx-2 probe insert), 10 mM Random Primer, and dH₂O to 36 µl final volume, and processed as described above for the 5'Panx-2 probe mixture.

In addition, 2 μ l each of reaction mixture, 5'Panx2-probe and 3'Panx2-probe were aliquoted into scintillation counting vials and read on the scintillation counter to measure the activity of the probe. *The 5' Panx-2 Probe had 326950.3 cpm (counts per minute) and the 3' Panx-2 probe had 299947.8 cpm.*

GENE TARGETING IN ES CELLS: DIGESTS TO CONFIRM THE SOUTHERN BLOT ANALYSIS

To confirm by Southern blot analysis that the selected restriction enzymes sites of **Spe1** were suitable for genotyping at the 5' loci (5'end of Panx2 Exon 2), control (embryonic stem cells) ES DNA, and genomic (wild-type) WT DNA samples were digested with suitable restriction enzymes. To 20 μ l of ES DNA or WT DNA (BM1 29, WT30, or WT31/32) samples was added 4 μ l of NEB 2 (10X) restriction buffer, 1.6 μ l Spermadine (0.1 M, CAS#124-20-9, AcrosOrganics, Fairlawn, NJ), 0.4 μ l 10 mg/mL BSA, 0.5 μ l Spe1 (40 units/ μ l) enzyme and dH₂O to a final volume of 40 μ l. Samples were incubated at 37°C overnight, then boosted the following day with an additional 0.5 μ l of Spe1 (40 units/ μ l) enzyme.

To confirm by Southern blot analysis that the selected restriction enzymes sites of **Xba1** and **HindIII** were suitable for genotyping at the 3' end of Panx2 Exon 2 site (3'loci), control ES DNA and genomic wild-type DNA samples were digested with suitable restriction enzymes. To 20 μ l of ES DNA or WT DNA (BM1 29, WT30, or WT31/32 DNA) samples was added 4 μ l of NEB 2 10X restriction buffer, 1.6 μ l (0.1 M) Spermadine, 0.4 μ l 10 mg/mL BSA, 2 μ l each of Xba1 (20 units/ μ l) and HindIII (20

units/ μ l) enzyme and dH₂O to a final volume of 40 μ l. Samples were incubated at 37°C overnight.

All digested samples were run on a 0.8% TPE (Tris-phosphate-EDTA) MetPhor agarose (Cat#50184, Lonza, Rockland, ME) gel at 30V, room temperature, overnight. The next day, 11 μ l of either radioactive 5'Panx2-probe or 3'Panx2-probe and EtBr was added to the gels, which were then washed in 2X SSC buffer for 1 minute. Gels were dried on Whatman paper, and the DNA cross-linked in a UV cross-linker oven.

The gels were stored in Pre-Hybridization buffer at 4°C until the addition of the 5' and 3' radioactive probes to the gel blots directly. Subsequently, the markers on the gel blots were also verified for radioactivity.

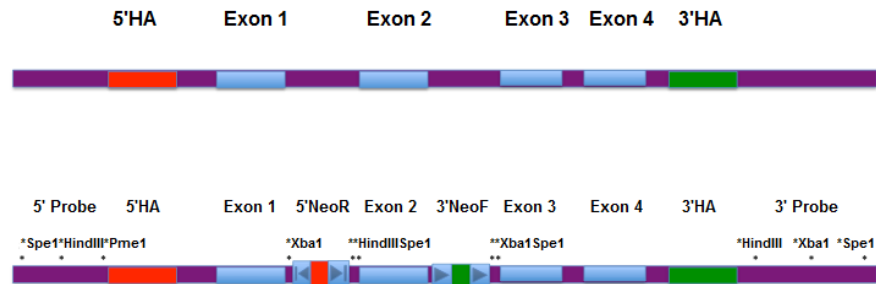


Figure A.19: Diagram showing the Southern blot design.

Top: This diagram shows the Panx2 gene with Exons 1-4, with the 5' and 3' HA homologous to Bac-Panx2 DNA for recombination. Bottom: This diagram shows the selection and placement of RE sites for Southern blot analysis. Following hybridization with the 3' probe, Spe 1 digest will give a 25.5 kb wild-type band and Xba1 will give an 11 kb wild-type band. Following hybridization with the 5' probe, Spe 1 digest will give a 25.5 kb wild-type band and HindIII will give a 15 kb wild-type band.

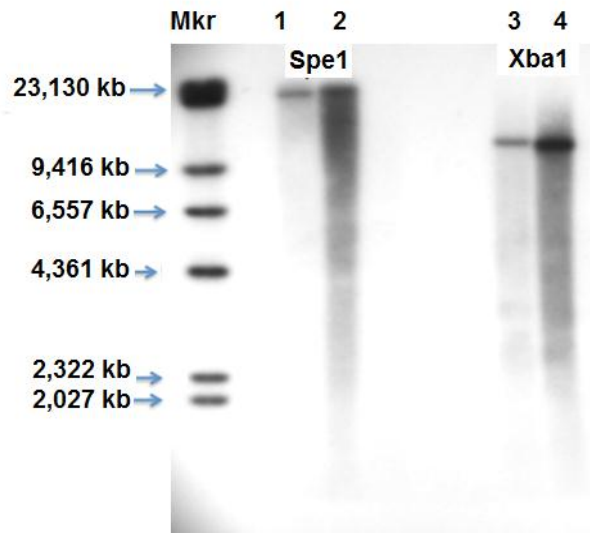


Figure A.20: Southern blot analysis of the WT DNA ES cells.

Following hybridization with the 3' probe, Spe 1 digest will give a 25.5 kb wild-type band and Xba1 will give an 11 kb wild-type band.

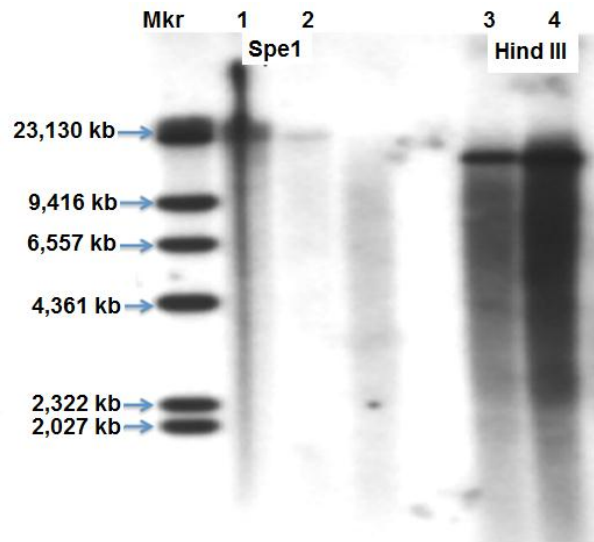


Figure A.21: Southern blot analysis of the WT DNA ES cells.

Following hybridization with the 5' probe, Spe 1 digest will give a 25.5 kb wild-type band and HindIII will give a 15 kb wild-type band.

PREPARATION OF PLASMID DNA FOR TRANSFECTION

DH10B *E.coli* cells containing BAC-Panx2 were cultured overnight in 200 ml LB broth, autoclaved in a 1L flask, and cooled before adding chloramphenicol at 25ug/ml, with shaking at 37⁰C. The next day, the LB broth was poured into 500 ml plastic centrifuge bottles and centrifuged at 5000 rpm for 15 minutes. The supernatant was discarded and the bacterial pellet was resuspended in 10 ml of chilled Buffer P1, before transferring the resuspended pellet solution to a clean plastic centrifuge tube. To this mixture 10 ml of Buffer P2 was added, the resuspended pellet mixed gently and incubated for 5 minutes at room temperature. Following the 5 minute incubation at RT, 10 ml of cold Buffer P3 was added, mixed immediately by gentle inversion and further incubated on ice for another 20 minutes. The mixture was centrifuged at 12,000 rpm at 4⁰C for 30 minutes. In the meanwhile, a Qiagen-tip 500 column was equilibrated by adding 10 ml of Buffer QBT and the column drained into a 50-ml tube. After centrifugation, the supernatant was drained into Falcon 50-ml tubes, which were then added to the equilibrated columns and allowed to flow through. The columns were washed twice with 30 ml of Buffer QC and the DNA eluted by 2 x 5 ml of Buffer QF, captured in a clean 50-ml tube. The DNA was precipitated by adding 7 ml of room-temperature isopropanol and the mixture centrifuged at 12,000 rpm for 30 minutes at 4⁰C. After centrifugation, the pellet was washed twice in 5 ml of 70% ethanol, by centrifugation at 12,000 rpm for 5 minutes at 4⁰C. Following the two washes the pellet was air-dried for 5 minutes then resuspended in 500 µl of dH₂O or TE. Approximately 15

μ l of the maxi-prepped BAC-Panx2 DNA was used for restriction enzyme digests to confirm the BAC-Panx2 DNA (www.Qiagen.com).

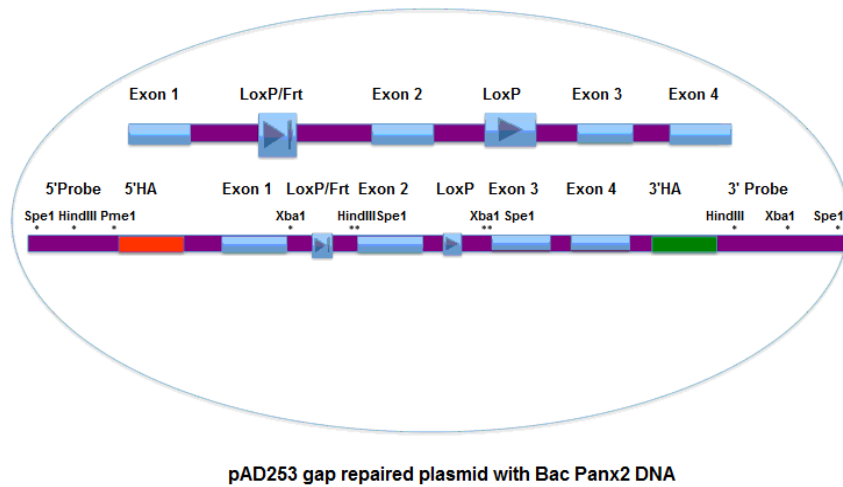


Figure A. 22: Diagram showing the expected pAD253 retrieval plasmid.

This will have the BAC-Panx2 DNA CKO construct for homologous recombination of genomic DNA in Cre/Flpe recombinase mice to generate the KO mutant.

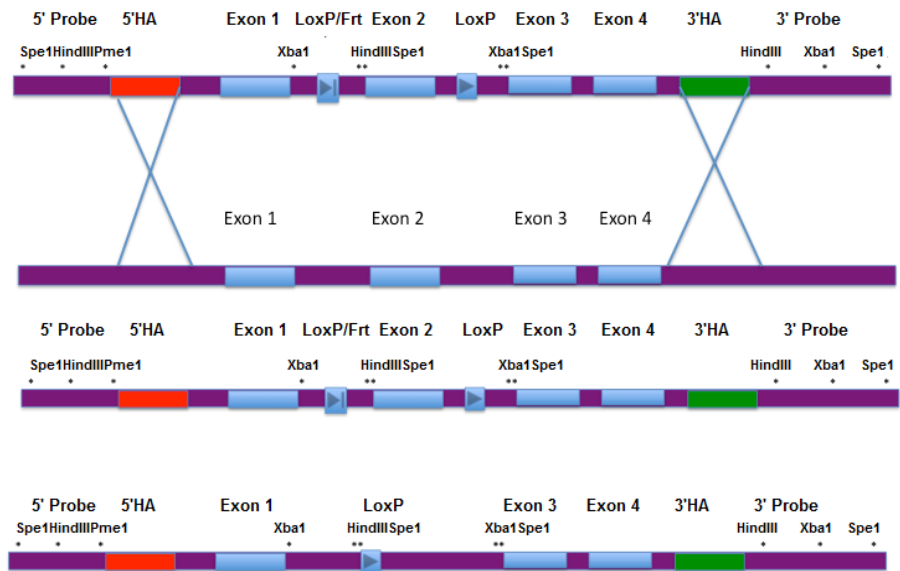


Figure A.23: Diagram showing the KO mutant mice DNA.

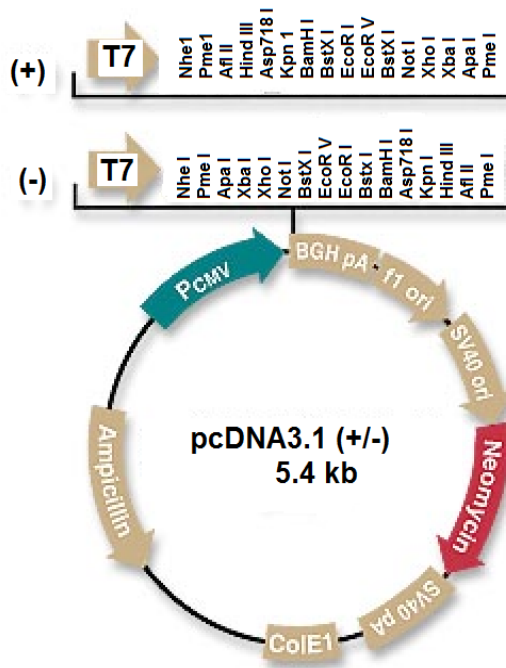


Figure A.24: Diagram showing the pcDNA3.1 vector used for sub-cloning.
(Data obtained from www.invitrogen.com)

A.3 RESULTS

RETRIEVAL OF THE GENOMIC FRAGMENT FROM BAC BY GAP REPAIR

To subclone DNA from a BAC clone into a vector of choice, a process known as gap repair is frequently used in homologous recombination.

BAC ISOLATION

To confirm the presence of BAC-Panx2 DNA in the DH10B *E. coli* electrocompetent cells, BAC-Panx2 DNA was digested with BamH1 and Not1 restriction

enzymes (RE). A map of the Panx2 BAC genomic DNA with RE enzyme sites showed that NotI was a non-cutter and that BamHI would cut at several sites to give a detailed banding pattern. Figure A-7 shows the identity of the correctly targeted BAC-Panx2 DNA clones. Using “M” as the marker with sizes corresponding to 12, 5, 2, 1.65 and 1 kb, the gel image shows that clones 1-4 and 6-10 have the expected sizes when digested with BamHI. The sizes are 6, 3.9, 3.5, 1.5, 1.4, 3, 1.9, and 2 kb. Therefore, clone number 5 does not have the correct banding pattern and was discarded, while clone number 11 was an internal control or another BAC-DNA. Therefore, BAC-Panx2 DNA was correctly inserted into the DH10B *E. coli* electro-competent cells.

PREPARATION OF ELECTRO-COMPETENT BACTERIAL STRAINS

DY380 (DH10B lambda cI857 (cro-bio< > Tet) competent cells inoculated in LB/Chloramphenicol (12.5 ug/mL) were incubated and grown at 32°C. Bacterial strains were grown at 32°C and for each required transformation only freshly prepared electro-competent cells were used. Pelleted DY380 cells resuspended in 50 µl ice-cold dH₂O were kept on ice to increase the electro-competency (Malureanu et al, 2011) before electroporation.

TRANSFERRING BAC-PANX2 DNA INTO E. COLI RECOMBINOGENIC BACTERIAL STRAIN

Freshly prepared Bac Panx2 DNA (600 ug or 1200 ug) were added to 50 µl of DY380 electrocompetent cells and electroporated, before selection using the chloramphenicol resistance (Cam^r) gene carried on the BAC vector backbone. We

obtained many colonies on both the Bac Panx2 DNA 600 ng and 1200 ng LB plates containing chloramphenicol at 12.5 ug/mL incubated at 32°C, compared to control plates which had no colonies. To confirm the presence and integrity of the Bac Panx2 DNA in the DY380 recombinogenic bacterial strain diagnostic restriction enzyme digests using multi-cutter BamH1 RE revealed the presence of Bac Panx2 DNA in the DY380 cells as compared to controls. The results indicate that clones 1-3, 5-7, 9-11, and 13-19 have the correct digest pattern (Data not shown).

RETRIEVING TARGETED GENE INTO TARGETED VECTOR BY GAP REPAIR

Following the successful transfer of Bac-Panx2 DNA into the DY380 recombinogenic bacterial strains, the DY380 electro competent cells were successfully induced for *exo*, *bet*, and *gam* expression by growing at 42 °C for 15 minutes, before electroporation of 100 ng of pAD253 retrieval plasmid DNA (pAD253-5'HA-3'HA) into induced DY380 electro competent cells. Selections of transformants using Ampicillin (50 ug/mL) revealed the presence of many colonies on the Induced/With DNA plates (42 °C) as compared to the absence of colonies on the Induced/No DNA plates (42 °C) the absence of colonies on the Induced/With DNA plates (32 °C), and the absence of colonies on the Induced/No DNA plates (32 °C). Isolation of Bac Panx2 DNA via mini-preparation using Qiagen mini-prep kit according to manufacturer's instructions and selecting recombinants for diagnostic restriction enzyme digests using BamH1 multi-cutter for Panx2 DNA confirmed the successful retrieval or gap repair of Bac Panx2 DNA into retrieval vector pAD253 (5'HA-3'HA) (Figure A-10). Specifically, Figure A-

10 confirms the successful and correct insertion of BAC-Panx2 with 5'HA and 3'HA into retrieval vector pAD253. Based on the expected sizes of BAC-Panx2 DNA when cut by RE BamH1, clones number 2, 4, 5, 7, 9, 11-16, 18 and 19, all have the expected sizes of 6, 3.9, 3.5, 1.5, 1.4, 3, 1.9 and 2 kb. The clone number 10 is an internal control of BAC-DNA.

INSERTING HOMOLOGY ARMS INTO TARGETING VECTOR PAD253

To increase the frequency of sub-cloning by gap repair, longer homology arms of 200-500 bp are recommended to reduce the likelihood of unwanted recombination products. The PCR primers (Table A-3) for the homology arms used in the pAD253 retrieval vector were designed to amplify two-300 bp regions of the Bac Panx2 DNA sequence such that the 5'HA and 3'HA marks the ends of the fragments to be subcloned by gap repair. Freshly prepared BAC Panx2 DNA template and primers were used to PCR amplify the homology arms 5'HA with several RE sites including Not1 and Xho1, as well as the 3'HA with several RE sites including Not1 and BamH1, to permit directional cloning of the PCR products into pAD253 retrieval vector (Figure A-7; A-8). Agarose gel electrophoresis confirmed the presence of the correct sized 300 bp PCR product which was subsequently purified using Qiagen spin columns. The 5'HA was digested with Not1/Xho1, the 3'HA digested with Not1/BamH1, and the pAD253 vector digested with Xho1/BamH1. The digested fragments were further purified before ligation of 5'HA (Not1/Xho1) and 3'HA (Not1/BamH1) into pAD253 retrieval vector

(Xho1/BamH1). The final pAD253 contained a Pme1 restriction enzyme site for linearization, needed to create a double-strand break for gap repair.

USING THE MINI-TARGETING VECTOR TO INSERT A LONE LOXP SITE INTO THE TARGETING CONSTRUCT GENERATING THE MINI-TARGETING VECTOR-3'NEO FORWARD (PLTM332)

The next step in creating a CKO-targeting vector is the introduction of a loxP site into the subcloned DNA, in this case the 3' end of Panx2 exon 2, by introducing a floxed neomycin resistance (Neo cassette) PLTM332 via homologous recombination into the subcloned plasmid DNA and by removing the Neo gene via Cre recombinase (Figure A6: B & C). The floxed Neo gene in PLTM332 is expressed from a hybrid PGK-EM7 promoter. PGK allows Neo to be expressed efficiently in mammalian cells while EM7 allows Neo to be expressed efficiently in bacterial cells (Figures A15 - A17). In the presence of Cre recombinase in the EL350 strain of *E. coli* bacterial cells, the floxed Neo gene will be removed leaving behind a single lone loxP site at the targeted locus.

To construct the mini-targeting vector (pcDNA3.1-5'HA-3'Neo F-3'HA) needed to introduce a floxed Neo gene at the correct location (3' end of the Panx2 Exon2) the vector pcDNA3.1 is first flanked with 300 bp homology arms homologous to the Bac Panx2 DNA targeting site. The 5'HA and 3'HA for pcDNA3.1 (+) were generated by PCR amplification of the BAC Panx2 DNA.

Here the PCR primers (Table A-4) were engineered to contain 5'HA restriction enzyme sites, Nhe1 and EcoR1, and 3'HA restriction enzymes sites, Not1 and EcoR1. Following PCR amplification, the products were purified, digested with restriction enzymes, and ligated to pcDNA3.1 vector digested with Nhe1/Not1. Colonies selected by

ampicillin (50 ug/mL) and checked by diagnostic restriction enzymes with Nhe1/Not1 confirmed the presence of the 600 bp insert in the pcDNA3.1 vector (5'HA/3'HA) (Figure A-18). In the second part to insert the Neo cassette into the pcDNA3.1 5'-3'HA complex, the floxed Neo cassette excised from PLTM332 vector was restriction enzyme digested with **HindIII/BglIII**, and ligated to pcDNA3.1 (5'HA/3'HA) similarly restriction enzyme digested with HindIII/BglIII. Colonies selected by Kanamycin (50 ug/mL) resistance, conferred by Neo cassette were picked and checked by restriction enzyme digest. None of the colonies contained the Neo cassette. Therefore, the first 3'Neo F PLTM332 mini-targeting vector was incomplete (Data not shown).

THE MINI-TARGETING VECTOR-5'NEO REVERSE (PLTM260)

Following PCR amplification of the 5'HA (Nhe1~AatII~Kpn1~EcoR1) and 3'HA (EcoR1~HindIII~AatII~Not1) with restriction enzymes sites, the products were purified, and restriction enzyme digested, and ligated to pcDNA3.1 vector digested with Nhe1/Not1 (Figures A11-A13). Colonies selected by ampicillin (50 ug/mL), and checked by diagnostic restriction enzymes with Nhe1/Not1 confirmed the presence of the 600 bp insert in the pcDNA3.1 vector (5'HA/3'HA). The floxed Neo cassette excised from PLTM260 vector was digested with **HindIII/Kpn1**, and ligated to pcDNA3.1 (5'HA/3'HA) similarly digested with HindIII/Kpn1. Colonies selected by Kanamycin (50 ug/mL) resistance, conferred by the Neo cassette, were picked and checked by restriction enzyme digest. The presence of the 1.9-2kb insert of the Neo-reverse cassette in the pcDNA3.1 (5.4 kB) ~5'HA~3'HA (600 bp) vector complex confirmed the identity of the

second mini-targeting vector (Figure A-14). The pcDNA3.1 5'HA-5'Neo R cassette-3'HA vector complex was linearized by restriction enzyme AatII, gel purified and frozen down at -20°C for homologous recombination in El250 *E. coli* bacterial cells containing Flpe recombinase. The second mini-targeting vector-5'Neo Reverse (PLTM260) was complete.

GENE TARGETING IN ES CELLS

To correctly identify recombinant ES clones after homologous recombination either upstream or downstream of the loxP site located at the 5' end of the Panx2 Exon 2 external and internal restriction enzyme sites were introduced into the targeting vector on various primers used to generate the homology arms.

The enzymes were selected to cut once outside targeting vector (the flanking site) and distal to the region to be floxed (the internal site). The enzymes can be the same for both ends, or they can be two different enzymes, one each for the 5' end and the other for the 3' end (Wang, Warren et al. 2007). To diagnose the 5' end of the Panx2 Exon2 location, Spe1 and HindIII restriction enzymes were engineered external to, or located outside the targeting construct, and Spe1 and HindIII restriction enzyme sites were also engineered internal to the 5' end of Panx2 Exon2, to determine successful recombinants.

A 5' probe using Spe1 restriction enzyme digests identifies a 25.5 kb wild type allele and a potential 12 kb 5' Neo R-PLTM260 targeted allele containing loxP and FRT sites. After Cre or Flp mediated recombination, the size of the 5'Neo R-PLTM260 targeted allele is reduced from 12 kb to 10 kb. The 25.5 kb wild-type allele is unchanged.

HindIII restriction enzyme digests will give a 15 kb wild type allele and a 12 kb mutant or targeted allele containing loxP and FRT sites. Upon Cre or Flp mediated deletion, the size of the mutant allele is reduced from 12 kb to 10 kb. The wild type 15 kb allele is unchanged.

To verify the 3' end of the Panx2 Exon2 targeting vector, Spe1 and Xba1 restriction enzymes were engineered external to or located outside the targeting construct, and Spe1 and Xba1 restriction enzyme sites were also engineered internal to the 3' end of the Panx2 Exon2 location, to determine successful recombinants.

A 3' probe using Spe1 restriction enzyme digests identifies a 25.5 kb wild type allele and a 9 kb 3' Neo R-PLTM332 targeted allele containing the lone loxP site.

Xba1 restriction enzyme digests will give an 11 kb wild type allele and a 9 kb 3' Neo R-PLTM332 targeted allele containing the lone loxP site.

Southern blot analysis confirmed the identity of the expected targets in WT ES cells showing the 25.5 kb wild type allele/band with Spe1 restriction enzyme digest and the 15 kb wild type allele/band with HindIII restriction enzyme digests, following hybridization with the 5' probe. Similarly, the wild type ES cells containing the expected 25.5 kb wild type allele/band with Spe1 restriction enzyme digest and the 11 kb wild type allele/band with Xba1 restriction enzyme digests, following hybridization with the 3' probe. Therefore, the Southern blot genotyping method was complete.

A.4 DISCUSSION

To determine the *in vivo* function of Panx2 gene, we attempted to construct a conditional knock-out targeting vector utilizing homologous recombineering. We were successful in cloning and constructing the 5'Neo Reverse mini-targeting vector containing (FRT-loxP-PGK-EM7-NeobpA-FRT-loxP) cloned into pcDNA3.1 vector. This would have been used in the second targeting event whereby the 5' NeoR loxP/FRT site would be inserted into the gap-repaired pAD253 vector. The pAD253 vector contained 5'HA and 3'HA homologous to mouse genomic Bac-Panx2. In the presence of EL250 Cre-Flpe recombinase cells via homologous recombination, the 5' Neo R cassette will be excised to leave loxP and FRT sites at the 5' of Exon 2 targeted for deletion.

We were also successful in retrieving Bac-Panx2 into the pAD253 retrieval vector containing both 5'HA and 3'HA, homologous to genomic mouse BAC-Panx2 DNA. The pAD253 retrieval vector would have become the gap-repaired plasmid to be used in the final construct to generate the KO, if all components to include the loxP and frt sites were successfully inserted and cloned.

In addition we were able to confirm the Southern blot analysis for genotyping potential homologous recombinants as evidenced by the presence of WT ES DNA bands at the appropriate size identified by the 5' and 3' hybridization probes.

Unfortunately, we were unable to generate the 3'NeoF selection cassette (loxP-PGK-EM7-NeobpA-loxP) for targeting to the 3' side of Exon 2 for deletion. As such, we

could not complete the first targeting event as this necessitated the entire 3' NeoF cassette cloned into the pcDNA3.1 vector containing both 5' HA and 3'HA, homologous to Bac-Panx2 DNA. Therefore, we could not proceed with cloning the 3'NeoF loxP into the gap-repaired pAD253 vector, containing the 5'HA and 3'HA homologous to Bac-Panx2 DNA. In the presence of EL350 Cre-recombinase cells via Homologous recombination, the 3' NeoF cassette would have been excised to leave a loxP site, 3' of Exon2 targeted for deletion. However, because we were unsuccessful in completing the 3' NeoF cassette, the first targeting event could not occur; and by default, neither could we proceed with the second targeting event to complete the Panx2 CKO construct.

Taken together, we can conclude that our efforts to generate a Panx2 CKO targeting vector were partially successful.

We were successful in inserting either the 5'HA and 3'HA, without the 3'NeoF cassette into pcDNA3.1 vector, or inserting the 3'HA and 3'NeoF cassette, without the 5'HA into pcDNA 3.1 vector (data not shown), as well as inserting the 5'HA and 3'NeoF cassette, without the 3'HA into pcDNA3.1 vector (data not shown). However, I was not successful in inserting all three components together, by the methods used.

To further characterize the function of Panx2 we performed several additional *in vitro* assays. Some notable experiments included a biotinylation assay, an epitope tagging assay, a shRNA assay, and finally a phosphatase assay.

Based on the publications in the literature, we initially hypothesized that Panx2 forms either hemi-channels or functional gap junction channels. We decided to perform a

biotinylation assay that would be instrumental to determine the cellular localization of Panx2 protein.

The biotinylation technique is based on the property of biotin to strongly and specifically bind to its partner, avidin. Sulfo-NHS-SS-Biotin is a thiol cleavable amine-reactive reagent with a molecular mass of 606.09. Biotin labels the surface membrane of proteins because it does not cross the cell membrane to label proteins in the cytoplasm in healthy cells. Furthermore, the MW of the SS of 606.09 is small enough to pass through open hemi-channels in healthy cells on the surface membrane. The size of the SS-Biotin is also small enough to block the hemi-channel pores by forming complexes with the extracellular lysines lining hemi-channel pores (Schalper, Palacios-Prado et al. 2008). With this knowledge in mind, we reasoned that if Panx2 was expressed on the cell surface in the normal mouse primary astrocytes, that it may form hemi-channels. If Panx2 formed endogenous gap junction intracellularly or in the cytoplasm, then the SS-Biotin may have labeled the Panx2 in KR158 mouse astrocytoma cell lines.

We were not successful in confirming the presence of Panx2 hemi-channel in the cell lines KR158 grade III astrocytoma and normal mouse primary astrocytes, or the presence of functional gap junction channels intracellularly. Importantly, in the study of Lai et al, Panx2 had been shown to localize within the cytosol of rat C6 cells and not at the plasma membrane (Lai, Bechberger et al. 2009). These results are in accordance with our observations that Panx2 does not form hemichannels (it is not found at the plasma membrane) and neither does it form functional gap junction intercellular channels (due to its location within the cytosol). Based on the more recent published reports, glycosylation

sites are present on Panx1 and Panx3 (Penuela, Bhalla et al. 2007; Penuela, Bhalla et al. 2009; Swayne, Sorbara et al. 2010). These glycosylation events preclude the formation of hemi-channels and possibly functional gap junction channels. It is also possible that Panx2 is glycosylated as well.

We also attempted to determine the possible location of Panx2 protein channels (Kim, Bonifant et al. 2008) in KR158 grade III astrocytoma cell line by epitope tagging of Panx2 cDNA at the C-terminal with FLAG-tag followed by transfection of this construct. Western blot analysis with FLAG antibodies did not demonstrate the presence of FLAG-Panx2 in epitope-tagged KR158 cells (Data not shown). One limitation of this assay may be due to poor transfection efficiency of the Panx2-cDNA into the KR158 cell line. Another limitation may be due to the failure of the Panx2 protein to be fully functional as the FLAG-tag may have impeded its folding. The third possibility is that the tag may have affected how the Panx2 protein interacted with other proteins necessary for its efficient functioning.

We also hypothesized that the knock-down of Panx2 will lead to increased tumorigenicity of glioma cells. To test this hypothesis, we made a shRNA to knock-down the expression levels of Panx2 in mouse primary astrocytes and KR158 grade III astrocytoma cell lines. Again, our data were inconclusive.

Online prediction tools available on the NETPHOS website identified potential phosphorylation sites within Panx2. Therefore, we performed a phosphatase assay with the expectations that removing phosphate groups would result in a band shift or the reduction of the number of Western blot bands to one. To do this, the lysates were

prepared from normal mouse primary astrocytes and dephosphorylated with alkaline phosphatase (AP). Dephosphorylation had no visible effect on the mobility of the Panx2 specific species. To confirm the efficiency of the AP treatment, the blots were stripped and re-probed for alpha-Actin, beta-Tubulin, and GAPDH, to ensure that equal amounts of proteins were loaded. The results indicate that equal amounts of protein lysates were loaded. However, later research by Penuela et al, demonstrated conclusively that the major post-translational event in Pannexins to include Panx1 and Panx3 is glycosylation, not phosphorylation (Penuela, Bhalla et al. 2007), a feature that distinguishes them from connexins.

In addition to N-glycosylation, the latest studies also identified possible sumoylation and palmitoylation sites within Panx2. In particular, in stem-like multipotent neuronal progenitor cells and in HEK293 cells ectopically expressing Pannexins, these proteins are partially S-palmitoylated (Swayne, Sorbara et al. 2010), while in their neuronally committed Type IIb and III progeny or in immature neurons only the non-palmitoylated form is present. It is possible that our Western blots showed multiple Panx2-specific bands due to differential S-palmitoylation or other modifications that we failed to capture.

Altogether, the initial results presented suggest that Panx2 is downregulated in mouse and human astrocytoma cell lines. However, we were unable to determine whether Panx2 is causally linked to astrocytoma progression.

UNANSWERED QUESTIONS & FUTURE DIRECTIONS

To determine the role of Panx2 in astrocytoma/GBM biology, we have attempted to make a Panx2 knockout, which involved making a Panx2 knockout construct. These attempts were not successful. However, other researchers studying the role of Panx1 and Panx2 in channel formation in neurons and the role they may play in ischemic brain damage, were successful in generating Panx2 ^{-/-}, Panx1 ^{-/-}; and Panx1 ^{-/-}/Panx2 ^{-/-} mice. These mice were viable and demonstrated no obvious signs of developmental or behavioral abnormalities (Bargiotas, Krenz et al. 2011; Qu, Misaghi et al. 2011). Furthermore, Dvorianchikova et al, 2012 generated neuron-specific conditional CKO Thy1-Cre/Panx1 knockout mice, as well as constitutive KO (CMV-Cre/Panx1) for the study of protective effects of Panx1 on retinal neurons undergoing ischemia. Both the conditional and the constitutive Panx1 knock-out mice were all fertile and could not be distinguished from the WT mice based on gross retinal morphology (Dvorianchikova, Ivanov et al. 2012). However, none of these mice have yet been evaluated for spontaneous or induced gliomagenesis, as such or after the crossing with glioma-prone mice. Therefore, the effects of Panx2 on astrocytoma/GBM biology remain unknown and warrant further investigations.

PANNEXIN BIBLIOGRAPHY

- Ambrosi, C., O. Gassmann, et al. (2010). "Pannexin1 and Pannexin2 channels show quaternary similarities to connexons and different oligomerization numbers from each other." The Journal of biological chemistry **285**(32): 24420-24431.
- Asklund, T., I. B. Appelskog, et al. (2004). "Histone deacetylase inhibitor 4-phenylbutyrate modulates glial fibrillary acidic protein and connexin 43 expression, and enhances gap-junction communication, in human glioblastoma cells." Eur J Cancer **40**(7): 1073-1081.
- Bao, B. A., C. P. Lai, et al. (2012). "Pannexin1 drives multicellular aggregate compaction via a signaling cascade that remodels the actin cytoskeleton." The Journal of biological chemistry **287**(11): 8407-8416.
- Bargiotas, P., A. Krenz, et al. (2011). "Pannexins in ischemia-induced neurodegeneration." Proceedings of the National Academy of Sciences of the United States of America **108**(51): 20772-20777.
- Boassa, D., C. Ambrosi, et al. (2007). "Pannexin1 channels contain a glycosylation site that targets the hexamer to the plasma membrane." The Journal of biological chemistry **282**(43): 31733-31743.
- Boassa, D., F. Qiu, et al. (2008). "Trafficking dynamics of glycosylated pannexin 1 proteins." Cell Commun Adhes **15**(1): 119-132.
- Bond, S. R., A. Lau, et al. (2011). "Pannexin 3 is a novel target for Runx2, expressed by osteoblasts and mature growth plate chondrocytes." Journal of bone and mineral research : the official journal of the American Society for Bone and Mineral Research **26**(12): 2911-2922.
- Bruzzone, R. and R. Dermietzel (2006). "Structure and function of gap junctions in the developing brain." Cell Tissue Res **326**(2): 239-248.
- Butt, A. M. (2011). "ATP: a ubiquitous gliotransmitter integrating neuron-glia networks." Seminars in cell & developmental biology **22**(2): 205-213.

- Celetti, S. J., K. N. Cowan, et al. (2010). "Implications of pannexin 1 and pannexin 3 for keratinocyte differentiation." Journal of cell science **123**(Pt 8): 1363-1372.
- Cotrina, M. L., J. H. Lin, et al. (1998). "Cytoskeletal assembly and ATP release regulate astrocytic calcium signaling." The Journal of neuroscience : the official journal of the Society for Neuroscience **18**(21): 8794-8804.
- D'Hondt, C., R. Ponsaerts, et al. (2009). "Pannexins, distant relatives of the connexin family with specific cellular functions?" BioEssays : news and reviews in molecular, cellular and developmental biology **31**(9): 953-974.
- de Rivero Vaccari, J. P., D. Bastien, et al. (2012). "P2X4 receptors influence inflammasome activation after spinal cord injury." The Journal of neuroscience : the official journal of the Society for Neuroscience **32**(9): 3058-3066.
- Deretic, V., S. Jiang, et al. (2012). "Autophagy intersections with conventional and unconventional secretion in tissue development, remodeling and inflammation." Trends in cell biology **22**(8): 397-406.
- Dvorianchikova, G., D. Ivanov, et al. (2012). "Genetic ablation of Pannexin1 protects retinal neurons from ischemic injury." PloS one **7**(2): e31991.
- Huang, Y.J., Y. Maruyama, et al. (2007). "The role of pannexin 1 hemichannels in ATP release and cell-cell communication in mouse taste buds." Proc Natl Acad Sci USA **104**(15): 6436-6441.
- Iglesias, R., G. Dahl, et al. (2009). "Pannexin 1: the molecular substrate of astrocyte "hemichannels"." The Journal of neuroscience : the official journal of the Society for Neuroscience **29**(21): 7092-7097.
- Ishikawa, M., T. Iwamoto, et al. (2011). "Pannexin 3 functions as an ER Ca²⁺ channel, hemichannel, and gap junction to promote osteoblast differentiation." J. Cell Biol. **193**(7): 1257-1274.
- Iwabuchi, S. and K. Kawahara (2011). "Functional significance of the negative-feedback regulation of ATP release via pannexin-1 hemichannels under ischemic stress in astrocytes." Neurochem Int **58**(3): 376-384.
- Kim, J. E. and T. C. Kang (2011). "The P2X7 receptor-pannexin-1 complex decreases muscarinic acetylcholine receptor-mediated seizure susceptibility in mice." The Journal of clinical investigation **121**(5): 2037-2047.
- Kim, J. S., C. Bonifant, et al. (2008). "Epitope tagging of endogenous genes in diverse human cell lines." Nucleic Acids Res **36**(19): e127.

- Krutovskikh, V. A., C. Piccoli, et al. (2002). "Gap junction intercellular communication propagates cell death in cancerous cells." Oncogene **21**(13): 1989-1999.
- Kuznetsov, S. G., D. C. Haines, et al. (2009). "Loss of Rad51c leads to embryonic lethality and modulation of Trp53-dependent tumorigenesis in mice." Cancer Res **69**(3): 863-872.
- Lai, C. P., J. F. Bechberger, et al. (2009). "Pannexin2 as a novel growth regulator in C6 glioma cells." Oncogene **28**(49): 4402-4408.
- Lai, C. P., J. F. Bechberger, et al. (2007). "Tumor-suppressive effects of pannexin 1 in C6 glioma cells." Cancer research **67**(4): 1545-1554.
- Lehmann, C., H. Lechner, et al. (2006). "Heteromerization of innexin gap junction proteins regulates epithelial tissue organization in Drosophila." Mol Biol Cell **17**(4): 1676-1685.
- Litvin, O., A. Tiunova, et al. (2006). "What is hidden in the pannexin treasure trove: the sneak peek and the guesswork." Journal of cellular and molecular medicine **10**(3): 613-634.
- Liu, P., N. A. Jenkins, et al. (2003). "A highly efficient recombineering-based method for generating conditional knockout mutations." Genome Research **13**: 476-484.
- Locovei, S., J. Wang, et al. (2006). "Activation of pannexin 1 channels by ATP through P2Y receptors and by cytoplasmic calcium." FEBS letters **580**(1): 239-244.
- Loewenstein, W. R. (1979). "Junctional intercellular communication and the control of growth." Biochimica et biophysica acta **560**(1): 1-65.
- Lyons, S. A., W. J. Chung, et al. (2007). "Autocrine glutamate signaling promotes glioma cell invasion." Cancer research **67**(19): 9463-9471.
- Ma, W., V. Compan, et al. (2012). "Pannexin 1 forms an anion-selective channel." Pflügers Archiv : European journal of physiology **463**(4): 585-592.
- Ma, W., H. Hui, et al. (2009). "Pharmacological characterization of pannexin-1 currents expressed in mammalian cells." J Pharmacol Exp Ther **328**(2): 409-418.
- Malureanu, L. A. (2011). "Targeting vector construction through recombineering." Transgenic Mouse Methods and Protocols, Methods in Molecular Biology, 2011, Volume **693**; 181-203.

- Mesnil, M., S. Crespin, et al. (2005). "Defective gap junctional intercellular communication in the carcinogenic process." Biochimica et biophysica acta **1719**(1-2): 125-145.
- Modena, P., E. Lualdi, et al. (2006). "Identification of tumor-specific molecular signatures in intracranial ependymoma and association with clinical characteristics." Journal of clinical oncology : official journal of the American Society of Clinical Oncology **24**(33): 5223-5233.
- Musil, L. S. and D. A. Goodenough (1991). "Biochemical analysis of connexin43 intracellular transport, phosphorylation, and assembly into gap junctional plaques." J Cell Biol **115**(5): 1357-1374.
- Nagasawa, K., H. Chiba, et al. (2006). "Possible involvement of gap junctions in the barrier function of tight junctions of brain and lung endothelial cells." Journal of cellular physiology **208**(1): 123-132.
- Oliveira, R., C. Christov, et al. (2005). "Contribution of gap junctional communication between tumor cells and astroglia to the invasion of the brain parenchyma by human glioblastomas." BMC Cell Biol **6**(1): 7.
- Oskam, N. T., E. H. Bijleveld, et al. (2000). "A region of common deletion in 22q13.3 in human glioma associated with astrocytoma progression." International journal of cancer. Journal international du cancer **85**(3): 336-339.
- Panchin, Y., I. Kelmanson, et al. (2000). "A ubiquitous family of putative gap junction molecules." Current biology : CB **10**(13): R473-474..
- Penuela, S., R. Bhalla, et al. (2007). "Pannexin 1 and pannexin 3 are glycoproteins that exhibit many distinct characteristics from the connexin family of gap junction proteins." Journal of cell science **120**(Pt 21): 3772-3783.
- Penuela, S., R. Bhalla, et al. (2009). "Glycosylation regulates pannexin intermixing and cellular localization." Molecular biology of the cell **20**(20): 4313-4323.
- Penuela, S., S. J. Celetti, et al. (2008). "Diverse subcellular distribution profiles of pannexin 1 and pannexin 3." Cell communication & adhesion **15**(1): 133-142.
- Penuela, S., R. Gehi, et al. (2013). "The biochemistry and function of pannexin channels." Biochimica et biophysica acta **1828**(1): 15-22.
- Qu, Y., S. Misaghi, et al. (2011). "Pannexin-1 is required for ATP release during apoptosis but not for inflammasome activation." Journal of immunology **186**(11): 6553-6561.

- Rubin, H. (2008). "Contact interactions between cells that suppress neoplastic development: can they also explain metastatic dormancy?" Advances in cancer research **100**: 159-202.
- Saunders, M. M., M. J. Seraj, et al. (2001). "Breast cancer metastatic potential correlates with a breakdown in homospecific and heterospecific gap junctional intercellular communication." Cancer research **61**(5): 1765-1767.
- Scemes, E., S. O. Suadicani, et al. (2007). "Connexin and pannexin mediated cell-cell communication." Neuron glia biology **3**(3): 199-208.
- Scemes, E., Spray, D.C., Meda, P. (2009). "Connexins, pannexins, innexins: novel roles of "hemi-channels". Pflugers Archiv: European journal of physiology **457**(6): 1207-26.
- Schalper, K. A., N. Palacios-Prado, et al. (2008). "Currently used methods for identification and characterization of hemichannels." Cell communication & adhesion **15**(1): 207-218.
- Sin, W. C., S. Crespin, et al. (2012). "Opposing roles of connexin43 in glioma progression." Biochimica et biophysica acta **1818**(8): 2058-2067.
- Sosinsky, G. E., D. Boassa, et al. (2011). "Pannexin channels are not gap junction hemichannels." Channels **5**(3): 193-197.
- Swayne, L. A., C. D. Sorbara, et al. (2010). "Pannexin 2 is expressed by postnatal hippocampal neural progenitors and modulates neuronal commitment." The Journal of biological chemistry **285**(32): 24977-24986.
- Tabernero, A., J. M. Medina, et al. (2006). "Glucose metabolism and proliferation in glia: role of astrocytic gap junctions." Journal of neurochemistry **99**(4): 1049-1061.
- Vladimer, G. I., R. Marty-Roix, et al. (2013). "Inflammasomes and host defenses against bacterial infections." Current opinion in microbiology **16**(1): 23-31.
- Wang, N., M. De Bock, et al. (2013). "Paracrine signaling through plasma membrane hemichannels." Biochimica et biophysica acta **1828**(1): 35-50.
- Wang, W., M. Warren, et al. (2007). "Induced mitotic recombination of p53 in vivo." Proc Natl Acad Sci U S A **104**(11): 4501-4505.

Zhu, D., S. Caveney, et al. (1991). "Transfection of C6 glioma cells with connexin 43 cDNA: analysis of expression, intercellular coupling, and cell proliferation." Proceedings of the National Academy of Sciences of the United States of America **88**(5): 1883-1887.

Zou, J. and F. T. Crews (2012). "Inflammasome-IL-1beta Signaling Mediates Ethanol Inhibition of Hippocampal Neurogenesis." Frontiers in neuroscience **6**: 77.

CURRICULUM VITAE

Yvette S. Connell-Albert received a Bachelor of Science Degree in Microbiology from the University of Maryland in College Park, Maryland, in 1994. She was employed as an Interdisciplinary Biologist/Microbiologist at the National Cancer Institute in Bethesda, Maryland, while pursuing a Master of Science Degree in Biotechnology from the Johns Hopkins University (JHU) in Baltimore, Maryland. She graduated in 2002 from JHU and was employed in a local biotechnology company before returning in 2004 to George Mason University in Fairfax, Virginia, to pursue a PhD degree in Functional Genomics. Most recently, she was in the Individual Graduate Partnership Program with George Mason University and the National Cancer Institute at Frederick, where she conducted her doctoral research studies in potential therapies against astrocytomas and glioblastomas.